Postgraduate Studies Program in Physics
Physics Department
School of Sciences
University of Ioannina
MASTER'S THESIS

Hawking Radiation from Primordial Black Holes

Charalampous Georgianna
ID: 818

Supervisor: Kanti Panagiota

Ioannina
September, 2024

One of the basic rules of the universe
is that nothing is perfect. Perfection simply doesn't exist..
Without imperfection, neither you nor I would exist.
Stephen Hawking

Acknowledgements

At this point, I would like to extend my sincere gratitude to Professor Mrs. Panagiota Kanti for her invaluable guidance and support throughout my thesis work. I also thank the committee members, Mr. Georgios Leontaris and Mr. Leandros Perivolaropoulos, for their careful evaluation and useful feedback. A warm thank you is also due to all the professors in both the theoretical and experimental fields for their significant contributions to my education. Lastly, I deeply appreciate the support and encouragement from my family and friends throughout this journey.

Abstract

The aim of this work is to study the equation of motion of a scalar field, its behavior as it propagates in the gravitational background of a Schwarzschild black hole and the associated effect of the emission of Hawking radiation. First, we review the useful mathematical tools of General Relativity, and then we derive the Schwarzschild metric in an extended, spherically-symmetric n-dimensional spacetime. We study the equation of a scalar field in this background, and derive its solution by using the approximated ″far″ and ″near″ the horizon solutions. We compute the absorption coefficients and greybody factors, and present the radiation spectra for the case of bulk scalar emission and brane-localized scalar emission for all modes with $l \geq 0$. Finally, we illustrate the conclusions via graphical representations of our results, and present specific numerical calculations for the case of primordial Schwarzschild black holes.

Contents

Intoduction

Transitioning from Newtonian mechanics to General Relativity marks a significant evolution in our understanding of gravity and the structure of the universe. Newtonian Mechanics was developed by Sir Isaac Newton in the 17th century and provided a framework for understanding the motion of objects under the influence of forces. Newton's law of universal gravitation stated that every point mass in the universe attracts every other point mass with a force that is directly proportional to the product of their masses and inversely proportional to the square of the distance between their centers. However, while Newtonian Mechanics was extremely successful in describing the motion of objects on Earth and in the solar system, it faced challenges in explaining certain phenomena, such as the precession of Mercury's perihelion and the bending of light by massive objects.

In the early 20th century, Albert Einstein developed Special Relativity, which revolutionized our understanding of space and time. Special Relativity showed that space and time are interconnected in a four-dimensional continuum called spacetime. Through this theory, it introduced the concept of relativistic effects, such as time dilation and length contraction, at high speeds. Building upon Special Relativity, Einstein formulated General Relativity in 1915. General Relativity provides a more comprehensive theory of gravity. According to General relativity, gravity arises due to the curvature of spacetime caused by the presence of mass and energy. Massive objects distort the fabric of spacetime, causing other objects to move along curved paths. General Relativity successfully explained the anomalous perihelion precession of Mercury and predicted the bending of light by massive objects, which was confirmed during a solar eclipse in 1919. The theory has been extensively tested and confirmed through various experiments and observations, including gravitational lensing, the existence of black holes, and the detection of gravitational waves.

Three key concepts of General Relativity are spacetime curvature, the equivalence principle, and the field equations. Spacetime curvature refers to the fact that mass and energy deform spacetime, affecting the motion of objects within it. Additionally, the equivalence principle states that the gravitational force experienced by an observer in free fall is indistinguishable from the inertial force experienced by an observer in an accelerating reference frame. Finally, Einstein's field equations describe the relationship between the curvature of spacetime and the distribution of matter and energy within it. Transitioning from Newtonian mechanics to general relativity therefore, represents a profound shift in our understanding of gravity, spacetime, and the fundamental nature of the universe. General relativity remains a cornerstone of modern theoretical physics and cosmology, providing the framework for understanding phenomena ranging from the dynamics of galaxies to the behavior of black holes.

More specifically for the force of gravity, this is one of the four fundamental forces of nature, along with electromagnetism, strong nuclear force, and weak force. Gravity is the natural force that attracts two bodies towards each other. It is a fundamental force of nature that exists between any two objects with mass or energy. This force is responsible for keeping planets in orbit around stars, and stars in orbit around the center of their galaxies. However, despite the properties we know about gravity and its actions, it remains for centuries a mysterious force, which theoretical physicists try to study and understand. For instance, gravity proves to be particularly resistant when one tries to unify it with the other three forces of nature.

Finally as pointed out according to General Relativity, gravity is not a force that is transmitted between objects, but rather a result of the curvature of spacetime caused by the presence of massive objects. This curvature of spacetime is what causes objects to move on a curved path in the presence of gravity. Then, through General relativity, the existence of black holes can be predicted, which are regions of spacetime where the curvature becomes infinitely steep. Anything that falls into a black hole is trapped inside, and can never escape. However, to better understand the theory of general relativity and, by extension, what it creates, it is important to study its geometry and mathematical formalism.

The purpose of this work is to understand the behavior of Schwarzschild black holes in n-dimensional spacetime by computing Hawking radiation in the form of bulk and brane-localized scalar emission. More specifically, in the first chapter we explain some useful mathematical tools of general relativity, which concern the metric tensor, the connection and covariant derivative, the Riemann tensor, the Ricci tensor, the Ricci scalar and the Einstein tensor and the Lagrangian formalism leading to the Einstein equations. Then, in the second chapter, the derivation of the Schwarzschild solution in n'-dimensions is presented, followed by a discussion on extra dimension theories and the derivation of the scalar field equation. Subsequently, in the third chapter we focus on the case of primordial Schwarzschild black holes that may have been formed in the early universe and we discuss then the concept of Hawking radiation via the bulk scalar field and brane-localized scalar emission for $l \geq 0$. In particular, we derive the radial equation in n-dimensions and transform it to a hypergeometric equation that describes the behavior of the scalar field ″near″ and ″far″ from the black hole event horizon, both for bulk and brane-localized scalar emission. Then, for these two emission channels, we calculate the absorption coefficient as well as the greybody factor. Then, in the fourth chapter, we present the results for the cases of the bulk scalar emission and the brane-localized scalar emission, for the absorption coefficients the graybody factors and the energy emission rates. In the fifth chapter, some calculations for early Schwarzschild black holes are presented, and in the sixth chapter, we close with the conclusions.

1 Mathematical tools of General Relativity

In this chapter we will present the basic mathematical quantities of the General Theory of Relativity, which were first introduced by Einstein. For these purposes, we rely on the following books of general relativity [1], [2], [3], [4] and [5].

1.1 The metric tensor

In general relativity, the metric tensor plays a fundamental role in describing the geometry of spacetime. It characterizes the curvature and distances in the spacetime manifold. The metric tensor is usually denoted by $g_{\mu\nu}$, where μ and ν are indices running from 0 to 3, representing the four dimensions of spacetime (three spatial dimensions and one time dimension).

Consequently, to be able to measure distances on a manifold, it is important to define the line-element ds^2 by means of the metric, which is written as:

$$ds^2 = g_{\mu\nu} dx^\mu dx^\nu, \tag{1}$$

with $\mu, \nu = 0, 1, 2, 3$ and where the metric tensor $g_{\mu\nu}$ provides us with all the information about the geometry of spacetime. Furthermore, the quantity ds^2 helps us measure distances in curved spacetimes and dx^μ, dx^ν are the elements of length.

In addition, the metric must be a symmetric tensor $g_{\mu\nu} = g_{\nu\mu}$ and an important property of metric that often helps us in practice is:

$$g^{\mu\alpha} g_{\alpha\nu} = \delta^\mu_\nu, \tag{2}$$

where δ^μ_ν is the Kronecker symbol:

$$\delta^\mu_\nu = \{ \begin{array}{ll} 1, & \text{if } \mu = \nu, \\ 0, & \text{if } \mu \neq \nu. \end{array} \tag{3}$$

A simple example of a tensor is that of the three-dimensional (3D) Euclidean space in spherical coordinates. In order to find the metric of this 3D space, we first express the coordinates, in spherical form:

$$x_1 = r sin\theta \, cos\phi, \quad x_2 = r sin\theta \, sin\phi, \quad x_3 = r cos\theta. \tag{4}$$

Thus, the line-element can be written as:

$$ds^2 = dx_1^2 + dx_2^2 + dx_3^2 = dr^2 + r^2 d\theta^2 + r^2 sin^2\theta d\phi^2 = g_{\mu\nu} dx^\mu \otimes dx^\nu \tag{5}$$

where: $g_{11} = 1$, $g_{22} = r^2$ and $g_{33} = r^2 sin^2\theta$.

It is also important to mention that the metric can always be written in the form of a $D \times D$ matrix with a non-zero determinant. So in the case of the above example, the metric can be written as:

$$g_{\mu\nu} = \begin{pmatrix} 1 & 0 & 0 \\ 0 & r^2 & 0 \\ 0 & 0 & r^2 sin^2\theta \end{pmatrix}. \tag{6}$$

Finally, it is worth mentioning an important property of the metric, that of *indexing up and down*, i.e. $A^\mu = g^{\mu\nu} B_\nu$, $A_\mu = g_{\mu\nu} B^\nu$, etc.

1.2 Connection and covariant derivatives

In General Relativity we are interested in spacetimes which do not have flat geometry, but their geometry exhibits curvature. So, we need a tensor that gives us information about the curvature of the manifold. The tensor we are interested in is called the Riemann tensor or the curvature tensor, while another tensor, called the Ricci tensor, will play a central role in the field equations. But before we define these quantities we will need the concept of the covariant derivative.

Covariant derivatives ∇_μ are a concept from differential geometry and differential calculus, particularly in the context of smooth manifolds equipped with additional structures such as a *connection*. They provide a way to differentiate vector fields (or tensor fields more generally) along curves or vector fields on the manifold while respecting the geometric structure, such as the metric or other connections.

Let as consider a random differentiable manifold M with a map $(x_1, ..., x_n)$ where at each point of the manifold we define a vector x^μ, thus creating a vector field. If in the manifold we define a tensor of order m then correspondingly we create a tensor field. Without loss of generality we can see that the differentiation of a tensor is not a tensor in general, because the differential of a tensor $dT^{\mu\nu...}_{\kappa\lambda...}$ will be equal to the difference of two tensors valued at different points in space-time. However, the transformation of a tensor is generally different from one point of space-time to another, and this is because its transformation depends on the coordinate system (the position). So let us consider a scalar field $\phi = \phi(x^\mu)$ and consider its partial derivative as follows:

$$\frac{\partial \phi}{\partial x^\mu} = \frac{\partial x^\nu}{\partial x^\mu} \frac{\partial \phi}{\partial x^\nu}. \tag{7}$$

Now, to create a tensor-transformed derivative, we define the covariant derivative as follows:

$$\nabla_\mu V^\nu = \partial_\mu V^\nu + \Gamma^\nu_{\ \mu\sigma} V^\sigma, \tag{8}$$

were V^μ is a vector field.

In the context of General Relativity, the coefficients $\Gamma^\nu_{\ \mu\sigma}$ are called Christoffel symbols, which in general are not tensors. The Christoffel symbols are given by the relation:

$$\Gamma^\lambda_{\ \mu\nu} = \frac{1}{2} g^{\lambda\sigma} (\partial_\mu g_{\nu\sigma} + \partial_\nu g_{\sigma\mu} - \partial_\sigma g_{\mu\nu}) \tag{9}$$

and have the property $\Gamma^{\lambda}_{\mu\nu} = \Gamma^{\lambda}_{\nu\mu}$.

At this point it is important to define through the connection, the geodesic equation for a curve $x^{\mu}(\lambda)$:

$$\frac{d^2x^{\mu}}{d\lambda^2} + \Gamma^{\mu}_{\rho\sigma}\frac{dx^{\rho}}{d\lambda}\frac{dx^{\sigma}}{d\lambda} = 0. \tag{10}$$

Geodesics are the free trajectories that particles and light follow in the presence of gravity, and in the absence of any other force. They can be thought of as the shortest distance between two points in spacetime.

For example, using Minkowski space with signature $(-1, +1, +1, +1)$, we can write the line element (metric):

$$ds^2 = -dt^2 + dx_1^2 + dx_2^2 + dx_3^2. \tag{11}$$

In this case, the Christoffel symbols are all zero since the metric is constant. Therefore, the geodesic equation simplifies to:

$$\frac{d^2x^{\mu}}{d\lambda^2} = 0. \tag{12}$$

This equation states that the acceleration of the particle is zero, meaning that the object moves in straight lines at constant velocity unless acted upon by external forces. This is consistent with the principle of inertia in special relativity, where free objects move in straight lines at constant velocity.

1.3 Riemann tensor, Ricci tensor, Ricci scalar and Einstein tensor

The Riemann tensor, named after the German mathematician Bernhard Riemann, is a fundamental concept in differential geometry and is particularly important in the study of curved spaces, such as those encountered in general relativity. In general, the Riemann tensor characterizes the curvature of a manifold. It's a mathematical object that encodes information about how geodesics (the paths of shortest distance) deviate from being straight lines due to the curvature of the space.

The Riemann tensor is defined in terms of the metric tensor, which describes the local geometry of a manifold, and its derivatives. For a manifold with n dimensions, the Riemann tensor is a rank-4 tensor with n^4 components, but due to symmetries, it has $n^2(n^2-1)/12$ independent components in a general manifold.

In component notation, the Riemann tensor $R^{\rho}{}_{\sigma\mu\nu}$ is given by:

$$R^{\rho}{}_{\sigma\mu\nu} = \partial_{\mu}\Gamma^{\rho}{}_{\nu\sigma} - \partial_{\nu}\Gamma^{\rho}{}_{\mu\sigma} + \Gamma^{\rho}{}_{\mu\lambda}\Gamma^{\lambda}{}_{\nu\sigma} - \Gamma^{\rho}{}_{\nu\lambda}\Gamma^{\lambda}{}_{\mu\sigma}, \tag{13}$$

where $\Gamma^{\rho}{}_{\nu\sigma}$ are the Christoffel symbols.

If we consider its fully covariant form $R_{\rho\sigma\mu\nu} = g_{\rho\lambda}R^{\lambda}{}_{\sigma\mu\nu}$, then we see the following basic properties of it:

- It is antisymmetric in the interchange of its first two or last two indices: $R_{\rho\sigma\mu\nu} = -R_{\sigma\rho\mu\nu} = -R_{\rho\sigma\nu\mu}$.

- The sum of cyclic permutations of the last three indices vanishes:

$$R_{\rho\sigma\mu\nu} + R_{\rho\mu\nu\sigma} + R_{\rho\nu\sigma\mu} = 0. \tag{14}$$

- The Bianchi identity can also be extracted to hold:

$$\nabla_{[\lambda} R_{\rho\sigma]\mu\nu} = 0. \tag{15}$$

A useful observation is the fact that the given tensor completely determines whether the manifold has curvature or not. If this tensor is zero, then we automatically get the flatness of space. So, the Riemann tensor is a way of measuring the curvature of a space, and plays a fundamental role in Einstein's theory of general relativity, which describes the behavior of gravity.

Furthermore, through the Riemann tensor we can make a contraction to form the Ricci tensor:

$$R_{\mu\nu} = R^{\lambda}{}_{\mu\lambda\nu}, \tag{16}$$

where the Ricci tensor is a symmetric tensor:

$$R_{\mu\nu} = R_{\nu\mu}, \tag{17}$$

as a consequence of the symmetries of the Riemann tensor.

The trace of the Ricci tensor is the Ricci scalar:

$$R = R^{\mu}{}_{\mu} = g^{\mu\nu} R_{\mu\nu}. \tag{18}$$

The Ricci scalar, denoted by R, is a scalar curvature quantity in differential geometry, specifically in the context of Riemannian geometry. It's a mathematical object used to describe the curvature of a Riemannian manifold, which is a generalization of the concept of curvature to higher dimensions.

The Ricci scalar is a fundamental quantity in Einstein's theory of general relativity. Together with the Ricci tensor, it appears in the Einstein field equations, which relate the curvature of spacetime to the distribution of matter and energy. Specifically, the Ricci tensor and Ricci scalar appear on the left-hand side of the Einstein field equations, representing the curvature of spacetime, while the right-hand side contains the stress-energy tensor, representing the distribution of matter and energy.

1.4 Lagrangian formulation and Einstein equations

As we pointed out, gravity can be described through Einstein's theory of general relativity. Then, we can look at gravity through two different perspectives: how the gravitational field influences the behavior of matter, and how matter determines the gravitational field. We initially consider a mass density ρ. According to Newtonian gravity, this mass density will create a gravitational potential which satisfies Poisson's equation:

$$\nabla^2\Phi = 4\pi G\rho, \tag{19}$$

where G is the gravitational constant, determining the strength of the gravitational force. This equation describes how the gravitational potential Φ is related to the mass density ρ. It essentially says that the Laplacian of the gravitational potential is proportional to the mass density, with the constant of proportionality being $4\pi G$.

Now, let's contrast this with general relativity. In general relativity, the behavior of particles and bodies under gravity is described by the curvature of spacetime rather than a force acting at a distance. Instead of trajectories being governed by forces, they are determined by the curvature of spacetime, which is in turn determined by the distribution of mass and energy. The equivalent to trajectories in general relativity is the concept of geodesics. A geodesic is the shortest path between two points in curved spacetime. In the absence of any forces, objects follow geodesics. These geodesics are determined by the geometry of spacetime, which is described by Einstein's field equations. The connection between Newton's equation and general relativity is that in the limit of weak gravitational fields and low velocities, general relativity reduces to Newtonian gravity. In this limit, the trajectories of particles described by geodesics closely resemble the trajectories predicted by Newtonian gravity.

Suppose now that we have a distribution of mass in space. Then, in order to find the gravitational potential it creates, we should solve the differential equation which is given by (19). In general relativity, the analogous statements will describe how the curvature of spacetime acts on matter to manifest itself as gravity, and how energy and momentum influence spacetime to create curvature.

In order at this point to be able to derive Einstein's equation, we consider the action:

$$S_{EH} = \frac{1}{16\pi G}\int d^4x\sqrt{-g}R = \frac{1}{16\pi G}\int d^4x\sqrt{-g}g^{\mu\nu}R_{\mu\nu}, \tag{20}$$

where g is the determinant of the metric tensor, and R the Ricci scalar quantity. This action is called Einstein-Hilbert action. Of course we can add the matter-energy distribution since we wrote the action only for the gravitational field in vacuum, so we get:

$$S = \frac{1}{16\pi G}\int d^4x\sqrt{-g}R + S_m, \tag{21}$$

where G is Newton's gravitational constant, while S_m is the action associated with matter and energy.

To obtain the equation of motion of the gravitational field we will consider the change of action with respect to $g^{\mu\nu}$ as follows (in equation (20)):

$$\delta S_{EH} = \frac{1}{16\pi G}\int d^nx[\delta(\sqrt{-g})g^{\mu\nu}R_{\mu\nu} + \sqrt{-g}R_{\mu\nu}\delta g^{\mu\nu} + \sqrt{-g}g^{\mu\nu}\delta R_{\mu\nu}] = 0. \tag{22}$$

Let us consider the third term in equation (22). In order to analyze this term, the following relations are derived:

$$\nabla_\lambda(\delta\Gamma^\rho{}_{\nu\mu}) = \partial_\lambda(\delta\Gamma^\rho{}_{\nu\mu}) + \Gamma^\rho{}_{\lambda\sigma}\delta\Gamma^\sigma{}_{\nu\mu} - \Gamma^\sigma{}_{\lambda\nu}\delta\Gamma^\rho{}_{\sigma\mu} - \Gamma^\sigma{}_{\lambda\mu}\delta\Gamma^\rho{}_{\nu\sigma} \tag{23}$$

$$\delta R^{\rho}{}_{\mu\lambda\nu} = \nabla_{\lambda}(\delta\Gamma^{\rho}{}_{\nu\mu}) - \nabla_{\nu}(\delta\Gamma^{\rho}{}_{\lambda\mu}) \tag{24}$$
$$\delta R_{\mu\nu} = \nabla_{\rho}(\delta\Gamma^{\rho}{}_{\nu\mu}) - \nabla_{\nu}(\delta\Gamma^{\rho}{}_{\rho\mu}) \tag{25}$$
$$\delta\Gamma^{\sigma}{}_{\mu\nu} = -\frac{1}{2}[g_{\lambda\mu}\nabla_{\nu}(\delta g^{\lambda\sigma}) + g_{\lambda\nu}\nabla_{\mu}(\delta g^{\lambda\sigma}) - g_{\mu\alpha}g_{\nu\beta}\nabla^{\sigma}(\delta g^{\alpha\beta})]. \tag{26}$$

Then, we can write for the third term of equation (22):

$$\int d^n x\sqrt{-g}g^{\mu\nu}\delta R_{\mu\nu} = \int d^n x\sqrt{-g}g^{\mu\nu}[\nabla_{\rho}(\delta\Gamma^{\rho}{}_{\nu\mu}) - \nabla_{\nu}(\delta\Gamma^{\rho}{}_{\rho\mu})]$$
$$= \int d^n x\sqrt{-g}\nabla_{\sigma}[g^{\mu\nu}(\delta\Gamma^{\rho}{}_{\mu\nu}) - g^{\mu\sigma}(\delta\Gamma^{\rho}{}_{\rho\mu})] = \int d^n x\sqrt{-g}\nabla_{\sigma}[g_{\mu\nu}\nabla^{\sigma}(\delta g^{\mu\nu}) - \nabla_{\rho}(\delta g^{\sigma\rho})]. \tag{27}$$

The integral in relation (27), is an integral with respect to the natural volume element of the covariant divergence of a vector. By Stokes theorem, this is equal to a boundary contribution at infinity, which we can set to zero by making the variation vanish at infinity.

The second term of equation (22) is in the desired form and therefore it remains for us to deal with the first term. So for the first term, we will use the relation:

$$\delta(\sqrt{-g}) = -\frac{1}{2}\sqrt{-g}g_{\mu\nu}\delta g^{\mu\nu} \tag{28}$$

and therefore:

$$\int d^n x\,\delta(\sqrt{-g})g^{\mu\nu}R_{\mu\nu} = -\frac{1}{2}\int d^n x\sqrt{-g}g_{\mu\nu}(g^{\mu\nu}R_{\mu\nu})\delta g^{\mu\nu}. \tag{29}$$

Therefore, equation (22) takes the form:

$$\delta S_{EH} = \frac{1}{16\pi G}\int d^n x\sqrt{-g}\left(R_{\mu\nu} - \frac{1}{2}g_{\mu\nu}R\right)\delta g^{\mu\nu} = 0, \tag{30}$$

leading to the result

$$R_{\mu\nu} - \frac{1}{2}g_{\mu\nu}R = 0, \tag{31}$$

which is the Einstein's equation in vacuum.

Furthermore, if we consider an action of the form:

$$S = \frac{1}{16\pi G}S_H + S_m, \tag{32}$$

where S_m is the action of the matter, we get:

$$\frac{1}{\sqrt{-g}}\frac{\delta S}{\delta g^{\mu\nu}} = \frac{1}{16\pi G}\left(R_{\mu\nu} - \frac{1}{2}Rg_{\mu\nu}\right) + \frac{1}{\sqrt{-g}}\frac{\delta S_M}{\delta g^{\mu\nu}} = 0. \tag{33}$$

If we define the energy-momentum tensor to be:

$$T_{\mu\nu} = -2\frac{1}{\sqrt{-g}}\frac{\delta S_M}{\delta g^{\mu\nu}}, \tag{34}$$

we obtain the complete Einstein's equation:

$$R_{\mu\nu} - \frac{1}{2}Rg_{\mu\nu} = 8\pi G T_{\mu\nu}, \tag{35}$$

where $R_{\mu\nu}$ is the Ricci tensor, R the Ricci scalar, $T_{\mu\nu}$ is the energy-momentum tensor and $g_{\mu\nu}$ the metric tensor.

The above equation describes the way spacetime is curved, through which we explain a series of gravitational phenomena. It is a system of second-order differential equations with respect to the spacetime metric, and its solution leads to various kinds of gravitational phenomena and objects described by a metric.

2 Black Holes in Four and Higher Dimensions

Black holes, their behavior and properties, are highly interesting objects of theoretical physics and astrophysics. In classical general relativity, black holes are described as regions of spacetime where gravitational forces are so intense that nothing, not even light, can escape from within a certain boundary called the event horizon. In four-dimensional spacetime (three spatial dimensions plus one time dimension), black holes are characterized by their mass, electric charge, and angular momentum.

The most famous solution describing a black hole in four dimensions is the Schwarzschild solution, which describes a non-rotating, uncharged black hole. This solution is characterized by a single parameter, the mass of the black hole, and it predicts a spherical event horizon. In addition to the Schwarzschild black hole, there are additional solutions that describe rotating black holes (Kerr black holes) and charged black holes (Reissner-Nordström black holes). These solutions introduce additional parameters to the metric tensor such as angular momentum and electric charge. One of the most intriguing aspects of black holes is their thermodynamics. In the 1970s, Stephen Hawking showed that black holes are not entirely black but emit radiation, now known as Hawking radiation, due to quantum effects near the event horizon. This discovery suggested a link between black holes and thermodynamics, leading to the development of black hole thermodynamics.

Black hole thermodynamics treats black holes as thermodynamic systems with temperature, entropy, and other thermodynamic properties. The laws of black hole mechanics, analogous to the laws of thermodynamics, were proposed by Jacob Bekenstein [6] and later refined by Hawking [7]. Recent research on black holes in four dimensions continues to explore various aspects, including their formation, evolution, and interactions with matter and other black holes.

Overall, the study of four-dimensional black holes remains a fascinating and active area of research in theoretical physics, with implications for our understanding of gravity, quantum mechanics, and the nature of spacetime itself.

In this chapter we will present the Schwarzschild solution in 4-dimensions as well as in higher-dimensions. For these purposes, we rely on the following books and papers: [1], [8], [9], [10], [11], [12], [13], [14], [15] [16] and [17].

2.1 The Schwarzschild solution

In this subsection, the most important and particularly simple solution will be presented, which is to consider a spherically symmetric curved space-time. In fact, to abstract things more, we will assume that this space-time is empty, i.e. the energy-momentum tensor is identically zero. Such spacetimes describe the outer region of a star, our planet, etc. In fact, the solution of such spacetime also describes black holes.

So we assume a metric of the form:

$$ds^2 = -A(r)\,dt^2 + B(r)\,dr^2 + r^2(d\theta_1^2 + sin^2\theta_1 d\phi). \tag{36}$$

Since we have assumed empty spacetime, the field equations take the form:

$$R_{\mu\nu} - \frac{1}{2}g_{\mu\nu}R = 0. \tag{37}$$

In order to solve equation (37), we will first calculate the Christoffel symbols and the Ricci tensor. We first calculate the Christoffel symbols, using equation (9):

$$\Gamma^0_{\ 01} = \frac{1}{2}\frac{A'(r)}{A(r)},\quad \Gamma^1_{\ 11} = \frac{1}{2}\frac{B'(r)}{B(r)},\quad \Gamma^1_{\ 00} = \frac{1}{2}\frac{A'(r)}{B(r)},\quad \Gamma^1_{\ 22} = -\frac{r}{B(r)},\quad \Gamma^1_{\ 33} = -\frac{r}{B(r)}sin^2\theta_1,$$
$$\Gamma^2_{\ 33} = -sin\theta_1\, cos\theta_1,\quad \Gamma^2_{\ 21} = \Gamma^3_{\ 31} = \frac{1}{r},\quad \Gamma^3_{\ 23} = \frac{cos\theta_1}{sin\theta_1}, \tag{38}$$

and then, from the equation (16) we can calculate the non-zero Ricci tensor components:

$$R_{00} = -\frac{A''(r)}{2B(r)} + \frac{A'(r)}{4B(r)}\left[\frac{A'(r)}{A(r)} + \frac{B'(r)}{B(r)}\right] - \frac{A'(r)}{rB(r)}, \tag{39}$$
$$R_{11} = \frac{A''(r)}{2A(r)} - \frac{A'(r)}{4A(r)}\left[\frac{A'(r)}{A(r)} + \frac{B'(r)}{B(r)}\right] - \frac{B'(r)}{rB(r)}, \tag{40}$$
$$R_{22} = \frac{1}{B(r)} - 1 + \frac{r}{2B(r)}\left[\frac{A'(r)}{A(r)} - \frac{B'(r)}{B(r)}\right], \tag{41}$$
$$R_{33} = sin^2\theta_1 R_{22}. \tag{42}$$

Then, using the Einstein's equation (31), we get:

$$R_{00} + \frac{A(r)}{B(r)}R_{11} + \frac{2A(r)}{r^2}R_{22} = 0, \tag{43}$$
$$R_{11} + \frac{B(r)}{A(r)}R_{00} - \frac{2B(r)}{r^2}R_{22} = 0 \Rightarrow \frac{A(r)}{B(r)}R_{11} + R_{00} - \frac{2A(r)}{r^2}R_{22} = 0. \tag{44}$$

Then, by adding equations (43) and (44) and employing the expressions (39)-(42), we get the equation:

$$2R_{00} + \frac{2A(r)}{B(r)}R_{11} = 0,$$
$$\Rightarrow \frac{A'(r)B'(r)}{4B^2(r)} + \frac{A'(r)A'(r)}{4A(r)B(r)} - \frac{A'(r)}{rB(r)} + \frac{A(r)}{B(r)}\left[-\frac{A'(r)A'(r)}{4A(r)A(r)} - \frac{A'(r)B'(r)}{4A(r)B(r)} - \frac{B'(r)}{rB(r)}\right] = 0,$$
$$\Rightarrow -\frac{A'(r)}{A(r)} = \frac{B'(r)}{B(r)}. \tag{45}$$

Also, demanding that $R_{22} = 0$, we obtain:

$$\frac{1}{B(r)} - 1 + \frac{r}{2B(r)}\frac{A'(r)}{A(r)} - \frac{r}{2B(r)}\frac{B'(r)}{B(r)} = 0. \tag{46}$$

After integrating the equation (45), we find the relation:

$$-lnA(r) + k = lnB(r) \Rightarrow A(r)B(r) = e^k \Rightarrow B(r) = \frac{\Lambda}{A(r)}, \tag{47}$$

with $e^k \equiv \Lambda$.

Now, substituting equation (47) into equation (46), we have:

$$\frac{A(r)}{\Lambda} - 1 + \frac{r}{\Lambda}A'(r) = 0 \Rightarrow rA'(r) + A(r) = \Lambda \Rightarrow \frac{d}{dr}(rA(r)) = \Lambda \Rightarrow A(r) = \Lambda\left(1 + \frac{C}{r}\right),$$

and then:

$$B(r) = \left(1 + \frac{C}{r}\right)^{-1}. \tag{48}$$

Therefore, $A(r)$ and $B(r)$, have the form:

$$A(r) = 1 + \frac{C}{r} \tag{49}$$

$$B(r) = \left(1 + \frac{C}{r}\right)^{-1}, \tag{50}$$

where C is a constant and Λ has been absorbed in the time coordinate.

To calculate the constant C, we apply Gauss's law:

$$\int g\, ds_2 = -4\pi GM, \tag{51}$$

where g is the intensity of the gravitational field and $ds_2 = r^2 sin\theta_1 d\theta_1 d\phi$.

Therefore equation (51) becomes:

$$gr^2 \int_0^{\pi} sin\theta_1\, d\theta_1 \int_0^{2\pi} d\phi = -4\pi GM \Rightarrow gr^2 4\pi = -4\pi GM \Rightarrow g = -\frac{GM}{r^2}. \tag{52}$$

In order, to find the potential and subsequently the constant C, we use the well-known relation $g = -\nabla\Phi$ and then:

$$\Phi = \int \frac{GM}{r^2} dr = -\frac{GM}{r}. \tag{53}$$

Taking as an approximation the limit of the weak gravitational field where $A(r) = -1 + 2\Phi$, we have:

$$2\Phi = \frac{C}{r} \Rightarrow \frac{-2GM}{r} = \frac{C}{r} \Rightarrow C = -2GM. \tag{54}$$

Thus, for equations (49) and (50), we have:

$$A(r) = 1 - \frac{2GM}{r} \equiv \left(1 - \frac{r_H}{r}\right), \tag{55}$$

$$B(r) = \left(1 - \frac{2GM}{r}\right)^{-1} \equiv \left(1 - \frac{r_H}{r}\right)^{-1}, \tag{56}$$

where $2GM$ is the Schwarzschild radius, $r_H = 2GM$, in 4-dimensions.

Thus, the metric takes the form:

$$ds^2 = -\left(1 - \frac{r_H}{r}\right) dt^2 + \left(1 - \frac{r_H}{r}\right)^{-1} dr^2 + r^2(d\theta_1^2 + sin^2\theta_1 d\phi),$$

and describes the outer region of a spherically symmetric gravitational object of mass M. This solution was named after the German physicist Karl Schwarzschild, who first derived it in 1916, just a few months after Einstein formulated his field equations.

It is important to comment on some features of this metric:

• At the radial coordinate $r = 2GM$, the term $1 - 2GM/r$ becomes zero, leading to a coordinate singularity. This is the event horizon, beyond which nothing can escape the gravitational pull of the black hole.

• The true physical singularity is at $r = 0$. As $r \to 0$, the curvature invariants become infinite and near $r = 0$, the tidal gravitational forces become infinitely strong, and no object can survive such conditions. The singularity at $r = 0$ is hidden behind the event horizon at $r = r_H$. This means that no information about the singularity can escape to an outside observer, preserving the cosmic censorship conjecture in classical General Relativity. So, any observer outside the black hole, i.e., at $r > r_H$, cannot detect or be affected by the singularity directly, due to the presence of the event horizon. As a consequence, the event horizon $r = r_H$ represents a one-way membrane. Any object or signal crossing this horizon from outside cannot return, effectively trapping all matter and information within. Furthermore, for an observer falling into the black hole, crossing $r = r_H$ would seem uneventful (locally), but they would inevitably reach the singularity at $r = 0$ in finite proper time. In summary, the real spacetime singularity at $r = 0$ is hidden inside the black hole's horizon and represents a region where classical General Relativity ceases to be valid, necessitating a theory of quantum gravity to fully understand its nature.

• The factor multiplying dt^2 in the metric shows that time flows differently at different distances from the black hole. Clocks near the black hole appear to run slower relative to distant observers, a phenomenon known as gravitational time dilation. According to the theory of General Relativity, this phenomenon is due to the gravity of the black hole curving spacetime in a way that affects all measurements of time and space near the black hole.

• The Schwarzschild solution describes a non-rotating, electrically neutral black hole. It does not account for the effects of angular momentum or electric charge.

The Schwarzschild solution serves as a cornerstone of black hole physics and provides the foundation for understanding many properties of black holes, including the event horizon, gravitational lensing, and the formation of singularities.

2.2 Theories with Extra Dimensions

The concept of dimensions has always fascinated both physicists and philosophers alike. While our everyday experience is confined to three spatial dimensions and one time dimension, theoretical physics has long entertained the possibility of additional spatial dimensions beyond the familiar three. These extra dimensions, though hidden from our direct perception, could fundamentally alter our understanding of the universe. But in how many dimensions does a black hole live? The number of spacelike dimensions in nature is a fundamental question that was first posed more than a century ago. Let us make a brief review of the most important models with extra dimensions.

Kaluza-Klein (KK) theory [18], one of the earliest attempts to unify gravity and electromagnetism, extends general relativity to five dimensions. Black holes in this framework, known as Kaluza-Klein black holes, can exhibit unique properties depending on the compactification of the extra dimension. These black holes can have interesting structures like ring-shaped horizons or black strings, which are extended in the fifth dimension. The stability and thermodynamic properties of these black holes depend on the nature of the compactification and the presence of additional fields. Kaluza-Klein theory can be extended to more than five dimensions, where black holes can have even more exotic horizon topologies and stability properties, influenced by the geometry of the extra dimensions [19], [20].

Also, string theory provides a framework where extra dimensions naturally arise. Typically, these models involve six or seven additional compactified dimensions. In particular, Calabi-Yau compactifications involve six additional spacelike dimensions, or three complex ones. In M theory, an eleventh spacelike dimension is assumed to be compactified on a circle. The properties of black holes in string theory are deeply tied to the underlying compactification geometry and the types of strings and branes present. D-branes, which are dynamical objects in string theory, can form black holes when multiple branes intersect and bind together. These configurations provide microscopic models of black holes that allow for the calculation of entropy and radiation properties, matching the predictions of Hawking radiation and the Bekenstein-Hawking entropy. String theory also predicts higher-dimensional black holes, such as those in ten or eleven dimensions. These higher-dimensional black holes can have unusual properties, such as non-spherical horizons and stability issues not present in four-dimensional black holes [21], [22].

Antoniadis [23] was the first to suggest that some extra dimension can be decompactified. Then, the ADD (Arkani-Hamed, Dimopoulos, Dvali) model [24], proposed in 1998, introduces large extra dimensions to address the hierarchy problem, specifically why gravity is much weaker compared to other fundamental forces. The central idea is that gravity propagates in all spatial dimensions, including the extra dimensions, while the Standard Model forces are confined to the usual four-dimensional spacetime. In the ADD model, extra dimensions are compactified, meaning they are curled up in such a way that they are not observable at low energies. The presence of these large extra dimensions modifies the gravitational potential at small distances, leading to deviations from the inverse-square law of gravity. At high energies, such as those achievable in particle colliders, black holes could form with much lower energy thresholds than traditionally expected [8]. These high-energy collisions would create microscopic black holes that decay quickly via Hawking radiation, emitting a burst of particles that could be detected experimentally.

Furthermore, the Randall-Sundrum (RS) models [25], proposed in 1999, offer another solution to the hierarchy problem by using a warped extra dimension. There are two main versions: RS1 and RS2. RS1 involves two branes: a visible (TeV) brane where our known universe resides, and a hidden (Planck) brane. The extra dimension is warped, meaning that the metric is not flat but exponentially decaying. This warping creates a significant energy difference between the two branes, naturally explaining the hierarchy between the weak force and gravity without requiring large extra dimensions. In the context of black holes, the RS1 model predicts that small black holes could form and be detected at TeV scales due to the localized gravity on the TeV brane. These black holes would have unique signatures due to the warped geometry, influencing their production and evaporation processes. RS2 eliminates the hidden brane and extends the extra dimension infinitely. This model suggests that while gravity propagates into the extra dimension, it remains localized near our four-dimensional universe due to the warping. The RS2 model implies the existence of black holes with horizons extending into the extra dimension, affecting their gravitational properties and Hawking radiation in observable ways [25].

Braneworld models, including ADD and RS models, predict that our universe is a 3-brane embedded in a higher-dimensional spacetime. Black holes in these models can exhibit behaviors significantly different from their four-dimensional counterparts. At scales near the extra dimension size, black holes could have extended ″black string″ or ″black cigar″ shapes. The localization of gravity on the brane means that black holes could have quasi-stable states where part of the horizon extends into the extra dimension. For black holes much larger than the extra dimension scale, they behave similarly to four-dimensional black holes, but with potential corrections from the higher-dimensional gravity. The evaporation and stability properties of these black holes are subjects of active research, particularly their potential detection via gravitational wave observatories [26], [27].

Finally, it is important to note that in this work, we will focus on the ADD model, where there exist analytical solutions for black holes. As a result, the extra dimensions employed in the next paragraph will all be flat (i.e., without curvature) and share the same size R. For the phenomenological constraints on the size R of the extra dimensions, from experiments (like Cavendish type) aimed at testing the form of gravitational interactions, no deviations from the usual Newtonian law have been found at distances up to the order of $52\mu m$. Therefore, if extra dimensions exist, they must be smaller than this scale. [28]

2.3 Schwarzschild solution in Higher-Dimensions

Higher-dimensional Schwarzschild black holes are theoretical objects described by solutions to Einstein's field equations in higher dimensions, extending beyond the standard four dimensions of spacetime. When considering higher dimensions, the mathematical analysis becomes more complex, but the concept and basic symmetries remain the same. In these scenarios, spacetime is assumed to have more than the usual three spatial dimensions and one time dimension. The Schwarzschild solution can be generalized to higher dimensions, resulting in black holes with different properties than those in four dimensions.

One key aspect of higher-dimensional Schwarzschild black holes is their event horizon, which is the boundary beyond which nothing, not even light, can escape the gravitational pull of the black hole. In higher dimensions, the structure of the event horizon and the properties of the black hole can vary significantly compared to four-dimensional cases.

Understanding higher-dimensional black holes is not only important for theoretical physics but also has implications for cosmology and the nature of spacetime at fundamental scales. However, it's worth noting that experimental evidence for the existence of higher-dimensional spacetime or higher-dimensional black holes remains elusive, and these concepts largely exist within the realm of theoretical physics and mathematical speculation.

We therefore model the metric of higher-dimensional black holes, according to the following relation:

$$ds^2 = -A(r)dt^2 + B(r)dr^2 + r^2 d\Omega^2_{2+n}, \tag{57}$$

where $d\Omega^2_{2+n} = d\theta^2_{n+1} + sin^2\theta_{n+1}(d\theta^2_n + sin^2\theta_n(... + sin^2\theta_2(d\theta^2_1 + sin^2\theta_1 d\phi^2)...))$.

Note that we consider the radius of the horizon to be much smaller than the size of the extra dimensions $r_H \ll R$. Furthermore, (57) is the general form of the spherically symmetric metric, where n stands for the number of extra, spacelike dimensions that exist in nature ($n' = 4+n$), and $d\Omega^2_{2+n}$ is the area of the $(2+n)$-dimensional unit sphere. As we expect, if in equation (57) we set $n = 0$, then we obtain the Schwarzschild metric in 4-dimensions.

The given metric (57), describes a spherically symmetric spacetime in a $(4+n)$-dimensional space, where n is the number of additional spatial dimensions beyond the usual four. Both metric functions A and B depend only on r and not on t. This implies that the spacetime is invariant under translations in time, $t \to t + constant$. This symmetry corresponds to the conservation of energy. The dependence of A and B only on r indicates spherical symmetry. The spacetime is thus invariant under rotations. Furthermore, the term $r^2 d\Omega^2_{2+n}$ describes the geometry of an $(n+2)$-dimensional sphere. This term is constructed from angular coordinates $\theta_1, \theta_2, \ldots, \theta_{n+1}, \phi$. The $d\Omega^2_{2+n}$ can be expanded as: $d\Omega^2_{2+n} = d\theta^2_{n+1} + sin^2\theta_{n+1}(d\theta^2_n + sin^2\theta_n(... + sin^2\theta_2(d\theta^2_1 + sin^2\theta_1 d\phi^2)...))$. This structure represents the metric on an $(n+2)$-dimensional sphere. The symmetries here are the rotational symmetries of the sphere, described by the group $SO(n+3)$. Each angular coordinate θ_i and ϕ describes rotations in a higher-dimensional generalization of spherical coordinates. These symmetries imply that the spacetime described by this metric is static (time-independent) and spherically symmetric in higher dimensions. This is a generalization of the Schwarzschild solution to higher dimensions, where the spatial part of the metric retains the spherical symmetry extended to higher-dimensional spheres. It is important at this point to mention that the shape of spacetime will change if the assumption of spherical symmetry changes.

At this point, we are interested in finding the form of the higher-dimensional metric - equation (57). In the same way as before, we can arrive at the following general relations for the Christoffel symbols and the Ricci tensor, respectively (detailed analyses for the cases where $n = 1$ and $n = 2$ are given in Appendix A):

$$\begin{aligned}
{\Gamma^0}_{01} = \frac{A'(r)}{2A(r)}, \quad {\Gamma^1}_{00} = \frac{A'(r)}{2B(r)}, \quad {\Gamma^1}_{11} = \frac{B'(r)}{2B(r)}, \quad {\Gamma^2}_{33} = {\Gamma^3}_{44} = ... = \Gamma^{N-1}_{NN} = -sin\theta_1\, cos\theta_1, \\
{\Gamma^4}_{43} = {\Gamma^5}_{53} = ... = \Gamma^N_{N3} = \frac{cos\theta_2}{sin\theta_2}, \quad {\Gamma^3}_{23} = {\Gamma^4}_{24} = {\Gamma^5}_{25} = ... = \Gamma^N_{2N} = \frac{cos\theta_1}{sin\theta_1}, \\
{\Gamma^2}_{21} = {\Gamma^3}_{31} = {\Gamma^4}_{41} = ... = \Gamma^{N-1}_{(N-1)1} = \frac{1}{r}, \quad {\Gamma^2}_{44} = {\Gamma^3}_{55} = ... = \Gamma^{N-2}_{NN} = -sin\theta_1\, cos\theta_1\, sin^2\theta_2, \\
{\Gamma^1}_{33} = -\frac{r}{B(r)}\, sin^2\theta_1, \quad {\Gamma^1}_{44} = -\frac{r}{B(r)}\, sin^2\theta_1\, sin^2\theta_2, \quad {\Gamma^1}_{55} = -\frac{r}{B(r)}\, sin^2\theta_1\, sin^2\theta_2\, sin^2\theta_3, \\
.., {\Gamma^1}_{NN} = -\frac{r}{B(r)}\, sin^2\theta_1\, sin^2\theta_2\, sin^2\theta_3 ... sin^2\theta_{N-2}, \quad {\Gamma^2}_{44} = -sin\theta_1\, cos\theta_1\, sin^2\theta_2, \\
{\Gamma^2}_{55} = -sin\theta_1\, cos\theta_1\, sin^2\theta_2\, sin^2\theta_3, \quad ..., \quad {\Gamma^2}_{NN} = -sin\theta_1\, cos\theta_1\, sin^2\theta_2\, sin^2\theta_3\, ...\, sin^2\theta_{N-2},
\end{aligned} \tag{58}$$

where $N = n' - 1$ and n' is the dimension of space ($n' = 4, 5, ..$), and:

$$R_{00} = -\frac{A''(r)}{2B(r)} + \frac{1}{4}\frac{A'(r)}{B(r)}\left[\frac{A'(r)}{A(r)} + \frac{B'(r)}{B(r)}\right] - \left(\frac{n'-2}{2}\right)\frac{A'(r)}{rB(r)}, \tag{59}$$

$$R_{11} = \frac{A''(r)}{2A(r)} - \frac{A'(r)}{4A(r)}\left[\frac{A'(r)}{A(r)} + \frac{B'(r)}{B(r)}\right] - \left(\frac{n'-2}{2}\right)\frac{B'(r)}{rB(r)}, \tag{60}$$

$$R_{22} = -n'' + \frac{n''}{B(r)} + \frac{r}{2B(r)}\left[\frac{A'(r)}{A(r)} - \frac{B'(r)}{B(r)}\right], \tag{61}$$

$$R_{33} = sin^2\theta_1 R_{22}, \tag{62}$$

$$R_{44} = sin^2\theta_1\, sin^2\theta_2 R_{22}, \tag{63}$$

$$R_{55} = sin^2\theta_1\, sin^2\theta_2\, sin^2\theta_3 R_{22}, \tag{64}$$

$$..., \tag{65}$$

$$R_{N'N'} = sin^2\theta_1\, sin^2\theta_2\, sin^2\theta_3 ... sin^2\theta_{N'-2} R_{22}, \tag{66}$$

where $n'' = n + 1 = 1, 2, 3, ...$ and N' is the last component of the Ricci tensor of the last calculated dimension.

Then, from the (00) and (11) components of the Einstein equations, we get:

$$\begin{aligned}
& R_{00} - \frac{1}{2}g_{00}\left(g^{00}R_{00} + g^{11}R_{11} + g^{22}R_{22} + g^{33}R_{33} + g^{44}R_{44} + ...\right) = 0 \\
& \Rightarrow R_{00} + \frac{1}{2}A(r)\left[-\frac{1}{A(r)}R_{00} + \frac{1}{B(r)}R_{11} + \frac{1}{r^2}R_{22} + \frac{1}{r^2 sin^2\theta_1}R_{33} + \frac{1}{r^2 sin^2\theta_1 sin^2\theta_2}R_{44} + ...\right] \\
& = 0 \Rightarrow \frac{1}{2}R_{00} + \frac{A(r)}{2B(r)}R_{11} + \frac{A(r)}{2r^2}R_{22} + \frac{A(r)}{2r^2 sin^2\theta_1}R_{33} + \frac{A(r)}{2r^2 sin^2\theta_1 sin^2\theta_2}R_{44} + ... = 0,
\end{aligned} \tag{67}$$

$$
\begin{aligned}
&R_{11} - \frac{1}{2} g_{11} \left(g^{00} R_{00} + g^{11} R_{11} + g^{22} R_{22} + g^{33} R_{33} + g^{44} R_{44} + ... \right) \\
&\Rightarrow R_{11} - \frac{1}{2} B(r) \left[-\frac{1}{A(r)} R_{00} + \frac{1}{B(r)} R_{11} + \frac{1}{r^2} R_{22} + \frac{1}{r^2 sin^2\theta_1} R_{33} + \frac{1}{r^2 sin^2\theta_1 sin^2\theta_2} R_{44} + ... \right] \\
&= 0 \Rightarrow \frac{1}{2} \frac{A(r)}{B(r)} R_{11} + \frac{1}{2} R_{00} - \frac{A(r)}{2r^2} R_{22} - \frac{A(r)}{2r^2 sin^2\theta_1} R_{33} - \frac{A(r)}{2r^2 sin^2\theta_1 sin^2\theta_2} R_{44} - ... = 0.
\end{aligned} \tag{68}
$$

By adding these equations - equation (67) and equation (68), we get the constraint:

$$
R_{00} + \frac{A(r)}{B(r)} R_{11} = 0. \tag{69}
$$

Substituting the components of the Ricci tensor, we have from equation (69):

$$
\begin{aligned}
&-\frac{A''(r)}{2B(r)} + \frac{1}{4} \frac{A'(r)}{B(r)} \left[\frac{A'(r)}{A(r)} + \frac{B'(r)}{B(r)} \right] - \left(\frac{n'-2}{2} \right) \frac{A'(r)}{rB(r)} + \frac{A(r)}{B(r)} \left[\frac{A''(r)}{2A(r)} \right. \\
&\left. - \frac{A'(r)}{4A(r)} \left(\frac{A'(r)}{A(r)} + \frac{B'(r)}{B(r)} \right) - \left(\frac{n'-2}{2} \right) \frac{B'(r)}{rB(r)} \right] = 0 \\
&\Rightarrow - \left(\frac{n'-2}{2} \right) \frac{1}{2r\, B(r)} \left(A'(r) + \frac{A(r)B'(r)}{B(r)} \right) = 0 \Rightarrow A'(r) + \frac{A(r)B'(r)}{B(r)} = 0 \\
&\Rightarrow \frac{A'(r)}{A(r)} = -\frac{B'(r)}{B(r)},
\end{aligned} \tag{70}
$$

and from the equation $R_{22} = 0$:

$$
-n'' + \frac{n''}{B(r)} + \frac{r}{2B(r)} \frac{A'(r)}{A(r)} - \frac{r}{2B(r)} \frac{B'(r)}{B(r)} = 0, \tag{71}
$$

where $n'' = n + 1 = 1, 2, 3, ...$

From equation (70) we get:

$$
-\frac{A'(r)}{A(r)} = \frac{B'(r)}{B(r)} \Rightarrow -ln[A(r)] + k = ln[B(r)] \Rightarrow A(r)B(r) = e^k \Rightarrow B(r) = \frac{\Lambda}{A(r)},
$$

where as before $e^k \equiv \Lambda$ and:

$$
B'(r) = \frac{-A'(r)\Lambda}{A^2(r)}. \tag{72}
$$

Then from (71) we can get:

$$
\begin{aligned}
-(n+1) + \frac{(n+1)}{\Lambda} A(r) + \frac{r}{\Lambda} A'(r) = 0 \Rightarrow -(n+1)\,\Lambda + (n+1)\, A(r) + r\, A'(r) = 0 \\
\Rightarrow \frac{d}{dr} \left(r^{n+1} A(r) \right) = (n+1)\, r^n \Lambda.
\end{aligned}
$$

By integrating , we find that $A(r)$ and $B(r)$ have the form:

$$
A(r) = \left(1 + \left(\frac{C}{r} \right)^{n+1} \right), \tag{73}
$$

$$B(r) = \left(1 + \left(\frac{C}{r}\right)^{n+1}\right)^{-1}, \tag{74}$$

where C is a constant.

To calculate the constant C, we apply Gauss law, as before:

$$\int g_* \, ds_{n+2} = -4\pi G_*^{(4+n)} M, \tag{75}$$

where g_* is the intensity of the gravitational field in the higher-dimensional spacetime and G_*^{4+n} the corresponding gravitational constant. Employing that $ds_{n+2} = r^{n+2} sin\theta_1 sin^2\theta_2 ... sin^n\theta_n d\theta_1 ... d\theta_n d\phi$, equation (75) becomes:

$$g_* \int ds = -4\pi G_*^{(4+n)} M \Rightarrow g_* \int r^{n+2} \prod_{i=1}^{n+1} sin^i\theta_i d\theta_i d\phi = -4\pi G_*^{(4+n)} M$$
$$\Rightarrow g_* r^{n+2} (2\pi) \prod_{i=1}^{n+1} \int sin^i\theta_i d\theta_i = -4\pi G_*^{(4+n)} M \Rightarrow g_* r^{n+2} \frac{\pi^{(n+1)/2}}{\Gamma\left(\dfrac{n+3}{2}\right)} = -2G_*^{(4+n)} M, \tag{76}$$

and finally:

$$g_* = \frac{-2G_*^{(4+n)} M}{r^{n+2} \pi^{(n+1)/2}} \Gamma\left(\frac{n+3}{2}\right), \tag{77}$$

where $G_*^{(4+n)} = \dfrac{1}{M_*^{n+2}}$ and M^* is the fundamental gravitational scale.

Therefore, to find the potential and subsequently the constant C, we use again the relation $g_* = -\nabla\Phi_* \rightarrow \Phi_* = -\int g_* dr$ and obtain:

$$\Phi_* = \frac{-2G_*^{(4+n)} M}{\pi^{(n+1)/2}} \frac{\Gamma\left(\dfrac{n+3}{2}\right)}{(n+1) r^{n+1}}. \tag{78}$$

Taking as an approximation the limit of the weak field and setting $2\Phi_* = \dfrac{r_H^{n+1}}{r^{n+1}}$, where $C = r_H^{n+1}$, we have:

$$r_H^{n+1} = \frac{4G_*^{(4+n)} M}{\pi^{n+1}} \frac{\Gamma\left(\dfrac{n+3}{2}\right)}{(n+1)} = \frac{4M}{M_*^{n+2} \pi^{(n+1)/2}} \frac{\Gamma\left(\dfrac{n+3}{2}\right)}{(n+1)}. \tag{79}$$

Then:

$$A(r) = \left(1 + \left(\frac{r_H}{r}\right)^{n+1}\right), \tag{80}$$

$$B(r) = \left(1 + \left(\frac{r_H}{r}\right)^{n+1}\right)^{-1}, \tag{81}$$

with the above definition, relation (79), of r_H^{n+1}.

The above form of metric describes the outer region of a spherically symmetric $(4+n)$-dimensional black hole of mass M. It is important to note that while in 4-dimensions the relation for the Schwarzschild radius r_H is linear with respect to M, in higher-dimensions, it is not. However, as can be seen from the metric of the higher-dimensions, in them we have greater spherical symmetry, compared to the 4-dimensions.

Some interesting features and implications of the higher-dimensional Schwarzschild solution include:

• Brane-world Scenarios: The Schwarzschild solution in higher dimensions is relevant for understanding how gravity behaves on branes (higher-dimensional analogs of membranes) embedded in higher-dimensional spacetimes.

• Cosmological Implications: Higher-dimensional solutions can have implications for cosmology, affecting our understanding of the early universe, inflation, and the large-scale structure of spacetime.

• Gravitational Collapse: Understanding gravitational collapse in higher dimensions is essential for predicting the final fate of massive stars and other astrophysical objects in scenarios where extra dimensions might play a role.

In summary, the Schwarzschild solution in higher dimensions offers a rich framework for exploring the gravitational dynamics and properties of spacetime in scenarios beyond the traditional four-dimensional Einstein gravity.

2.4 A scalar field in a curved background

In physics, a scalar field in a curved background refers to a situation where a scalar field, is defined in a spacetime with curvature. This typically arises in the context of general relativity, where spacetime is curved due to the presence of mass and energy. In general relativity, the curvature of spacetime is described by the metric tensor, which encapsulates information about distances and angles in the curved spacetime. When a scalar field is introduced into this curved spacetime, its behavior is influenced by the curvature of spacetime itself.

The dynamics of a scalar field in a curved background can be described by its field equation, which generalizes the usual scalar field equation to account for the curvature of spacetime. Studying scalar fields in curved spacetimes is important in various areas of theoretical physics, including cosmology (the study of the large-scale structure, inflation and evolution of the universe) and particle physics (the study of elementary particles and their interactions).

At this point, we will first derive the scalar field equation. We consider first the Lagrangian of a free scalar field:

$$L = \frac{1}{2} g^{\mu\nu} \partial_\mu \Phi \partial_\nu \Phi \tag{82}$$

and we compute the variation δL induced by a small variation $\delta\Phi$.

So, let's consider the variation $\Phi \to \Phi + \delta\Phi$. The corresponding variation of derivative, is given by $\partial_\mu \Phi \to \partial_\mu(\phi + \delta\Phi) = \partial_\mu \Phi + \partial_\mu(\delta\Phi)$ and then the corresponding variation in the Lagrangian density is given by:

$$L \to \frac{1}{2} g^{\mu\nu} (\partial_\mu \Phi + \partial_\mu(\delta\Phi))(\partial_\nu \Phi + \partial_\nu(\delta\Phi))$$

$$L \to \frac{1}{2} g^{\mu\nu} (\partial_\mu \Phi \partial_\nu \Phi + \partial_\mu \Phi \partial_\nu(\delta\Phi) + \partial_\mu(\delta\Phi)\partial_\nu \Phi + \partial_\mu(\delta\Phi)\partial_\nu(\delta\Phi))$$

$$L \to L + \frac{1}{2} g^{\mu\nu} (\partial_\mu \Phi \partial_\nu(\delta\Phi) + \partial_\mu(\delta\Phi)\partial_\nu \Phi + \partial_\mu(\delta\Phi)\partial_\nu(\delta\Phi))$$

and keeping only the 1st-order $\delta\Phi$ terms:

$$L + \delta L \simeq L + g^{\mu\nu} \partial_\mu \Phi \partial_\nu(\delta\Phi) \Rightarrow \delta L = g^{\mu\nu} \partial_\mu \Phi \partial_\nu(\delta\Phi).$$

The variation of the action $S = \int L\sqrt{-g}\, d^4x$ is then:

$$\delta S = \int \delta L \sqrt{-g}\, d^4x = \int [g^{\mu\nu} \partial_\mu \Phi \partial_\nu(\delta\Phi)] \sqrt{-g}\, d^4x = -\int [\partial_\nu(\sqrt{-g} g^{\mu\nu} \partial_\mu \Phi)] \delta\Phi\, d^4x$$
$$= -\int \frac{\sqrt{-g}}{\sqrt{-g}} [\partial_\nu(\sqrt{-g} g^{\mu\nu} \partial_\mu \Phi)] \delta\Phi\, d^4x,$$

where the boundary term becomes zero and we multiply and divide by $\sqrt{-g}$, to create the invariant volume element.

For the action to be stationary ($\delta S = 0$) for arbitrary $\delta\Phi$, the integrand must vanish:

$$\frac{1}{\sqrt{-g}} \partial_\nu(\sqrt{-g} g^{\mu\nu} \partial_\mu \Phi) = 0. \tag{83}$$

This is the Euler-Lagrange equation for the scalar field Φ derived from the given Lagrangian density (relation (82)).

The given equation - equation (83) - is a fundamental result in the study of scalar fields in curved spacetime, particularly in the context of general relativity and quantum field theory. It is therefore important to highlight some features of the equation:

- The equation is written in a covariant form, which means it is valid in an arbitrary coordinate system and in an arbitrary number of dimensions. This is essential in general relativity where spacetime curvature is described by the metric tensor, and coordinate transformations are allowed.

- The presence of the $\sqrt{-g}$ factor ensures that the equation is invariant under general coordinate transformations. This means that the physics described by this equation remains unchanged even if we choose different coordinate systems to describe spacetime.

- In the context of quantum field theory, this equation governs the behavior of scalar fields, such as the Higgs field, in curved spacetime.

- The equation has significant implications for cosmology and the study of black holes, where spacetime curvature is prominent. Understanding how scalar fields behave in such curved spacetime environments is essential for theoretical predictions and observational tests.

Overall, the equation represents a deep connection between the geometry of spacetime described by general relativity and the dynamics of scalar fields described by quantum field theory. Its solutions provide valuable insights into the nature of spacetime and the fundamental forces of the universe. As we will see, this equation is used to study Hawking radiation.

3 Hawking Radiation from Higher-Dimensional Black Holes

3.1 Hawking radiation

In 1975 Hawking [7] published a shocking result: if one takes quantum theory into account, it seems that black holes are not quite black! Instead, they should ″glow″ by emitting *Hawking radiation*, consisting of photons, neutrinos, and to a lesser extent all sorts of massive particles. This has never been observed, since the only black holes we have evidence for are those with lots of hot gas falling into them, whose radiation would completely swamp this tiny effect. Indeed, if the mass of a black hole is M solar masses, Hawking predicted it should glow like a blackbody of temperature $6 \times 10^{-8}/MKelvin$, so only for very small black holes would this radiation be significant. The most drastic consequence is that a black hole, left alone and unfed, should radiate away its mass, slowly at first but then faster and faster as it shrinks, finally dying in a blaze of glory like a hydrogen bomb.

But, how does this work? Virtual particle pairs are constantly being created near the horizon of the black hole, as they are everywhere. Normally, they are created as a particle-antiparticle pair and they quickly annihilate each other. But near the horizon of a black hole, it's possible for one to fall in before the annihilation can happen, in which case the other one escapes as Hawking radiation.

In more detail, this procedure is as follows:

• According to quantum field theory, empty space isn't really empty. Pairs of virtual particles and antiparticles continuously pop in and out.

• When this process occurs near the event horizon of a black hole, one of the particles (the antiparticle) may fall into the black hole while the other escapes.

• The particle that escapes is asymptotically detected as Hawking radiation. This process leads to a gradual loss of mass and energy by the black hole over time.

• The probability of a particle escaping or being absorbed by the black hole depends on various factors, including the black hole's mass and properties, as well as the energy of the emitted particles.

In particular, studying the absorption probability involves complex calculations and theories, often utilizing quantum field theory in curved spacetime. It's a crucial aspect of understanding the dynamics of black holes and the universe at large.

Although it has never been directly observed, Hawking radiation is a prediction supported by combined models of general relativity and quantum mechanics. If shown to be factual, Hawking radiation would mean black holes can emit energy and therefore shrink in size, with the tiniest of these insanely dense objects exploding rapidly in a puff of heat (and the largest slowly evaporating over trillions of years in a cold breeze).

3.2 Scalar emission in the Bulk

As explained in Chapter 2, in this thesis we will focus on the ADD model [24] which predicts an arbitrary number of compact, flat, spacelike dimensions. In what follows, the word bulk will refer to the higher-dimensional space in which our observable universe, or brane, may be embedded. In theories like string theory and braneworld scenarios, the universe we perceive is a brane within this higher-dimensional bulk. The bulk contains additional dimensions beyond the familiar three spatial dimensions and one time dimension. These extra dimensions are compactified or curled up at very small scales, making them effectively unobservable in everyday life. However, they can have profound effects on the behavior of matter and energy at very high energies or small scales [8].

The equation (83) is the Klein-Gordon equation in curved spacetime, describing the dynamics of a scalar field Φ. This equation is crucial in the study of quantum field theory in curved spacetime, particularly in the context of black hole physics. Hawking radiation, the theoretical prediction that black holes emit radiation due to quantum effects near the event horizon, is derived by applying quantum field theory to the curved spacetime of a black hole. Solving the Klein-Gordon equation in this context helps to understand how particle-antiparticle pairs propagate near the event horizon, leading to the emission of Hawking radiation. To solve equation (83), we will consider the separated ansatz solution.

The separated ansatz solution, is a common approach in solving partial differential equations (PDEs) that exhibit some form of spherical symmetry. More specific, this solution employs a technique called separation of variables. This technique assumes that the solution to the PDE can be written as a product of functions, each depending on only one of the variables involved (in this case, time, radial coordinate, and angular coordinates). Thus, we write:

$$\Phi(t, r, \theta_i, \phi) = e^{-i\omega t} R_{\omega l}(r)\, \tilde{Y}_l(\Omega), \tag{84}$$

where $\tilde{Y}_l(\Omega)$ is the $(3+n)$ spatial dimensional generalization of the usual spherical harmonic functions depending on the angular coordinates. Furthermore, the term $e^{-i\omega t}$ represents the time dependence of the solution. The exponential factor introduces oscillations with frequency ω, which can have significant physical implications depending on the system being studied. Moreover, the function $R_{\omega l}$ captures the radial dependence of the solution and the function $\tilde{Y}_l(\Omega)$ represents the angular dependence of the solution. In three-dimensional space, $\tilde{Y}_l(\Omega)$ reduces to the usual spherical harmonics $Y_l^m(\theta, \phi)$, which are solutions to the angular part of Laplace's equation. In higher-dimensional spaces ($3+n$ dimensions in this case), more general functions are needed to describe the angular dependence.

So, at this point, we are interested in deriving the radial equation for the scalar field. To do this, we employ the metric of equation (57), the scalar field equation (83) and the ansatz solution (84). We start from the case of 4-dimensions where we have:

$$g^{\mu\nu}_{(d=4)} = \begin{pmatrix} -1/h(r) & 0 & 0 & 0 \\ 0 & h(r) & 0 & 0 \\ 0 & 0 & 1/r^2 & 0 \\ 0 & 0 & 0 & 1/(r^2 sin^2\theta_1) \end{pmatrix} \tag{85}$$

and from which we easily calculate that $g = -r^4 sin^2\theta_1 \Rightarrow \sqrt{-g} = r^2 sin\theta_1$. Furthermore, $-1/h(r)$ and $h(r)$ are the coefficients in front of the dt^2 and dr^2 elements, of the metric.

Then, from equation (83), we have:

$$-\partial_t\left(\frac{1}{h(r)}\partial_t\Phi\right) + \frac{1}{r^2}\partial_r\left(r^2 h(r)\partial_r\Phi\right) + \frac{1}{r^2 sin\theta_1}\partial_{\theta_1}\left(sin\theta_1\partial_{\theta_1}\Phi\right) + \frac{1}{r^2 sin^2\theta_1}\partial^2_\phi\Phi = 0 \tag{86}$$

and thus assuming the general solution of the form (84), we obtain for equation (86):

$$\begin{aligned} &-\frac{1}{h(r)}\partial_t\left(\partial_t e^{-i\omega t}YR\right) + \frac{1}{r^2}\partial_r\left[r^2 h(r)\partial_r\left(e^{-i\omega t}YR\right)\right] \\ &+\frac{1}{sin\theta_1}\partial_{\theta_1}\left[\frac{1}{r^2}sin\theta_1\partial_{\theta_1}\left(e^{-i\omega t}YR\right)\right] + \frac{1}{r^2 sin^2\theta_1}\partial^2_\phi\left(e^{-i\omega t}YR\right) = 0. \end{aligned} \tag{87}$$

Multiplying this equation by $(r^2 e^{-i\omega t})/(RY)$, we obtain the relation:

$$\frac{1}{R}\frac{d}{dr}\left(r^2 h(r)\frac{dR}{dr}\right) = -\frac{\omega^2 r^2}{h(r)} - \frac{1}{Y}\frac{1}{sin\theta_1}\frac{d}{d\theta_1}\left(sin\theta_1\frac{d}{d\theta_1}Y\right) - \frac{1}{Y}\frac{1}{sin^2\theta_1}\frac{d^2Y}{d\phi^2}, \tag{88}$$

where

$$\frac{1}{sin^2\theta_1}\frac{d^2Y}{d\phi^2} + \frac{1}{sin\theta_1}\frac{d}{d\theta_1}\left(sin\theta_1\frac{d}{d\theta_1}Y\right) = -l(l+1)Y, \tag{89}$$

with l the angular momentum number.

Therefore, the radial equation takes the form:

$$\left[\omega^2 - \frac{h(r)}{r^2}l(l+1)\right]R + \frac{h(r)}{r^2}\frac{d}{dr}\left(h(r)\,r^2\frac{dR}{dr}\right) = 0. \tag{90}$$

Continuing this process inductively, in an arbitary number of dimensions, we can finally arrive at the following general form for the radial equation (the details for the case of 5 and 6 dimensions are given in the Appendix B):

$$\frac{h(r)}{r^{n+2}}\frac{d}{dr}\left[h(r)\,r^{n+2}\frac{dR}{dr}\right] + \left[\omega^2 - \frac{h(r)}{r^2}l(l+n+1)\right]R = 0. \tag{91}$$

In order to understand the physical implications of this equation, we can transform it to a more convenient form by defining a new ″tortoise″ radial coordinate by [29]:

$$\frac{dr_*}{dr} = \frac{1}{h(r)}. \tag{92}$$

Defining also a new radial function through the relation $R(r) = u(r)/r^{(n+2)/2}$, the scalar field equation in the bulk (91) becomes:

$$h'(r)\,r^{-(n+2)/2}\frac{du(r)}{dr_*}+h^2(r)\,r^{-(n+2)/2}\left[-\frac{h'(r)}{h^2(r)}\frac{du(r)}{dr_*}+\frac{1}{h^2(r)}\frac{d^2u(r)}{dr_*^2}\right]$$
$$-h(r)\,h'(r)\,\frac{(n+2)}{2}r^{-(n+4)/2}\,u(r)-\frac{h^2(r)}{4}n\,(n+2)\,u(r)\,r^{-(n+6)/2}$$
$$+\left[\omega^2-\frac{h(r)}{r^2}l(l+n+1)\right]\frac{u(r)}{r^{(n+2)/2}}=0,$$

or in Schrödinger-like form:

$$-\frac{d^2u(r)}{dr_*^2}+h(r)\left[\frac{l(l+n+1)}{r^2}+\frac{(n+2)\,h'(r)}{2r}+\frac{n\,(n+2)\,h(r)}{4r^2}\right]u=\omega^2u. \qquad (93)$$

From the above equation, we may easily read the gravitational potential $V(r)$ that a scalar particle, feels while propagating in the bulk. The potential $V(r)$ is therefore given by the relation:

$$V(r)=h(r)\left[\frac{l(l+n+1)}{r^2}+\frac{(n+2)\,h'(r)}{2r}+\frac{n\,(n+2)\,h(r)}{4r^2}\right], \qquad (94)$$

where $h(r)=1-\left(\frac{r_H}{r}\right)^{n+1}$ and $h'(r)=\frac{(n+1)}{r}[1-h(r)]$. Substituting these into equation (94) and considering $r_H=1$ [1], we obtain the graphs shown in Figure 1. Regarding the results shown in Figure 1, it is evident that the graphs take the form of a potential barrier, which prevents the scalar field from entirely escaping to infinity. As a result, the absorption (or transmission) coefficient will not be equal to 1. Additionally, from Figure 1, it is apparent that for a fixed l (n), the larger the n (l), is the higher the potential barrier $V(r)$ is. Additionally, from the two graphs in Figure 1, a symmetry between n and l is observed (as the graph with fixed n and varying l has exactly the same behavior and takes the same values as the graph with fixed l and varying n), which could be further investigated in future work.

Now, we need to solve equation (91) and use the solution to determine the absorption coefficient and the greybody factor. Due to its complexity, we will solve equation (91) in the $near-horizon$ and in the $far-field$ regimes. Then, these two solutions must smoothly connect at an intermediate zone for a viable complete solution to exist.

First, in the case of the $near-horizon$, we do the variable change $r\rightarrow h(r)$, where:

$$h(r)=1-\left(\frac{r_H}{r}\right)^{n+1}\Rightarrow\frac{dh(r)}{dr}=\frac{n+1}{r}(1-h(r)) \qquad (95)$$

and we get for (91):

[1] In this way, we essentially normalize the length scale in order to create indicative graphs: we require the horizon to be at 1, and r represents a multiple of the horizon. For example, if we create a graph up to $r=100$, this means we are examining the specific function up to a distance one hundred times that of the horizon. In this way, it is as if we are conducting the analysis for any black hole, which may have a random mass and therefore a different horizon.

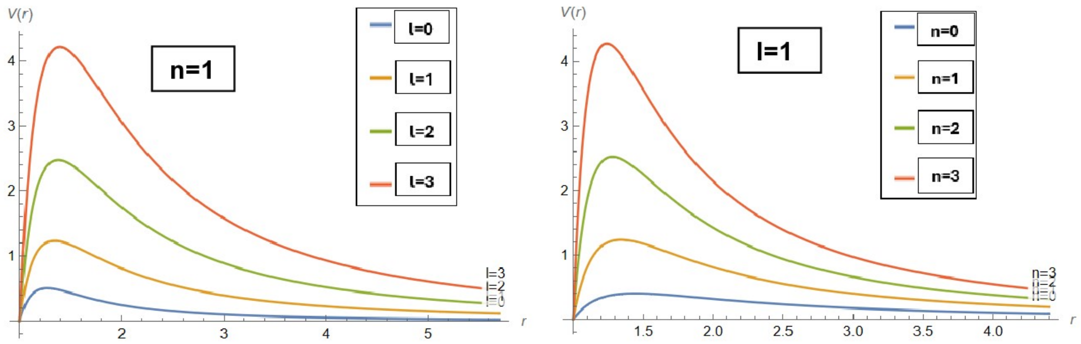

Figure 1: The gravitational potential $V(r)$ in scalar emission in the Bulk, where the left-hand side shows its behaviour for a constant n ($n=1$) and varying l, and the right-hand side shows its behaviour for a constant l ($l=1$) and varying n.

$$\frac{h(r)}{r^{n+2}}\frac{d}{dr}\left[h(r)\,r^{n+1}\frac{dR}{dh}(n+1)(1-h)\right]+\left[\omega^2-\frac{h(r)}{r^2}l(l+n+1)\right]R=0\Rightarrow$$
$$\frac{h^2(r)}{r^2}(n+1)^2(1-h)^2\frac{d^2R}{dh^2}+\frac{h(r)}{r^2}(n+1)^2(1-h)^2\frac{dR}{dh}+\left[\omega^2-\frac{h(r)}{r^2}l(l+n+1)\right]R=0, \tag{96}$$

where finally:

$$h(1-h)\frac{d^2R}{dh^2}+(1-h)\frac{dR}{dh}+\left[\frac{(\omega r_H)^2}{(n+1)^2(1-h)h}-\frac{l(l+n+1)}{(n+1)^2(1-h)}\right]R=0, \tag{97}$$

is the $near-horizon$ form of the radial equation. Next, we redefine $R(h)$, $R(h)=h^{\alpha}(1-h)^{\beta}F(h)$ and obtain:

$$\begin{aligned}
&h(1-h)\,\alpha\,(\alpha-1)\,h^{\alpha-2}(1-h)^{\beta}F(h)-h(1-h)\,\alpha\,h^{\alpha-1}\beta\,(1-h)^{\beta-1}F(h)\\
&+h(1-h)\,\alpha\,h^{\alpha-1}(1-h)^{\beta}\frac{dF(h)}{dh}-h(1-h)\,\alpha\,h^{\alpha-1}(1-h)^{\beta-1}\,\beta\,F(h)\\
&+h(1-h)\,h^{\alpha}(\beta-1)(1-h)^{\beta-2}\,\beta\,F(h)-h(1-h)\,h^{\alpha}(1-h)^{\beta-1}\,\beta\frac{dF(h)}{dh}\\
&+h(1-h)\,\alpha\,h^{\alpha-1}(1-h)^{\beta}\frac{dF(h)}{dh}-h(1-h)\,\beta\,h^{\alpha}(1-h)^{\beta-1}\frac{dF(h)}{dh}\\
&+h(1-h)\,h^{\alpha}(1-h)^{\beta}\frac{d^2F(h)}{dh^2}+(1-h)\Big[\alpha\,h^{\alpha-1}(1-h)^{\beta}F(h)-h^{\alpha}(1-h)^{\beta-1}\beta\,F(h)\\
&+\,h^{\alpha}(1-h)^{\beta}\frac{dF(h)}{dh}\Big]+\left[\frac{(\omega r_H)^2}{(n+1)^2\,h\,(1-h)}-\frac{l(l+n+1)}{(n+1)^2(1-h)}\right]h^{\alpha}(1-h)^{\beta}F(h)=0.
\end{aligned}$$

After several operations, we obtain the relation:

$$\begin{aligned}
h(1-h)\frac{d^2F(h)}{dh^2}&+\Big[2\alpha(1-h)-2h\beta+1-h\Big]\frac{dF(h)}{dh}-(2\alpha\beta+\beta+\alpha^2)F(h)\\
&+\left[\frac{\alpha^2}{h}-\beta(\beta-1)+\frac{\beta}{1-h}(\beta-1)+\frac{(\omega r_H)^2}{(n+1)^2h}+\frac{(\omega r_H)^2}{(n+1)^2(1-h)}\right.\\
&\left.-\frac{l(l+n+1)}{(n+1)^2(1-h)}\right]F(h)=0.
\end{aligned} \tag{98}$$

The above differential equation hints to the form of a hypergeometric equation which is given by [30]:

$$h(1-h)\frac{d^2F(h)}{dh^2} + [c-(1+a+b)h]\,\frac{dF(h)}{dh} - abF(h) = 0. \tag{99}$$

For a perfect match with the above, the terms $1/h$ and $1/(1-h)$ in relation (98) must be set to zero. Therefore:

$$\frac{\alpha^2}{h} + \frac{(\omega r_H)^2}{(n+1)^2 h} = 0 \Rightarrow \alpha^2 = -\frac{(\omega r_H)^2}{(n+1)^2} \Rightarrow \alpha_\pm = \pm\frac{i\omega r_H}{n+1}, \tag{100}$$

$$\frac{\beta}{1-h}(\beta-1) + \frac{(\omega r_H)^2}{(n+1)^2(1-h)} - \frac{l(l+n+1)}{(n+1)^2(1-h)} = 0 \Rightarrow \beta^2 - \beta + \frac{(\omega r_H)^2}{(n+1)^2} - \frac{l(l+n+1)}{(n+1)^2} = 0. \tag{101}$$

From equation (101), we get the solutions:

$$\beta_\pm = \frac{1}{2} \pm \frac{1}{n+1}\sqrt{\left(l+\frac{n+1}{2}\right)^2 - (\omega r_H)^2}. \tag{102}$$

Therefore, we have:

$$h(1-h)\frac{d^2F(h)}{dh^2} + \Big[2\alpha(1-h) - 2\beta h + 1 - h\Big]\frac{dF(h)}{dh} - \left[2\alpha\beta + \alpha^2 + \beta^2\right] F(h) = 0.$$

By defining the constants:

$$a = b = \alpha + \beta, \tag{103}$$

$$c = 1 + 2\alpha, \tag{104}$$

the above equation takes the exact form of the hypergeometric equation (99) with the constants given by the relations (101), (102), (103) and (104).

Equation (99) admits many pairs of partial solutions, which may expressed in different forms. We choose the pair of solutions [30]:

$$W_{1(0)} = F(a,b,c;h) = (1-h)^{c-a-b}\,F(c-a,c-b,c;h) \tag{105}$$

$$W_{2(0)} = h^{1-c}\,F(a-c+1,b-c+1,2-c;h) = h^{1-c}(1-h)^{c-a-b}F(1-a,1-b,2-c;h) \tag{106}$$

and thus we obtain the general solution for (99):

$$R_{NH}(h) = A_-\,h^{\alpha_\pm}(1-h)^{\beta}F(a,b,c;h) + A_+\,h^{-\alpha_\pm}(1-h)^{\beta}F(a-c+1,b-c+1,2-c;h). \tag{107}$$

Let us investigate a bit more carefully the behaviour of this solution close to the horizon. Choosing the solution $\alpha = \alpha_-$ where $\alpha_- = -\frac{i\omega r_H}{n+1}$, we can obtain the following form, for (107):

$$R_{NH}(h) = A_- e^{-i\omega r_H ln(h)/(n+1)}(1-h)^{\beta}F(a,b,c;h)$$

$$+A_+ e^{i\omega r_H ln(h)/(n+1)}(1-h)^\beta F(a-c+1, b-c+1, 2-c; h), \tag{108}$$

where we may write

$$h^{-i\omega r_H/(n+1)} \to e^{-i\omega r_H ln(h)/(n+1)}, \tag{109}$$

$$h^{i\omega r_H/(n+1)} \to e^{i\omega r_H ln(h)/(n+1)}. \tag{110}$$

Additionally, from the fact that $h \to 0$, we have $(1-h) \to 1$. Also, using the property of the hypergeometric function that $F(a, b, c; h \to 0) \to 1$ and $F(a-c+1, b-c+1, 2-c, h \to 0) \to 1$, we have:

$$R_{NH}(h) = A_- e^{-i\omega r_H ln(h)/(n+1)} + A_+ e^{i\omega r_H ln(h)/(n+1)}. \tag{111}$$

We employ the *tortoise* coordinate, defined as:

$$y = \frac{ln[h(r)]}{r_H^{n+1}(n+1)}, \tag{112}$$

with $h(r) = 1 - \left(\frac{r_H}{r}\right)^{n+1}$ and we obtain the general solution *near the black hole horizon*:

$$R_{NH}(h) \simeq A_- e^{-i\omega r_H^{n+2} y} + A_+ e^{i\omega r_H^{n+2} y}. \tag{113}$$

If we had chosen the solution $\alpha = \alpha_+$, then we would have gotten the same form of solution, with the only difference being that the coefficients A_+ and A_- would be interchanged. Having chosen the solution $\alpha = \alpha_-$, we now require $A_+ = 0$, since at the horizon of the black hole we can have only incoming waves and no outgoing ones, according to classical General Relativity.

We now turn to the $far-field\ zone$, where we may show that the limit $r \gg r_H$ and the redefinition $R(r) = \frac{f(r)}{r^{(n+1)/2}}$ reduce equation (91) to a Bessel differential equation of the form:

$$\frac{d^2 f}{dr^2} + \frac{1}{r}\frac{df}{dr} + \left[\omega^2 - \frac{1}{r^2}\left(l + \frac{n+1}{2}\right)^2\right] f = 0. \tag{114}$$

We start from equation (91) setting $h(r) = 1$. Then, we get:

$$\begin{aligned}
&\frac{1}{r^{n+2}}\left[(n+2)\, r^{n+1}\frac{dR}{dr} + r^{n+2}\frac{d^2R}{dr^2}\right] + \left[\omega^2 - \frac{l(l+n+1)}{r^2}\right] R = 0 \\
&\Rightarrow f'(r)\,(n+2)\, r^{(n+1)/2} - \frac{(n+1)(n+2)}{2} f(r)\, r^{(n-1)/2} + f''(r)\, r^{(n+3)/2} \\
&- f(r)\frac{(n+1)(n-1)}{4} r^{(n-1)/2} - (n+1) f'(r)\, r^{(n+1)/2} + \frac{(n+1)^2}{2} f(r)\, r^{(n-1)/2} \\
&+ \left[\omega^2 - \frac{1}{r^2} l(l+n+1)\right] f(r) r^{(n+3)/2} = 0 \Rightarrow f''(r) + \frac{1}{r} f'(r) - \frac{(n+1)^2}{4r^2} f(r) \\
&+ \left[\omega^2 - \frac{l(l+n+1)}{r^2}\right] f(r) = 0 \\
&\Rightarrow \frac{d^2 f(r)}{dr^2} + \frac{1}{r}\frac{df(r)}{dr} + \left[\omega^2 - \frac{1}{r^2}\left(l + \frac{n+1}{2}\right)^2\right] f(r) = 0.
\end{aligned}$$

The general solution for the radial function $R(r)$ is then given by:

$$R_{FF}(r) = \frac{B_+}{r^{(n+1)/2}} J_{l+(n+1)/2}(\omega r) + \frac{B_-}{r^{(n+1)/2}} Y_{l+(n+1)/2}(\omega r), \tag{115}$$

where J and Y are the Bessel functions of the first and second kinds, respectively.

Therefore, we have found solutions in two different regions, one far from the black hole's horizon and one *near*. Now, through these two solutions, we must find the complete solution that will describe the scalar field over the entire radial regime. What we need to do is to *stretch* the *near solution* towards large values of r and take the small r limit of the far *solution*. To construct a complete solution, we need to match these two asymptotic solutions in an intermediate region.

To this end, we first shift the hypergeometric function to large values of r. This can be done using a standard linear transformation formula [30]:

$$F(a,b,c;h) = \frac{\Gamma(c)\,\Gamma(c-a-b)}{\Gamma(c-a)\,\Gamma(c-b)} F(a,b,a+b-c+1;1-h)$$
$$+(1-h)^{c-a-b}\frac{\Gamma(c)\,\Gamma(a+b-c)}{\Gamma(a)\,\Gamma(b)} F(c-a,c-b,c-a-b+1;1-h). \tag{116}$$

Near the horizon, we can have only one wave propagating, as nothing can escape from the black hole (and its horizon), and therefore:

$$R_{NH}(h) \simeq A_- h^\alpha (1-h)^\beta F(a,b,c;h), \tag{117}$$

with $A_+ = 0$ and we choose $\beta = \beta_-$ and $\alpha = \alpha_-$. So, from equation (117), we have:

$$\begin{aligned}
R_{NH}(h) &\simeq A_- h^\alpha (1-h)^\beta F(a,b,c;h) \\
&= A_- h^a (1-h)^\beta \frac{\Gamma(c)\,\Gamma(c-a-b)}{\Gamma(c-a)\,\Gamma(c-b)} F(a,b,a+b-c+1;1-h) \\
&+ A_- h^\alpha (1-h)^\beta (1-h)^{c-a-b}\frac{\Gamma(c)\,\Gamma(a+b-c)}{\Gamma(a)\,\Gamma(b)} F(c-a,c-b,c-a-b+1;1-h) \\
&= A_- h^\alpha (1-h)^\beta \frac{\Gamma(1+2\alpha)\,\Gamma(1-2\beta)}{\Gamma(1+\alpha-\beta)\,\Gamma(1+\alpha-\beta)} F(a,b,a+b-c+1;1-h) \\
&+ A_- h^\alpha (1-h)^\beta (1-h)^{1-2\beta}\frac{\Gamma(1+2\alpha)\Gamma(2\beta-1)}{\Gamma(\alpha+\beta)\,\Gamma(\alpha+\beta)} F(c-a,c-b,c-a-b+1;1-h) \\
&= A_- \left[1-\left(\frac{r_H}{r}\right)^{n+1}\right]^\alpha \left[\left(\frac{r_H}{r}\right)^{n+1}\right]^\beta \frac{\Gamma(1+\alpha+\beta)\,\Gamma(2-\alpha-\beta)}{\Gamma(1+\alpha-\beta)\,\Gamma(1+\alpha-\beta)} \\
&F\left(a,b,a+b-c+1;\left(\frac{r_H}{r}\right)^{n+1}\right) \\
&+ A_- \left[1-\left(\frac{r_H}{r}\right)^{n+1}\right]^\alpha \left[\left(\frac{r_H}{r}\right)^{n+1}\right]^{1-\beta} \frac{\Gamma(1+\alpha+\beta)\,\Gamma(\alpha+\beta-1)}{\Gamma(\alpha+\beta)\,\Gamma(\alpha+\beta)} \\
&F\left(c-a,c-b,c-a-b+1;\left(\frac{r_H}{r}\right)^{n+1}\right),
\end{aligned}$$

and as $h \to 1$, we have $\left(\frac{r_H}{r}\right)^{n+1} \to 0$, and thus:

$$F(a,b,a+b-c+1;0) \to 1, \tag{118}$$

$$F(c-a, c-b, c-a-b+1; 0) \to 1. \tag{119}$$

Then, we have:

$$\begin{aligned}
R_{NH}(h) &= A_- \left[1 - \left(\frac{r_H}{r}\right)^{n+1}\right]^\alpha \left[\left(\frac{r_H}{r}\right)^{n+1}\right]^\beta \frac{\Gamma(1+\alpha+\beta)\,\Gamma(1-\alpha-\beta)}{\Gamma(1+\alpha-\beta)^2} \\
&+ A_- \left[1 - \left(\frac{r_H}{r}\right)^{n+1}\right]^\alpha \left[\left(\frac{r_H}{r}\right)^{n+1}\right]^{1-\beta} \frac{\Gamma(1+\alpha+\beta)\,\Gamma(\alpha+\beta-1)}{\Gamma(\alpha+\beta)^2} \\
&= A_- \left[1 - \left(\frac{r_H}{r}\right)^{n+1}\right]^\alpha \left[\left(\frac{r_H}{r}\right)^{n+1}\right]^\beta \\
&\left[\frac{\Gamma(1+2\alpha)\,\Gamma(1-2\beta)}{\Gamma(1+\alpha-\beta)^2} + \left[\left(\frac{r_H}{r}\right)^{n+1}\right]^{1-2\beta} \frac{\Gamma(1+2\alpha)\,\Gamma(2\beta-1)}{\Gamma(1+\alpha-\beta)^2}\right] \\
&\simeq A_-\Gamma(1+2\alpha)\left[\left(\frac{r}{r_H}\right)^l \frac{\Gamma(1-2\beta)}{\Gamma(1+\alpha-\beta)^2} + \left(\frac{r_H}{r}\right)^{l+n+1} \frac{\Gamma(2\beta-1)}{\Gamma(\alpha+\beta)^2}\right]
\end{aligned} \tag{120}$$

and as before, we chose $\alpha = \alpha_-$ and $\beta = \beta_-$, with $\beta_- \simeq \frac{1}{2} - \frac{1}{n+1}\left(l + \frac{n+1}{2}\right) = -\frac{l}{n+1}$ as $\omega r_H \to 0$. The approximation $\omega r_H \to 0$ corresponds to considering the low-energy (or equivalently, the long-wavelength) limit of the scalar modes. In this regime, the wavelength of the scalar field is much larger than the size of the black hole horizon. This simplification is useful because it allows for a more tractable analytical treatment of the scalar field. Furthermore, since $r \gg r_H$, then $\left(\frac{r_H}{r}\right) \to 0$, and thus $\left[1 - \left(\frac{r_H}{r}\right)^{n+1}\right]^\alpha \to 1$. Also:

$$\begin{aligned}
\left[\left(\frac{r_H}{r}\right)^{n+1}\right]^{\beta_-} &= \left[\left(\frac{r_H}{r}\right)^{n+1}\right]^{-l/(n+1)} = \left(\frac{r}{r_H}\right)^l \\
\left[\left(\frac{r_H}{r}\right)^{n+1}\right]^{1-\beta_-} &= \left[\left(\frac{r_H}{r}\right)^{n+1}\right]^{1-l/(n+1)} = \left(\frac{r_H}{r}\right)^{n+1+l}
\end{aligned} \tag{121}$$

and therefore, the solution *near the black hole horizon*, which we have *stretched* towards large r, is:

$$R_{NH}(h) \simeq A_-\Gamma(1+2\alpha)\left[\left(\frac{r}{r_H}\right)^l \frac{\Gamma(1-2\beta)}{\Gamma(1+\alpha-\beta)^2} + \left(\frac{r_H}{r}\right)^{l+n+1} \frac{\Gamma(2\beta-1)}{\Gamma(\alpha+\beta)^2}\right]. \tag{122}$$

Now, concerning the process of approaching *small distances starting from the large ones* and the process of *pulling the far solution inwards*, we will again consider in equation (115) that $\omega r_H \ll 1$. From the first and second kind order Bessel equations, we will have for equation (115):

$$R_{FF}(r) = \frac{B_+}{r^{(n+1)/2}} \frac{1}{\Gamma\left(l + \frac{n+3}{2}\right)} \left(\frac{\omega r}{2}\right)^{l+(n+1)/2} - \frac{B_-}{\pi\, r^{(n+1)/2}}\Gamma\left(l + \frac{n+1}{2}\right)\left(\frac{\omega r}{2}\right)^{-l-(n+1)/2}$$

$$\Rightarrow R_{FF}(r) = \frac{B_+ r^l}{\Gamma\left(l + \frac{n+3}{2}\right)}\left(\frac{\omega}{2}\right)^{l+(n+1)/2} - \frac{B_-}{\pi\, r^{n+1+l}}\left(\frac{2}{\omega}\right)^{l+(n+1)/2}\Gamma\left(l + \frac{n+1}{2}\right)$$

$$\Rightarrow R_{FF}(r) = \frac{B_+ r^l}{\Gamma(l+\dfrac{n+3}{2})}\left(\frac{\omega}{2}\right)^{l+(n+1)/2} - \frac{B_-}{\pi\, r^{l+n+1}}\left(\frac{2}{\omega}\right)^{l+(n+1)/2}\Gamma\left(l+\frac{n+1}{2}\right). \quad (123)$$

So, matching the two solutions (122) and (123), we obtain a relation between the two integration constants at infinity and the one at the horizon:

$$A_- \frac{\Gamma(1+2\alpha)}{r_H^l}\frac{\Gamma(1-2\beta)}{\Gamma(1+\alpha-\beta)^2} = \frac{B_+}{\Gamma(l+\dfrac{n+3}{2})}\left(\frac{\omega}{2}\right)^{l+(n+1)/2} \quad (124)$$

$$A_-\Gamma(1+2\alpha)\, r_H^{l+n+1}\frac{\Gamma(2\beta-1)}{\Gamma(\alpha+\beta)^2} = -\frac{B_-}{\pi}\left(\frac{2}{\omega}\right)^{l+(n+1)/2}\Gamma\left(l+\frac{n+1}{2}\right), \quad (125)$$

or alternatively:

$$B_+ = \frac{A_-}{r_H^l}\frac{\Gamma(1+2\alpha)\,\Gamma(1-2\beta)\,\Gamma\left(l+\dfrac{n+3}{2}\right)}{\Gamma(1+\alpha-\beta)^2}\left(\frac{2}{\omega}\right)^{l+(n+1)/2} \quad (126)$$

$$B_- = -A_-\pi\, r_H^{l+n+1}\frac{\Gamma(1+2\alpha)\,\Gamma(2\beta-1)}{\Gamma(\alpha+\beta)^2\,\Gamma\left(l+\dfrac{n+1}{2}\right)}\left(\frac{\omega}{2}\right)^{l+(n+1)/2}. \quad (127)$$

Dividing the two relations, we get:

$$\begin{aligned}\frac{B_+}{B_-} &= -\frac{\Gamma(1-2\beta)\,\Gamma\left(l+\dfrac{n+3}{2}\right)\Gamma(\alpha+\beta)^2\,\Gamma\left(l+\dfrac{n+1}{2}\right)\left(\dfrac{2}{\omega}\right)^{l+(n+1)/2}}{\pi\, r_H^{2l+n+1}\,\Gamma(1+\alpha-\beta)^2\,\Gamma(2\beta-1)\left(\dfrac{\omega}{2}\right)^{l+(n+1)/2}} \\ \Rightarrow \frac{B_+}{B_-} &= -\left(\frac{2}{\omega r_H}\right)^{2l+n+1}\frac{\Gamma(1-2\beta)\,\Gamma(\alpha+\beta)^2\,\Gamma\left(l+\dfrac{n+1}{2}\right)^2\left(l+\dfrac{n+1}{2}\right)}{\pi\,\Gamma(1+\alpha-\beta)^2\,\Gamma(2\beta-1)}.\end{aligned} \quad (128)$$

Under the above constraint, the near-horizon and far-field solutions are smoothy matched in the low-energy limit, thus completing the derivation of the solution for the scalar field over the whole radial regime. After having completed the determination of the solution for the radial function $R(r)$ and in order to compute the absorption coefficient, we turn our attention to the form of the scalar field at infinity. We need to determine the amplitudes of the incoming and outgoing modes, thus, we expand equation (115) in the limit $r\to\infty$, and we find:

$$\begin{aligned}R^{(\infty)} = &\frac{B_+}{r^{(n+1)/2}}\frac{e^{-i\omega r}}{\sqrt{2\pi\omega r}}e^{i[(n+1)\pi/4+l\pi/2+\pi/4]} + \frac{B_+}{r^{(n+1)/2}}\frac{e^{i\omega r}}{\sqrt{2\pi\omega r}}e^{-i[(n+1)\pi/4+l\pi/2+\pi/4]} \\ &- \frac{i\,B_-}{r^{(n+1)/2}}\frac{e^{i\omega r}}{\sqrt{2\pi\omega r}}e^{-i[(n+1)\pi/4+l\pi/2+\pi/4]} + \frac{i\,B_-}{r^{(n+1)/2}}\frac{e^{-i\omega r}}{\sqrt{2\pi\omega r}}e^{i[(n+1)\pi/4+l\pi/2+\pi/4]},\end{aligned} \quad (129)$$

or

$$R^{(\infty)} = A_{in}^{(\infty)}\frac{e^{-i\omega r}}{\sqrt{r^{n+2}}} + A_{out}^{(\infty)}\frac{e^{i\omega r}}{\sqrt{r^{n+2}}}, \quad (130)$$

where:

$$A_{in}^{(\infty)} = \frac{(B_+ + iB_-)}{\sqrt{2\pi\omega}} e^{i\pi(l+n/2+1)/2} \tag{131}$$

$$A_{out}^{(\infty)} = \frac{(B_+ - iB_-)}{\sqrt{2\pi\omega}} e^{-i\pi(l+n/2+1)/2}. \tag{132}$$

The reflection coefficient R_l is defined as the ratio of the outgoing amplitude over the incoming one at infinity. Then, the absorption coefficient A_l is given by:

$$\begin{aligned} |A_l|^2 = 1 - |R_l|^2 = 1 - \left| \frac{(B_+ - iB_-)e^{-i\pi(l+n/2+1)/2}e^{i\omega r}}{(B_+ + iB_-)e^{i\pi(l+n/2+1)/2}e^{-i\omega r}} \right|^2 = 1 - \left| \frac{B_+ - iB_-}{B_+ + iB_-} \right|^2 \\ \Rightarrow |A_l|^2 = 1 - \left[\frac{(B_+ - iB_-)(B_+^* + iB_-^*)}{(B_+ + iB_-)(B_+^* - iB_-^*)} \right] = \frac{2i(B^* - B)}{BB^* + i(B^* - B) + 1}, \end{aligned} \tag{133}$$

where $B \equiv B_+/B_-$ is defined in equation (127).

The above analytic result can take a simplified form in the low-energy limit $\omega r_H \ll 1$, in which case $BB^* \gg i(B^* - B) \gg 1$, and we may write:

$$|A_l|^2 = \frac{4\pi^2}{2^{4l/(n+1)}} \left(\frac{\omega r_H}{2}\right)^{2l+n+2} \frac{\Gamma\left(1 + \frac{l}{n+1}\right)^2}{\Gamma\left(\frac{1}{2} + \frac{l}{n+1}\right)^2 \Gamma\left(l + \frac{n+3}{2}\right)^2} + ... \tag{134}$$

The Greybody factor, or the absorption cross-section, $\sigma_{l,n}(\omega)$, is given by the expression [8]:

$$\sigma_{l,n}(\omega) = \frac{2^n}{\pi} \Gamma\left(\frac{n+3}{2}\right)^2 \frac{A_H}{(\omega r_H)^{n+2}} N_l |A_l|^2, \tag{135}$$

where N_l is the multiplicity of states corresponding to the same partial wave l, given for a $(4+n)$-dimensional space-time by:

$$N_l = \frac{(2l+n+1)(l+n)!}{l!(n+1)!} \tag{136}$$

and A_H is the horizon area of the $(4+n)$-dimensional black hole defined as:

$$\begin{aligned} A_H = r_H^{n+2} \int_0^{2\pi} d\phi \prod_{k=1}^{n+1} \int_0^{\pi} sin^k\theta_{k+1} d\theta_{k+1} = r_H^{n+2}(2\pi) \prod_{k=1}^{n+1} \sqrt{\pi} \frac{\Gamma[(k+1)/2]}{\Gamma[(k+2)/2]} \\ \to A_H = r_H^{n+2}(2\pi)\pi^{(n+1)/2} \Gamma\left(\frac{n+3}{2}\right)^{-1}. \end{aligned} \tag{137}$$

Substituting the relation (134) into the equation (135), we arrive at the expression:

$$\sigma_{l,n}(\omega) = \frac{\pi}{2^{4l/(n+1)}} \left(\frac{\omega r_H}{2}\right)^{2l} \frac{\Gamma\left(1 + \frac{l}{n+1}\right)^2 \Gamma\left(\frac{n+3}{2}\right)^2}{\Gamma\left(\frac{1}{2} + \frac{l}{n+1}\right)^2 \Gamma\left(l + \frac{n+3}{2}\right)^2} N_l A_H + ... \tag{138}$$

Since $\omega r_H \ll 1$, the greybody factor decreases as l increases, therefore, the main contribution to $\sum_l \sigma_{l,n}$ comes from the lowest partial wave with $l = 0$. It is easy to see that the above expression evaluated for $l = 0$ simply reduces to A_H, thus, revealing the fact that even in the higher-dimensional case, the greybody factor for scalar fields at the low-energy regime is given by the area of the horizon. This behaviour is similar to the one obtained in the four-dimensional case; here, however, the area of the horizon changes as n varies.

As in the four-dimensional case, the contribution to the greybody factor from the dominant partial wave comes out to be independent of the number of extra dimensions. Looking at the dependence of the higher partial waves on n, we obtain a suppression of the greybody factor as the dimensionality of the bulk increases. However, in order to be absolutely certain about this behaviour we would have to include next-to-leading-order corrections in the simplified expression of $\sigma_{l,n}(\omega)$ - (138), or simply deal with the full analytic result derived from equation (133). In either case, however, the derived dependence would only hold in the low-energy regime and no information could be derived from these expressions for the dependence of the greybody factor, and thus of the emission rates, in the high-energy regime [8].

3.3 Scalar emission on the brane

In string theory and related theories in theoretical physics, a brane (short for membrane) is a spatially extended mathematical object that generalizes the notion of a point particle to higher dimensions. Branes can have various dimensions, such as zero-dimensional (point particles), one-dimensional (strings), two-dimensional (surfaces or membranes), and higher-dimensional versions. Branes can be thought of as the boundaries or surfaces within a higher-dimensional space, which can host particles, strings, or even entire universes. The brane is what we see and perceive as 4-dimensional observers.

So, we now turn to the study of the case where the scalar field is confined in a $(4+n)$-dimensional Schwarzschild spacetime. The scalar field propagates in a four-dimensional background whose metric tensor is given by the induced metric at the location of the brane. The induced metric follows from the $(4 + n)$-dimensional one by fixing the values of the extra angular coordinates: $\theta_n = \pi/2$ for $n \geq 2$, and it may be written as:

$$ds^2 = -h(r)dt^2 + h(r)^{-1}dr^2 + r^2(d\theta^2 + sin^2\theta d\phi^2), \tag{139}$$

where $h(r) = 1 - \left(\frac{r_H}{r}\right)^{n+1}$.

The scalar field equation may be separated in the same way as before. Then, the ansatz solution (relation (84)), allows us to write the equation for the radial part as:

$$\frac{h(r)}{r^2}\frac{d}{dr}\left[h(r)\,r^2\frac{dR}{dr}\right] + \left[\omega^2 - \frac{h(r)}{r^2\,l(l+1)}\right]R = 0. \tag{140}$$

By using the definition $R(r) = u(r)/r$, and the same tortoise coordinate defined in equation (92), the scalar field equation in the brane (140), takes the Schrodinger-like form [28]:

$$
\begin{aligned}
&h'(r)\frac{r}{h(r)}\frac{du(r)}{dr_*} + h(r)\,r\left(-\frac{h'(r)}{h^2(r)}\frac{du(r)}{dr_*} + \frac{1}{h^2(r)}\frac{d^2u(r)}{dr_*^2}\right) - h'(r)\,u(r)\\
&+\left[\frac{\omega^2 r^2}{h(r)} - l(l+1)\right]\frac{u(r)}{r} = 0\\
&\Rightarrow \frac{-d^2u(r)}{dr_*^2} + h(r)\left[\frac{l(l+1)}{r^2} + \frac{h'(r)}{r}\right]u(r) = \omega^2 u(r),
\end{aligned}
$$

where the potential $V(r)$ is given by the relation:

$$
V(r) = \left(\frac{l(l+1)}{r^2} + \frac{h'(r)}{r}\right) h(r), \tag{141}
$$

where $h(r) = 1 - \left(\frac{r_H}{r}\right)^{n+1}$ and $h'(r) = \frac{(n+1)}{r}[1 - h(r)]$. Substituting these into equation (141) and considering $r_H = 1$ (as before), we obtain the graphs shown in Figure 2. Regarding the results shown in Figure 2, it is evident that the graphs take the form of a potential barrier, which prevents the scalar field from entirely escaping to infinity. As a result, the absorption (or transmission) coefficient will not be 1. Additionally, from Figure 2, it is apparent that for a fixed l (n), the larger the n (l), is the higher the potential barrier $V(r)$ is. However, we observe that while in the case of the Bulk (Figure 1), the two graphs of $V(r)$ for different n and fixed l, as well as for different l and fixed n, exhibit almost identical behavior and the same $V(r)$ value at the peak, this is not the case for the Brane channel (Figure 2). Specifically, from Figure 2, it is apparent that for a fixed n and varying l, the larger l is, the higher is the peak value of $V(r)$ on the figure, compared to the case of a fixed l and varying n. For example, when $n = 1$ and $l = 3$, the potential $V(r)$ has a peak at approximately $V(r) \simeq 3.5$, whereas for $l = 1$ and $n = 3$, the potential peaks at approximately $V(r) \simeq 1.5$. Finally, it is important to comment on the fact that the potential for propagation in the Bulk and on the Brane are not the same (as shown in Figures 1 and 2). Specifically, in the case of the Bulk (for both fixed l and varying n, as well as fixed n and varying l), the potential $V(r)$ has higher values compared to the Brane case, for the same values of n and l. As observed, the difference is more pronounced for a fixed l and varying n, where in the Bulk case the potential $V(r)$ takes on significantly larger values compared to the Brane case. Consequently, the absorption coefficient is expected to be higher in the Brane channel.

The presence of the metric function $h(r)$ makes once again the derivation of the general solution extremely difficult (in equation (140)). We will follow the same method as in the previous section and compute the solution in the two radial domains, $near - horizon$ and $far - field$.

We start with the solution in the $near - horizon$ (NH) region. Initially, we make the

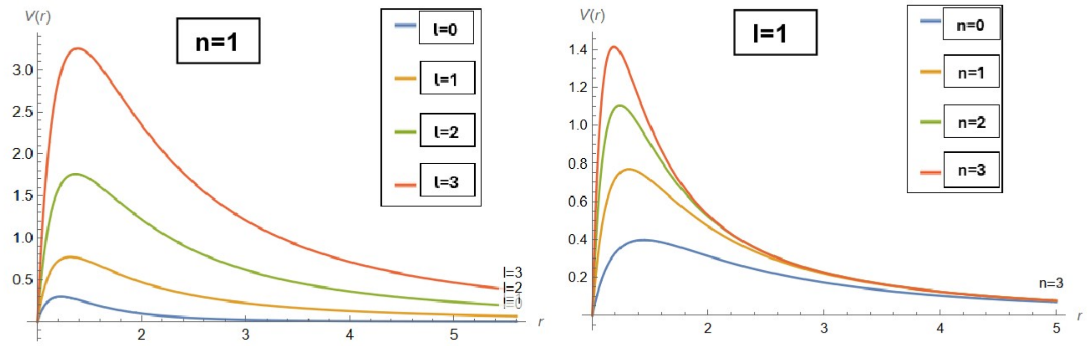

Figure 2: The gravitational potential $V(r)$ in scalar emission on the Brane, where the left-hand side shows its behaviour for a constant n ($n = 1$) and varying l, and the right-hand side shows its behaviour for a constant l ($l = 1$) and varying n.

variable change $r \to h(r)$ where $h(r) = 1 - \left(\frac{r_H}{r}\right)^{n+1}$ and $\frac{dh}{dr} = \frac{(n+1)}{r}(1-h)$, thus:

$$\frac{h(r)}{r^2}\frac{d}{dr}\left[h(r)r\frac{dR}{dh}(n+1)(1-h)\right] + \left[\omega^2 - \frac{h(r)}{r^2}l(l+1)\right]R = 0$$
$$\Rightarrow h(1-h)\frac{d^2R}{dh^2}\left[\frac{h}{r^2}(n+1)^2 - \frac{h^2}{r^2}(n+1)^2\right] + \left[\omega^2 - \frac{h}{r^2}l(l+1)\right]R$$
$$+\frac{h}{r^2}(n+1)\left[(n+1)(1-h) + h - 2h(n+1)(1-h) - h^2)\right]\frac{dR}{dh} = 0.$$

Then, we multiply by $\frac{r^2}{h(1-h)(n+1)^2}$, and thus:

$$h(1-h)\frac{d^2R}{dh^2} + \frac{dR}{dh}\left(1 - 2h + \frac{h}{(n+1)}\right)\frac{r^2}{h}\frac{1}{(n+1)^2(1-h)}\left[\omega^2 - \frac{h}{r^2}l(l+1)\right]R = 0, \tag{142}$$

obtaining finally the equation:

$$h(1-h)\frac{d^2R}{dh^2} + \left[1 - \frac{(2n+1)h}{(n+1)}\right]\frac{dR}{dh} + \left[\frac{(\omega r_H)^2}{h(1-h)(n+1)^2} - \frac{l(l+1)}{(n+1)^2(1-h)}\right]R = 0. \tag{143}$$

Then, we redefine, as before, $R(h)$, $R(h) = h^\alpha(1-h)^\beta F(h)$ and obtain the equation:

$$h^{\alpha+1}(1-h)^{\beta+1}\frac{d^2F(h)}{dh^2} + \left[2\alpha h^\alpha(1-h)^{\beta+1} - \alpha h^{\alpha+1}\beta(1-h)^\beta + h^\alpha(1-h)^\beta\right.$$
$$\left.-\frac{(2n+1)}{(n+1)}h^{\alpha+1}(1-h)^\beta\right]\frac{dF(h)}{dh} + \left[\alpha(\alpha-1)h^{\alpha-1}(1-h)^{\beta+1} - 2\alpha\beta h^\alpha(1-h)^\beta\right.$$
$$\left.+h^\alpha\beta(\beta-1)(1-h)^{\beta-1} + \alpha h^{\alpha-1}(1-h)^\beta\right]F(h) + \left[-h^\alpha\beta(1-h)^{\beta-1}\right.$$
$$\left.-\frac{(2n+1)}{(n+1)}\alpha h^\alpha(1-h)^\beta + \frac{(2n+1)}{(n+1)}h^{\alpha+1}\beta(1-h)^{\beta-1}\right]F(h)$$
$$+\left[\frac{(\omega r_H)^2}{h(1-h)(n+1)^2} - \frac{l(l+1)}{(n+1)^2(1-h)}\right]h^\alpha(1-h)^\beta F(h) = 0.$$

If we divide by $h^\alpha(1-h)^\beta$, we get:

$$
\begin{aligned}
&h(1-h)\frac{d^2F(h)}{dh^2}+\left[2\alpha(1-h)-2h\beta+1-\frac{(2n+1)}{(n+1)}h\right]\frac{dF(h)}{dh}\\
&+[\alpha(\alpha-1)\frac{(1-h)}{h}-2\alpha\beta+\frac{h}{(1-h)}\beta(\beta-1)+\frac{\alpha}{h}-\frac{\beta}{1-h}-\frac{(2n+1)}{(n+1)}\alpha\\
&+\frac{(2n+1)}{(n+1)}\beta\frac{h}{1-h}]F(h)+\left[\frac{(\omega r_H)^2}{h(1-h)(n+1)^2}-\frac{l(l+1)}{(1-h)(n+1)^2}\right]F(h)=0.
\end{aligned}
$$

The term in the form of $\frac{h}{1-h}$ can be written as $-\left[\frac{(1-h)-1}{(1-h)}\right]=-1+\frac{1}{1-h}$. Furthermore, for the term $\frac{1}{h}\frac{1}{1-h}$, from the previous analysis, we have that it is equal to $\left(\frac{1}{h}+\frac{1}{1-h}\right)$. Putting everything together, we obtain:

$$
\begin{aligned}
h(1-h)\frac{d^2F(h)}{dh^2}+\left[2\alpha(1-h)-2\beta h+1-\frac{2n+1}{n+1}h\right]\frac{dF(h)}{dh}+\left[\frac{\alpha^2}{h}-\alpha^2+\alpha-2\alpha\beta\right]F(h)\\
+\left[-\beta(\beta-1)+\beta\frac{\beta-1}{1-h}-\frac{\beta}{1-h}-\frac{2n+1}{n+1}\alpha-\frac{2n+1}{n+1}\beta+\frac{2n+1}{n+1}\frac{\beta}{1-h}\right]F(h)\\
+\left[\frac{(\omega r_H)^2}{(n+1)^2}\left(\frac{1}{h}-\frac{1}{1-h}\right)-\frac{l(l+1)}{(n+1)^2}\frac{1}{1-h}\right]F(h)=0.
\end{aligned}
$$

As in the previous analysis, the terms of the form $\frac{1}{h}$ and $\frac{1}{1-h}$ should vanish in order to obtain a hypergeometric equation. Thus, we obtain the equation:

$$
\begin{aligned}
h(1-h)\frac{d^2F(h)}{dh^2}+\left[2\alpha(1-h)-2\beta h+1-\frac{2n+1}{n+1}h\right]\frac{dF(h)}{dh}\\
+\left[-\alpha^2+\alpha-2\alpha\beta-\beta(\beta-1)\right]F(h)+\left[-\frac{2n+1}{n+1}\alpha-\frac{2n+1}{n+1}\beta\right]F(h)=0,
\end{aligned}
\tag{144}
$$

with:

$$
\alpha^2+\frac{(\omega r_H)^2}{(n+1)^2}=0\rightarrow\alpha_\pm=\pm i\frac{\omega r_H}{n+1},
\tag{145}
$$

$$
\begin{aligned}
&\beta(\beta-1)-\beta+\frac{2n+1}{n+1}\beta+\frac{(\omega r_H)^2}{(n+1)^2}-\frac{l(l+1)}{(n+1)^2}=0\\
\Rightarrow&\beta_\pm=\frac{1}{2(n+1)}\left[1\pm\sqrt{(2l+1)^2-4(\omega r_H)^2}\right].
\end{aligned}
\tag{146}
$$

Then, from equation (144) we have:

$$
h(1-h)\frac{d^2F(h)}{dh^2}+\left[c-(1+a+b)\,h\right]\frac{dF(h)}{dh}-abF(h)=0,
\tag{147}
$$

where $a=\alpha+\beta+\frac{n}{n+1}$, $b=\alpha+\beta$ and $c=1+2\alpha$.

We choose again the pair of solutions [30]:

$$W_{1(0)} = F(a,b,c;h) = (1-h)^{c-a-b}F(c-a,c-b,c;h), \tag{148}$$

$$W_{2(0)} = h^{1-c}F(a-c+1,b-c+1,2-c;h) = h^{1-c}(1-h)^{c-a-b}F(1-a,1-b,2-c;h). \tag{149}$$

As before this choice will be convenient because near the horizon where $h \to 0$ (since $r \to r_H$), the hypergeometric function goes to unity, $F(a,b,c;h \to 0) \to 1$.

Choosing the solution $\alpha = \alpha_-$ where $\alpha_- = -\dfrac{i\omega r_H}{n+1}$ and from the fact that $F(a,b,c;h \to 0) \to 1$ very near the horizon, we can obtain the approximated form:

$$\begin{aligned} R_{NH}(h) &= A_- h^{\alpha_-}(1-h)^{\beta_-}F(a,b,c;0) + A_+ h^{-\alpha_-}(1-h)^{\beta_-}F(a-c+1,b-c+1,2-c;0) \\ &= A_- e^{-i\omega\, r_H ln(h)/(n+1)} + A_+ e^{i\omega\, r_H ln(h)/(n+1)}, \end{aligned} \tag{150}$$

where:

$$h^{-i\omega r_H/(n+1)} \to e^{-i\omega r_H ln(h)/(n+1)}, \tag{151}$$

$$h^{i\omega r_H/(n+1)} \to e^{i\omega r_H ln(h)/(n+1)}. \tag{152}$$

We employ again the *tortoise* coordinate and we take the equation:

$$R_{NH}(h) \simeq A_- e^{-i\omega\, r_H^{n+2} y}, \tag{153}$$

where $A_+ = 0$ as before, because near the horizon, we can have only one wave propagating towards the black hole, as nothing can escape from the black hole (and its horizon).

As before, trying to stretch the $near-horizon$ solution, we will use the relation:

$$\begin{aligned} &R_{NH}(h) \simeq A_- h^{\alpha}(1-h)^{\beta}F(a,b,c;h) = A_- h^{\alpha}(1-h)^{\beta}\frac{\Gamma(c)\,\Gamma(c-a-b)}{\Gamma(c-a)\,\Gamma(c-b)} \\ &F(a,b,a+b-c+1;1-h) + A_- h^{\alpha}(1-h)^{\beta}(1-h)^{c-a-b}\frac{\Gamma(c)\,\Gamma(a+b-c)}{\Gamma(a)\,\Gamma(b)} \\ &F(c-a,c-b,c-a-b+1;1-h). \end{aligned} \tag{154}$$

In the limit $r \gg r_H$ or $h \to 1$ and from the fact that as $h \to 0$ we have $F(a,b,c;h \to 0) \to 1$ and $F(a-c+1,b-c+1,2-c,h \to 0) \to 1$ and then, we get:

$$R_{NH}(h) = A_- h^{\alpha}(1-h)^{\beta}\frac{\Gamma(c)\,\Gamma(c-a-b)}{\Gamma(c-a)\,\Gamma(c-b)} + A_- h^{\alpha}(1-h)^{\beta}(1-h)^{c-a-b}\frac{\Gamma(c)\,\Gamma(a+b-c)}{\Gamma(a)\,\Gamma(b)}. \tag{155}$$

Furthermore, we know that $a = \alpha + \beta + \dfrac{n}{n+1}$, $b = \alpha + \beta$ and $c = 1 + 2\alpha$.

As we said, we choose $\alpha = \alpha_-$ and $\beta = \beta_-$, with $\beta_- \simeq \dfrac{1}{2} - \dfrac{1}{n+1}\left(l + \dfrac{n+1}{2}\right) = -\dfrac{l}{n+1}$ as $\omega r_H \to 0$. Then, we take:

$$R_{NH}(h) = A_-(1-h)^{\beta}\frac{\Gamma(1+2\alpha)\,\Gamma\!\left(1-2\beta-\dfrac{n}{n+1}\right)}{\Gamma\!\left(1+a-\beta-\dfrac{n}{n+1}\right)\Gamma(1+\alpha-\beta)}$$

$$+A_{-}(1-h)^{\beta}(1-h)^{1-2\beta-n/(n+1)}\frac{\Gamma(a+2\alpha)\,\Gamma\left(2\beta-1+\dfrac{n}{n+1}\right)}{\Gamma\left(\alpha+\beta+\dfrac{n}{n+1}\right)\Gamma(\alpha+\beta)}.$$

So, the solution *near the black hole horizon*, which we have *stretched* towards large r, is:

$$\begin{aligned}R_{NH}(h) &\simeq A_{-}\Gamma(1+2\alpha)\left(\frac{r}{r_H}\right)^{l}\frac{\Gamma\left(1-2\beta-\dfrac{n}{n+1}\right)}{\Gamma\left(1+\alpha-\beta-\dfrac{n}{n+1}\right)\Gamma(1+\alpha-\beta)}\\ &+A_{-}\Gamma(1+2\alpha)\left(\frac{r_H}{r}\right)^{l+1}\frac{\Gamma\left(2\beta-1+\dfrac{n}{n+1}\right)}{\Gamma\left(\alpha+\beta+\dfrac{n}{n+1}\right)\Gamma(\alpha+\beta)}.\end{aligned} \tag{156}$$

The $far-field$ solution can easily be found working in the limit $r \gg r_H$ and has the form:

$$R_{FF}(r)=\frac{B_{+}}{r^{1/2}}J_{l+1/2}(\omega r)+\frac{B_{-}}{r^{1/2}}Y_{l+1/2}(\omega r), \tag{157}$$

which can also be derived from relation (116), if we set $n=0$. As before, we will assume again that $\omega r_H \ll 1$. Then, from the first and second order Bessel equations, we will have for equation (157):

$$R_{FF}(r)=\frac{B_{+}r^{l}}{\Gamma(l+3/2)}\left(\frac{\omega}{2}\right)^{l+1/2}-\frac{B_{-}}{\pi\, r^{l+1}}\left(\frac{2}{\omega}\right)^{l+1/2}\Gamma(l+1/2). \tag{158}$$

So, matching the two solutions (156) and (158), we obtain a relation between the two integration constants at infinity and then, dividing the two solutions, we get:

$$\frac{B_{+}}{B_{-}}=-\left(\frac{2}{\omega\, r_H}\right)^{2l+1}\frac{\Gamma\left(l+\dfrac{1}{2}\right)^{2}\left(l+\dfrac{1}{2}\right)\Gamma\left(1-2\beta-\dfrac{n}{n+1}\right)\Gamma(\alpha+\beta)\,\Gamma\left(\alpha+\beta+\dfrac{n}{n+1}\right)}{\pi\,\Gamma(1+\alpha-\beta)\,\Gamma\left(1+\alpha-\beta-\dfrac{n}{n+1}\right)\Gamma\left(2\beta-1+\dfrac{n}{n+1}\right)}. \tag{159}$$

Again, the above constraint completes the derivation of the analytic solution for the scalar field on the brane. As before, we next turn our attention to the form of the scalar field at infinity. We need to determine the amplitudes of the incoming and outgoing modes, thus, we expand equation (157) in the limit $r\to\infty$, and we find:

$$R^{(\infty)}=A_{in}^{(\infty)}\frac{e^{-i\omega r}}{r}+A_{out}^{(\infty)}\frac{e^{i\omega r}}{r}, \tag{160}$$

with

$$A_{in}^{(\infty)}=\frac{(B_{+}+iB_{-})}{\sqrt{2\pi\omega}}e^{i\pi(l+1)/2}, \tag{161}$$

$$A_{out}^{(\infty)} = \frac{(B_+ - iB_-)}{\sqrt{2\pi\omega}} e^{-i\pi(l+1)/2}. \tag{162}$$

In addition, we already know that the reflection coefficient R_l is defined as the ratio of the outgoing amplitude over the incoming one at infinity. Then, the absorption coefficient A_l is given by:

$$|A_l|^2 = \frac{2i(B^* - B)}{BB^* + i(B^* - B) + 1}, \tag{163}$$

where $B \equiv B_+/B_-$ which is defined in equation (158).

The above analytic result can take a simplified form in the low-energy limit $\omega r_H \ll 1$, in which case we have:

$$|A_l|^2 = \frac{16\pi}{(n+1)^2} \left(\frac{\omega r_H}{2}\right)^{2l+2} \frac{\Gamma\left(\frac{l+1}{n+1}\right)^2 \Gamma\left(1 + \frac{l}{n+1}\right)^2}{\Gamma\left(\frac{1}{2} + l\right)^2 \Gamma\left(1 + \frac{2l+1}{n+1}\right)^2}. \tag{164}$$

Finally, the greybody factor $\sigma_{l,n}(\omega)$ is equal to:

$$\sigma_l(\omega) = \frac{4\pi^2(2l+1)}{(n+1)^2} \left(\frac{\omega r_H}{2}\right)^{2l} \frac{\Gamma\left(\frac{l+1}{n+1}\right)^2 \Gamma\left(1 + \frac{l}{n+1}\right)^2}{\Gamma\left(\frac{1}{2} + l\right)^2 \Gamma\left(1 + \frac{2l+1}{n+1}\right)^2} r_H^2 \tag{165}$$

As can be seen from this relation, for every n when $l = 0$, the greybody factor for scalar fields at the low-energy regime is given by the area of the horizon.

3.4 Energy Emission of black holes in the case of a bosonic field

An important quantity determined by the greybody factor and related to Hawking radiation is the energy emitted per unit of time from the black hole, which is found by combining the number of particles emitted with the amount of energy they carry. This energy emission rate is given by the relation [8]:

$$\frac{dE(\omega)}{dt} = \sum_l \sigma_{l,n}(\omega) \frac{\omega^3}{exp(\omega/T_H) - 1} \frac{d\omega}{2\pi^2} \tag{166}$$

where $''$-1$''$ was chosen because we are referring to bosonic fields.

The equation provided describes the rate at which energy is emitted from a black hole due to the Hawking radiation process [7]. This formula encapsulates several critical aspects of the physical mechanisms at play, combining quantum field theory with general relativity to describe a phenomenon that lies at the intersection of these two foundational pillars of modern physics.

The equation for the energy emission rate $dE(\omega)/dt$ encompasses several important variables and concepts. First of all, the summation over l, runs over different angular momentum quantum numbers l. The presence of this summation indicates that the radiation emitted by the black hole can occur in different angular momentum modes. Each mode represents a specific solution to the wave equation in the curved spacetime around the black hole. Moreover, the absorption cross-section $\sigma_{l,n}(\omega)$, represents the probability that a particle with frequency ω and angular momentum quantum number l will be absorbed by the black hole. It is referred to as the greybody factor, modifying the pure blackbody spectrum due to the curvature of spacetime near the black hole.

Furthermore, the energy term $\dfrac{\omega^3}{exp(\omega/T_H) - 1}$, is akin to the Planck distribution for blackbody radiation, but adapted for a black hole. Here, ω is the frequency of the emitted particle, and T_H is the Hawking temperature of the black hole. The factor ω^3 arises from the density of states for the radiation. Furthermore, the differential $d\omega$ suggests that the equation sums contributions from all possible frequencies of the emitted radiation. This integral is over the range of frequencies that the black hole can emit. Also, the normalization factor $\dfrac{d\omega}{2\pi^2}$ ensures that the units and scaling of the equation are consistent, particularly in the context of the chosen dimensional analysis.

The energy emission rate described by this equation is pivotal for understanding the ultimate fate of black holes. As black holes emit Hawking radiation, they lose mass and energy, leading to a gradual decrease in their size. Over astronomical timescales, this radiation could cause black holes to evaporate completely, a process ending in a burst of high-energy radiation as the black hole reaches extremely small sizes and high temperatures.

From a theoretical perspective, Hawking radiation provides a unique window into the quantum aspects of gravity. It challenges and enriches our understanding of fundamental physics, suggesting that black holes are not entirely closed systems but instead interact with their surroundings in subtle yet profound ways. This interaction bridges the gap between classical descriptions of gravity and quantum mechanics, offering insights that could pave the way toward a theory of quantum gravity.

In conclusion, equation (166) elegantly encapsulates the emission of energy from a black hole via Hawking radiation. It synthesizes quantum field theory, statistical mechanics, and general relativity into a single framework. This formulation not only highlights the intricate dance of particles and energy near the event horizon but also underscores the deep connections between the macroscopic and microscopic realms of physics.

4 Evaluation of Results

In this chapter we will present the results for the cases of the bulk scalar emission and the brane-localized scalar emission, for the absorption coefficients the graybody factors and the energy emission rates. More specifically, the next two sections present detailed plots for these two emission channels and analyzes the derived results in both cases.

4.1 Bulk scalar emission for $l \geq 0$

In this section, we discuss the results obtained for the absorption coefficients, graybody factors and energy emission rates in the case of Bulk scalar emission for $l \geq 0$. The graphs come from the analytical solutions of the expressions, with the approximation that $\omega r_H \ll 1$. Therefore, for bigger values of ωr_H, we do not expect them to give us the correct results.

For the absorption coefficients in the case of Bulk Scalar emission for $l \geq 0$ given by equation (134), we obtain the graphs of Figure 3. More specifically and as can be seen from Figure 3, in the case where we have constant l and different n, the larger the n, the smaller the value of the absorption coefficient. At the same time, we observe from Figure 3 that the larger l is, the curve raises from the zero value at higher values on the horizontal axis. Furthermore, it appears that the larger the l (or n) (for constant l and variable j, and for constant n and variable l, respectively), the smaller the absorption coefficient becomes. This happens because for larger values of l or n, ωr_H takes on a larger power value which decreases the value of the absorption coefficient. In contrast, it is found that for small values of n and small values of l, the absorption coefficient has larger values. In general, as can be seen from the relationship (134) as well as from the graphs in Figure 3, as l increases, the absorption coefficient decreases, since as l increases, the value of the denominator in the relationship (134) increases.

Furthermore, Figure 4 shows the graphs for the relation (138) for different l and n. The greybody factor is given in units of the horizon area A_H, since the quantity A_H is a purely geometric quantity and does not depend on ω. Since $\omega r_H \ll 1$, the greybody factor decreases as l increases, therefore, the main contribution comes from the lowest partial wave with $l = 0$. As can be seen from both relation (138) and Figure 4, for $l = 0$ and $n = 0$ the greybody factor is equal to 1. Furthermore, the greybody factor is equal to 1 for $l = 0$ and for arbitrary n. In addition, the larger l is, the smaller the greybody factor is, since for large l the denominator becomes larger. At the same time, for constant l and variable n, the greybody factor does not change much, except for large values of l where the coefficient decreases.

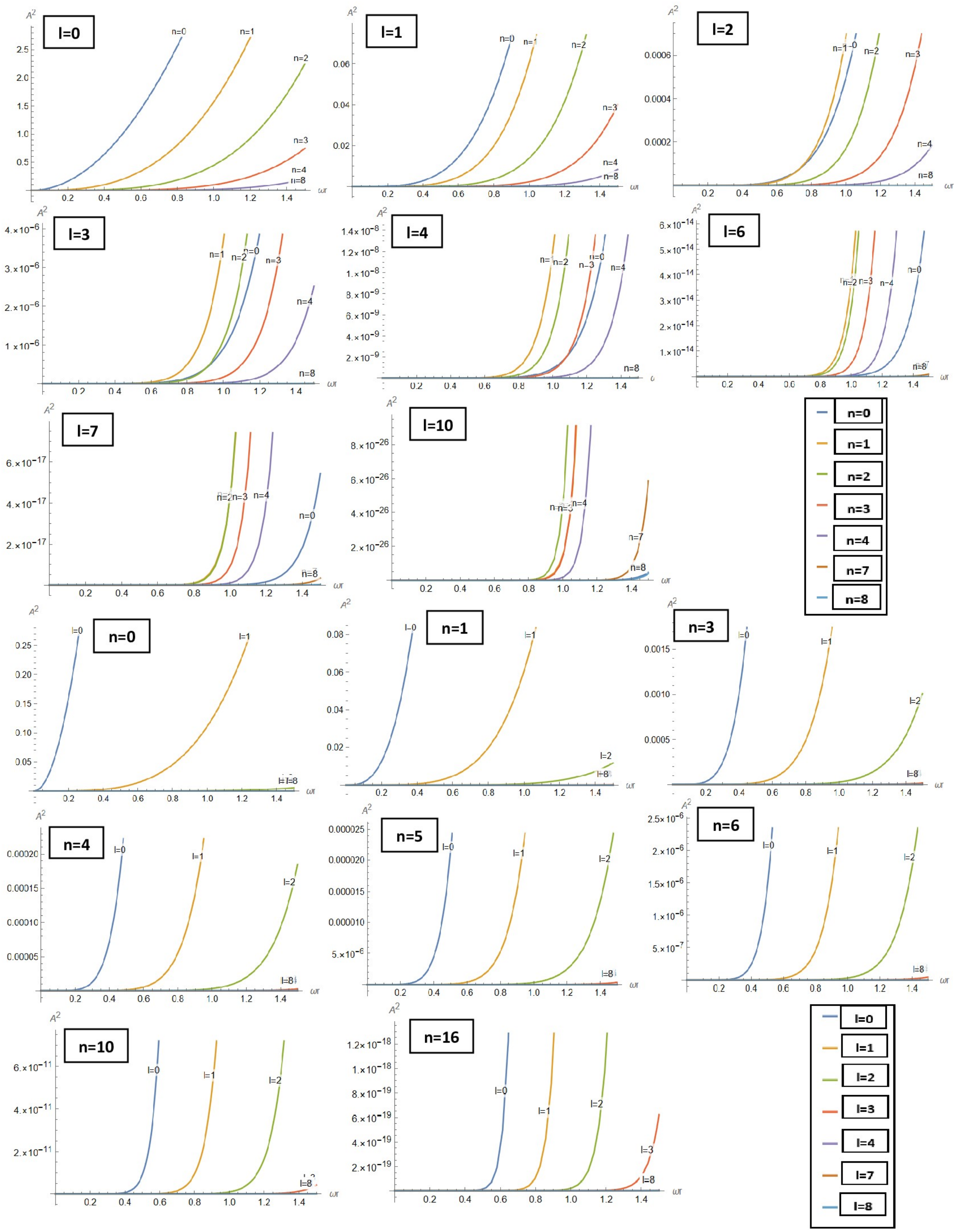

Figure 3: Absorption coefficients for Bulk Scalar emission with $l \geq 0$, for different l and n, respectively.

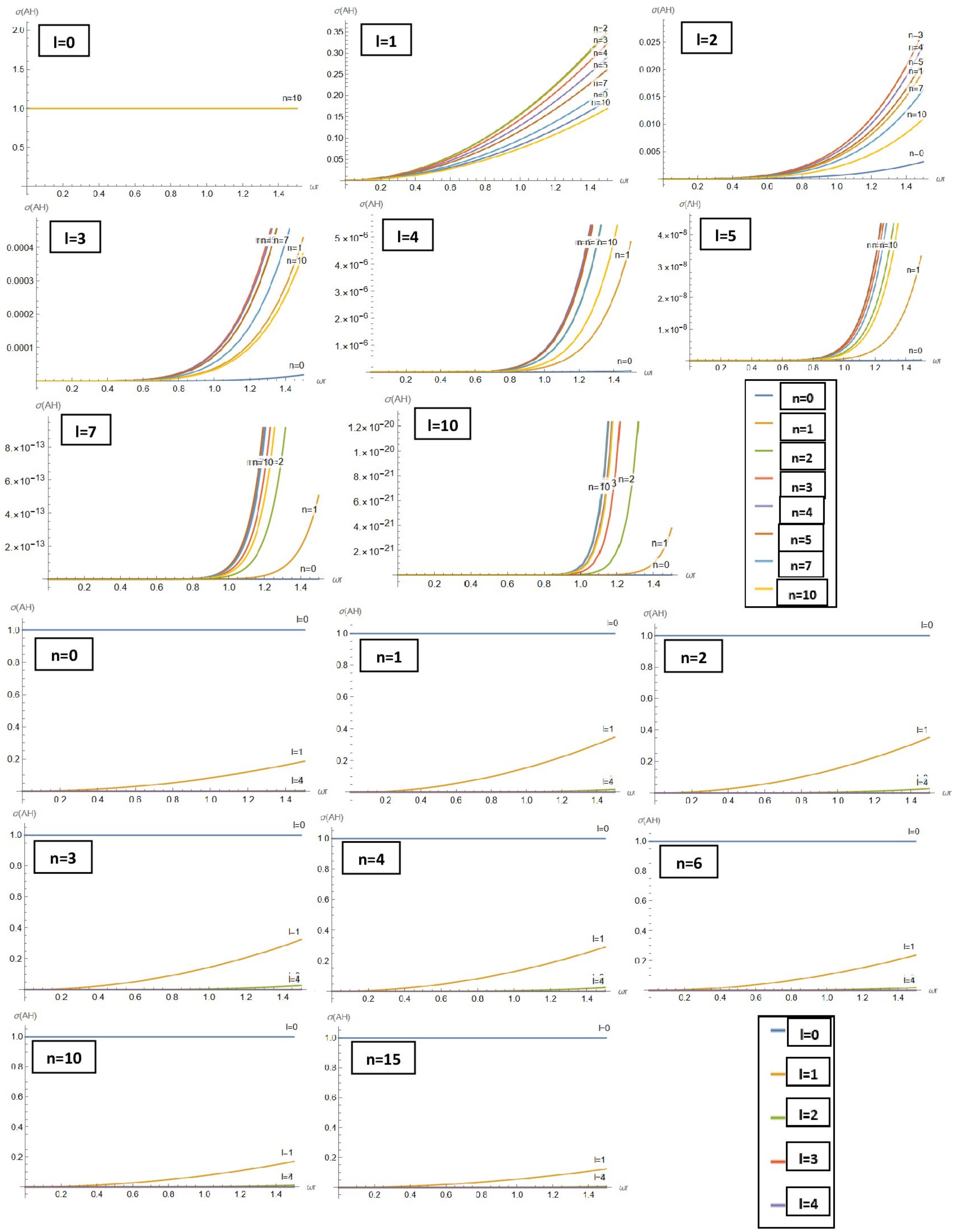

Figure 4: Greybody factors for Bulk Scalar emission with $l \geq 0$ for different l and n, respectively.

In Tables 1 and 2, the lowest-order values of the absorption coefficients and greybody factors are calculated, in the case of the bulk scalar field, for different n and l. From the results of these tables, the conclusions derived from Figures 3 and 4 are confirmed. More specifically and as seen from Table 1, the absorption coefficient in the case of bulk scalar field decreases by keeping n constant and increasing l, while the same also applies to the greybody factor, given in the same table. Similarly, as can be seen from the results in Table 2, the absorption coefficient decreases as we keep l constant and increase n, while in the case of the greybody factor, it remains relatively constant for l constant and n varying.

In more detail and with regard to the results of Table 1, it can be seen the increase in the power of the term (ωr_H), at each n, both in the case of the absorption coefficient and the greybody factor. On the other hand and as can be seen from Table 2 and for l constant, we see that while the power of the term (ωr_H) increases in the case of the absorption coefficient, in the case of the greybody factor, the power of the term (ωr_H) remains constant for fixed l.

Table 1. Absorption coefficients and greybody factor for a (4+n) bulk scalar field			
$n=0$	$l=0$	$\|A\|^2 \simeq (\omega r_H)^2$	$\sigma \simeq A_H$
	$l=1$	$\|A\|^2 \simeq 1\times 10^{-2}(\omega r_H)^4$	$\sigma \simeq 1\times 10^{-1}(\omega r_H)^2 A_H$
	$l=2$	$\|A\|^2 \simeq 1\times 10^{-3}(\omega r_H)^6$	$\sigma \simeq 1\times 10^{-4}(\omega r_H)^4 A_H$
	$l=5$	$\|A\|^2 \simeq 1\times 10^{-13}(\omega r_H)^{12}$	$\sigma \simeq 1\times 10^{-12}(\omega r_H)^{10} A_H$
$n=1$	$l=0$	$\|A\|^2 \simeq (\omega r_H)^3$	$\sigma \simeq A_H$
	$l=1$	$\|A\|^2 \simeq 1\times 10^{-1}(\omega r_H)^5$	$\sigma \simeq 1\times 10^{-1}(\omega r_H)^2 A_H$
	$l=2$	$\|A\|^2 \simeq 1\times 10^{-4}(\omega r_H)^7$	$\sigma \simeq 1\times 10^{-3}(\omega r_H)^4 A_H$
	$l=5$	$\|A\|^2 \simeq 1\times 10^{-11}(\omega r_H)^{13}$	$\sigma \simeq 1\times 10^{-11}(\omega r_H)^{10} A_H$
$n=2$	$l=0$	$\|A\|^2 \simeq 1\times 10^{-1}(\omega r_H)^4$	$\sigma \simeq A_H$
	$l=1$	$\|A\|^2 \simeq 1\times 10^{-2}(\omega r_H)^6$	$\sigma \simeq 1\times 10^{-1}(\omega r_H)^2 A_H$
	$l=2$	$\|A\|^2 \simeq 1\times 10^{-4}(\omega r_H)^8$	$\sigma \simeq 1\times 10^{-3}(\omega r_H)^4 A_H$
	$l=5$	$\|A\|^2 \simeq 1\times 10^{-10}(\omega r_H)^{14}$	$\sigma \simeq 1\times 10^{-9}(\omega r_H)^{10} A_H$
$n=3$	$l=0$	$\|A\|^2 \simeq 1\times 10^{-2}(\omega r_H)^5$	$\sigma \simeq A_H$
	$l=1$	$\|A\|^2 \simeq 1\times 10^{-3}(\omega r_H)^7$	$\sigma \simeq 1\times 10^{-1}(\omega r_H)^2 A_H$
	$l=2$	$\|A\|^2 \simeq 1\times 10^{-5}(\omega r_H)^9$	$\sigma \simeq 1\times 10^{-3}(\omega r_H)^4 A_H$
	$l=5$	$\|A\|^2 \simeq 1\times 10^{-12}(\omega r_H)^{15}$	$\sigma \simeq 1\times 10^{-9}(\omega r_H)^{10} A_H$
$n=7$	$l=0$	$\|A\|^2 \simeq 1\times 10^{-5}(\omega r_H)^9$	$\sigma \simeq A_H$
	$l=1$	$\|A\|^2 \simeq 1\times 10^{-7}(\omega r_H)^{11}$	$\sigma \simeq 1\times 10^{-2}(\omega r_H)^2 A_H$
	$l=2$	$\|A\|^2 \simeq 1\times 10^{-9}(\omega r_H)^{13}$	$\sigma \simeq 1\times 10^{-5}(\omega r_H)^4 A_H$
	$l=5$	$\|A\|^2 \simeq 1\times 10^{-21}(\omega r_H)^{19}$	$\sigma \simeq 1\times 10^{-12}(\omega r_H)^{10} A_H$

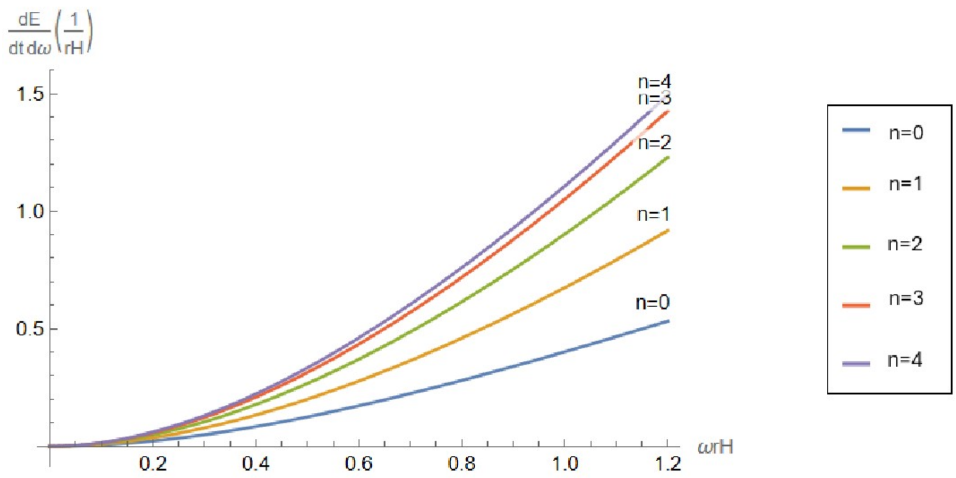

Figure 5: Energy emission rates of black holes in the case of Bulk Scalar emission with $l \geq 0$ for different n.

Table 2. Absorption coefficients and greybody factor for a (4+n) bulk scalar field			
$l=0$	$n=0$	$\lvert A\rvert^2 \simeq (\omega r_H)^2$	$\sigma \simeq A_H$
	$n=2$	$\lvert A\rvert^2 \simeq 1\times 10^{-1}(\omega r_H)^4$	$\sigma \simeq A_H$
	$n=3$	$\lvert A\rvert^2 \simeq 1\times 10^{-2}(\omega r_H)^5$	$\sigma \simeq A_H$
	$n=7$	$\lvert A\rvert^2 \simeq 1\times 10^{-5}(\omega r_H)^9$	$\sigma \simeq A_H$
$l=1$	$n=0$	$\lvert A\rvert^2 \simeq 1\times 10^{-1}(\omega r_H)^4$	$\sigma \simeq 1\times 10^{-2}(\omega r_H)^2 A_H$
	$n=2$	$\lvert A\rvert^2 \simeq 1\times 10^{-3}(\omega r_H)^6$	$\sigma \simeq 1\times 10^{-1}(\omega r_H)^2 A_H$
	$n=3$	$\lvert A\rvert^2 \simeq 1\times 10^{-4}(\omega r_H)^7$	$\sigma \simeq 1\times 10^{-1}(\omega r_H)^2 A_H$
	$n=7$	$\lvert A\rvert^2 \simeq 1\times 10^{-8}(\omega r_H)^{11}$	$\sigma \simeq 1\times 10^{-2}(\omega r_H)^2 A_H$
$l=2$	$n=0$	$\lvert A\rvert^2 \simeq 1\times 10^{-4}(\omega r_H)^6$	$\sigma \simeq 1\times 10^{-4}(\omega r_H)^4 A_H$
	$n=2$	$\lvert A\rvert^2 \simeq 1\times 10^{-4}(\omega r_H)^8$	$\sigma \simeq 1\times 10^{-3}(\omega r_H)^4 A_H$
	$n=3$	$\lvert A\rvert^2 \simeq 1\times 10^{-5}(\omega r_H)^9$	$\sigma \simeq 1\times 10^{-3}(\omega r_H)^4 A_H$
	$n=7$	$\lvert A\rvert^2 \simeq 1\times 10^{-9}(\omega r_H)^{13}$	$\sigma \simeq 1\times 10^{-2}(\omega r_H)^4 A_H$
$l=5$	$n=0$	$\lvert A\rvert^2 \simeq 1\times 10^{-6}(\omega r_H)^{12}$	$\sigma \simeq 1\times 10^{-12}(\omega r_H)^{10} A_H$
	$n=2$	$\lvert A\rvert^2 \simeq 1\times 10^{-11}(\omega r_H)^{14}$	$\sigma \simeq 1\times 10^{-9}(\omega r_H)^{10} A_H$
	$n=3$	$\lvert A\rvert^2 \simeq 1\times 10^{-12}(\omega r_H)^{15}$	$\sigma \simeq 1\times 10^{-9}(\omega r_H)^{10} A_H$
	$n=7$	$\lvert A\rvert^2 \simeq 1\times 10^{-17}(\omega r_H)^{19}$	$\sigma \simeq 1\times 10^{-9}(\omega r_H)^{10} A_H$

Finally, regarding the visualization of the graphical representations of energy emission rates, relation (166) was used, with $\sigma_{l,n}(\omega)$ given by relation (138). To calculate the term $\sum_l \sigma_{l,n}(\omega)$ the values of the greybody factor were added for the first 8 values of l (from $l = 0$ to $l = 7$) and for constant n. There is not much variation with the number of modes so here we present a general case, with 8 modes. In Figure 5, we observe that as n increases the energy emission rate increases as ωr_H increases. More specifically, for the same value of ωr_H, it can be seen that the larger n is, the higher the energy emission rate is. This was to be anticipated, because the temperature of the black hole is given by the relation $T_H = (n+1)/4\pi r_H$, therefore, for fixed r_H, the temperature of the black hole increases as n increases. This simply means that the energy of the black hole available for the emission of particles also increases, and this is reflected in the enhancement of the power and flux rates.

4.2 Brane-localized scalar emission for $l \geq 0$

In this section, we discuss the results obtained for the absorption coefficients, graybody factors and energy emssion rates in the case of Brane-localized scalar emission for $l \geq 0$. The graphs come from the analytical solutions of the expressions, with the approximation that $\omega r_H \gg 1$. Therefore, for bigger values of ωr_H, we do not expect them to give us the correct results. Initially, in Figures 6 and 7 we show the graphs of the absorption coefficients and the greybody factors, in the case of the Brane-localized Scalar emission, for different n and l.

As shown in Figure 6 and in the case of fixed l and different n, for $l = 0$ the absorption coefficient has the same value for all n, while as l increases and n decreases, the absorption coefficient decreases. At the same time and as shown in Figure 6 for constant n and different l, the absorption coefficient is very small for large values of l, while in general there are no large changes for different values of n. Additionally and regarding the results of Figure 7 for the greybody factor, in the case where we have constant l and different n, when $l = 0$ the greybody factor has a constant value for all n and as l increases, the greybody factor decreases. At the same time, from the results of Figure 6 for constant n and different l, in the case of $l = 0$ we always have (for every n) a constant non-zero value of the absorption coefficient, while for larger l the absorption coefficient is very small. Moreover, more generally with changes of n, the absorption coefficient does not change.

As before, in Tables 3 and 4, the lowest-order values of the absorption coefficients and greybody factors are calculated, in the case of the brane-localized scalar emission, for different n and l. From the results of these tables, the conclusions drawn from Figures 6 and 7 are confirmed. More specifically and as can be seen from Table 3, the absorption coefficient in the case of the brane-localized scalar emission, decreases by keeping n constant and increasing l, while the same applies to the greybody factor, given in the same table. On the other hand and as can be seen from the results in Table 4, both the absorption coefficient and the greybody factor remain almost constant as we keep l constant and increase n.

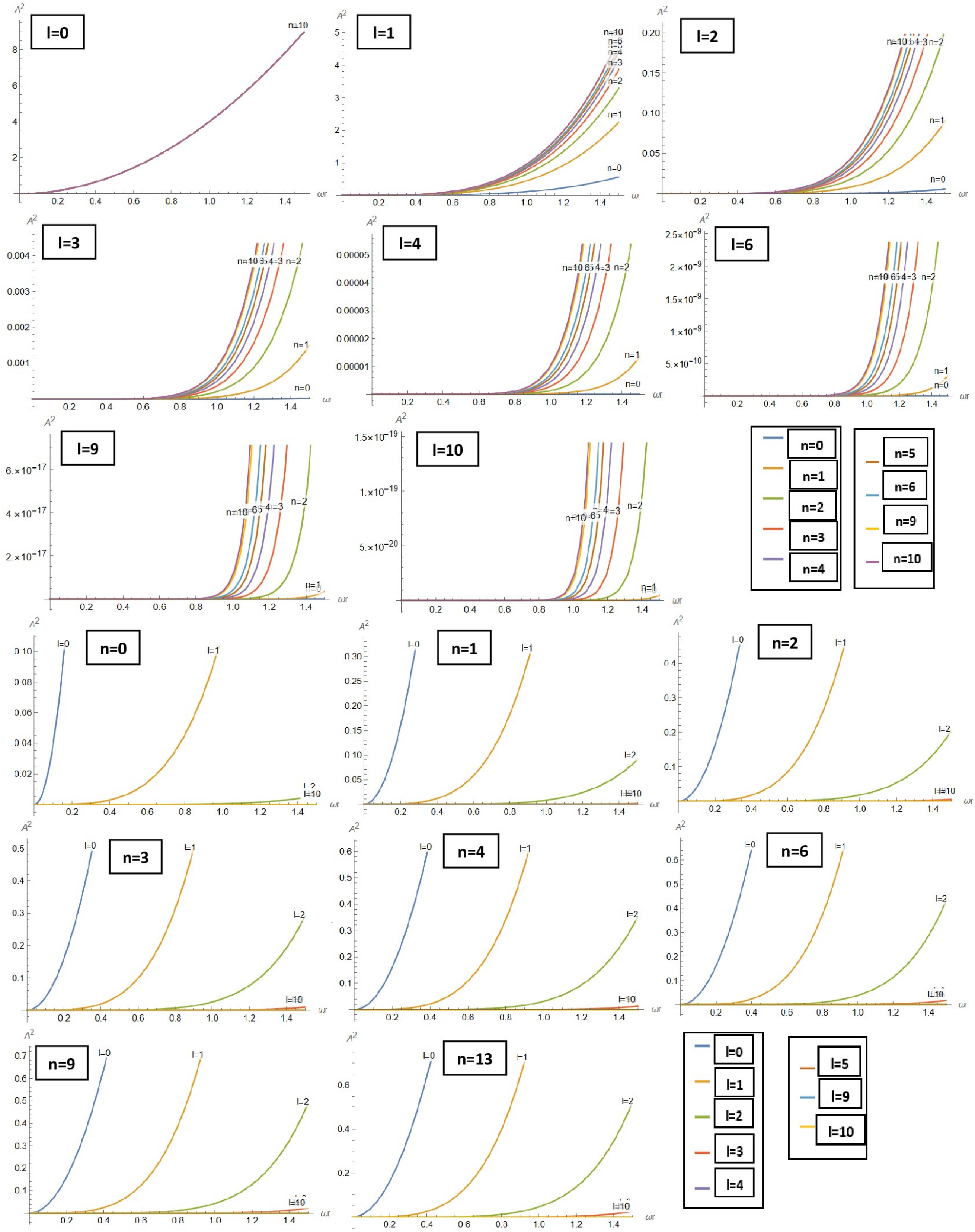

Figure 6: Absorption coefficients for Brane-localized Scalar emission with $l \geq 0$ for different l and n, respectively.

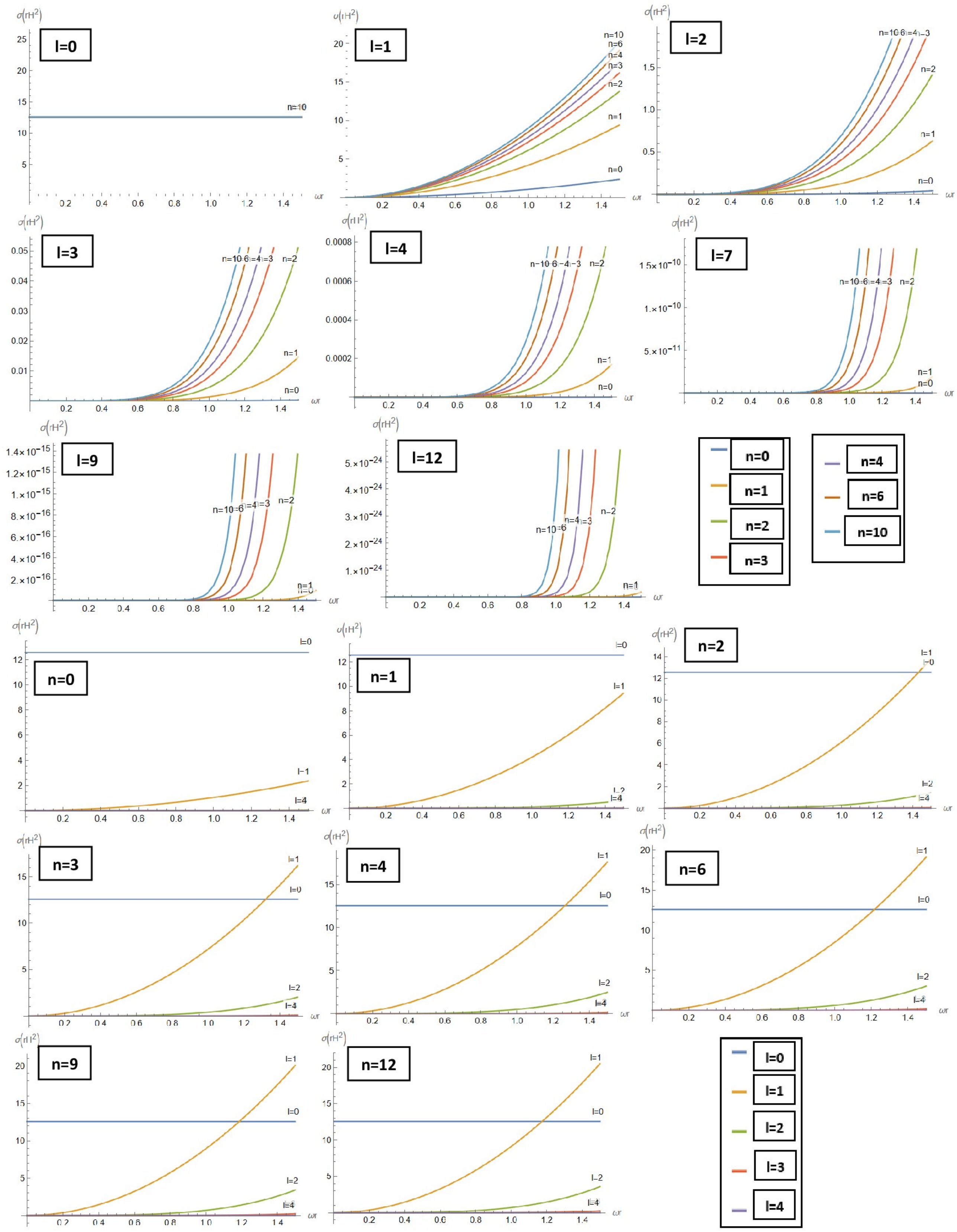

Figure 7: Greybody factors for Brane-localized Scalar emission with $l \geq 0$ for different l and n, respectively.

Table 3. Absorption coefficients and greybody factor for a brane-localized scalar			
$n=0$	$l=0$	$\lvert A\rvert^2 \simeq 4(\omega r_H)^2$	$\sigma \simeq 4\pi r_H^2$
	$l=1$	$\lvert A\rvert^2 \simeq 0.11(\omega r_H)^4$	$\sigma \simeq (\omega r_H)^2 r_H^2$
	$l=2$	$\lvert A\rvert^2 \simeq 0.0005(\omega r_H)^6$	$\sigma \simeq 1\times 10^{-3}(\omega r_H)^4 r_H^2$
	$l=4$	$\lvert A\rvert^2 \simeq 9.14\times 10^{-10}(\omega r_H)^{10}$	$\sigma \simeq 1\times 10^{-8}(\omega r_H)^8 r_H^2$
$n=1$	$l=0$	$\lvert A\rvert^2 \simeq 4(\omega r_H)^2$	$\sigma \simeq 4\pi r_H^2$
	$l=1$	$\lvert A\rvert^2 \simeq 0.33(\omega r_H)^4$	$\sigma \simeq (\omega r_H)^2 r_H^2$
	$l=2$	$\lvert A\rvert^2 \simeq 0.008(\omega r_H)^6$	$\sigma \simeq 1\times 10^{-1}(\omega r_H)^4 r_H^2$
	$l=4$	$\lvert A\rvert^2 \simeq 2.34\times 10^{-7}(\omega r_H)^{10}$	$\sigma \simeq 1\times 10^{-4}(\omega r_H)^8 r_H^2$
$n=2$	$l=0$	$\lvert A\rvert^2 \simeq 4.01(\omega r_H)^2$	$\sigma \simeq 4\pi r_H^2$
	$l=1$	$\lvert A\rvert^2 \simeq 0.65(\omega r_H)^4$	$\sigma \simeq (\omega r_H)^2 r_H^2$
	$l=2$	$\lvert A\rvert^2 \simeq 0.04(\omega r_H)^6$	$\sigma \simeq (\omega r_H)^4 r_H^2$
	$l=4$	$\lvert A\rvert^2 \simeq 0.000001(\omega r_H)^{10}$	$\sigma \simeq 1\times 10^{-5}(\omega r_H)^8 r_H^2$
$n=3$	$l=0$	$\lvert A\rvert^2 \simeq 4.01(\omega r_H)^2$	$\sigma \simeq 4\pi r_H^2$
	$l=1$	$\lvert A\rvert^2 \simeq 0.2(\omega r_H)^4$	$\sigma \simeq (\omega r_H)^2 r_H^2$
	$l=2$	$\lvert A\rvert^2 \simeq 0.02(\omega r_H)^6$	$\sigma \simeq 1\times 10^{-1}(\omega r_H)^4 r_H^2$
	$l=4$	$\lvert A\rvert^2 \simeq 0.000003(\omega r_H)^{10}$	$\sigma \simeq 1\times 10^{-5}(\omega r_H)^8 r_H^2$
$n=6$	$l=0$	$\lvert A\rvert^2 \simeq 4(\omega r_H)^2$	$\sigma \simeq 4\pi r_H^2$
	$l=1$	$\lvert A\rvert^2 \simeq 0.90(\omega r_H)^4$	$\sigma \simeq (\omega r_H)^2 r_H^2$
	$l=2$	$\lvert A\rvert^2 \simeq 0.005(\omega r_H)^6$	$\sigma \simeq 1\times 10^{-1}(\omega r_H)^4 r_H^2$
	$l=4$	$\lvert A\rvert^2 \simeq 0.000007(\omega r_H)^{10}$	$\sigma \simeq 1\times 10^{-4}(\omega r_H)^8 r_H^2$

Table 4. Absorption coefficients and greybody factor for a brane-localized scalar			
$l=0$	$n=0$	$\lvert A\rvert^2 \simeq (\omega r_H)^2$	$\sigma \simeq 4\pi r_H^2$
	$n=1$	$\lvert A\rvert^2 \simeq (\omega r_H)^2$	$\sigma \simeq 4\pi r_H^2$
	$n=2$	$\lvert A\rvert^2 \simeq (\omega r_H)^2$	$\sigma \simeq 4\pi r_H^2$
	$n=3$	$\lvert A\rvert^2 \simeq (\omega r_H)^2$	$\sigma \simeq 4\pi r_H^2$
	$n=6$	$\lvert A\rvert^2 \simeq (\omega r_H)^2$	$\sigma \simeq 4\pi r_H^2$
$l=1$	$n=0$	$\lvert A\rvert^2 \simeq 1\times 10^{-1}(\omega r_H)^4$	$\sigma \simeq (\omega r_H)^2 r_H^2$
	$n=1$	$\lvert A\rvert^2 \simeq 1\times 10^{-1}(\omega r_H)^4$	$\sigma \simeq (\omega r_H)^2 r_H^2$
	$n=2$	$\lvert A\rvert^2 \simeq 1\times 10^{-1}(\omega r_H)^4$	$\sigma \simeq (\omega r_H)^2 r_H^2$
	$n=3$	$\lvert A\rvert^2 \simeq 1\times 10^{-1}(\omega r_H)^4$	$\sigma \simeq (\omega r_H)^2 r_H^2$
	$n=6$	$\lvert A\rvert^2 \simeq 1\times 10^{-1}(\omega r_H)^4$	$\sigma \simeq (\omega r_H)^2 r_H^2$
$l=2$	$n=0$	$\lvert A\rvert^2 \simeq 1\times 10^{-4}(\omega r_H)^6$	$\sigma \simeq 1\times 10^{-3}(\omega r_H)^4 r_H^2$
	$n=1$	$\lvert A\rvert^2 \simeq 1\times 10^{-2}(\omega r_H)^6$	$\sigma \simeq 1\times 10^{-1}(\omega r_H)^4 r_H^2$
	$n=2$	$\lvert A\rvert^2 \simeq 1\times 10^{-2}(\omega r_H)^6$	$\sigma \simeq 1\times 10^{-1}(\omega r_H)^4 r_H^2$
	$n=3$	$\lvert A\rvert^2 \simeq 1\times 10^{-2}(\omega r_H)^6$	$\sigma \simeq 1\times 10^{-1}(\omega r_H)^4 r_H^2$
	$n=6$	$\lvert A\rvert^2 \simeq 1\times 10^{-2}(\omega r_H)^6$	$\sigma \simeq 1\times 10^{-1}(\omega r_H)^4 r_H^2$
$l=4$	$n=0$	$\lvert A\rvert^2 \simeq 1\times 10^{-10}(\omega r_H)^{10}$	$\sigma \simeq 1\times 10^{-8}(\omega r_H)^8 r_H^2$
	$n=1$	$\lvert A\rvert^2 \simeq 1\times 10^{-7}(\omega r_H)^{10}$	$\sigma \simeq 1\times 10^{-6}(\omega r_H)^8 r_H^2$
	$n=2$	$\lvert A\rvert^2 \simeq 1\times 10^{-6}(\omega r_H)^{10}$	$\sigma \simeq 1\times 10^{-5}(\omega r_H)^8 r_H^2$
	$n=3$	$\lvert A\rvert^2 \simeq 1\times 10^{-6}(\omega r_H)^{10}$	$\sigma \simeq 1\times 10^{-5}(\omega r_H)^8 r_H^2$
	$n=6$	$\lvert A\rvert^2 \simeq 1\times 10^{-6}(\omega r_H)^{10}$	$\sigma \simeq 1\times 10^{-4}(\omega r_H)^8 r_H^2$

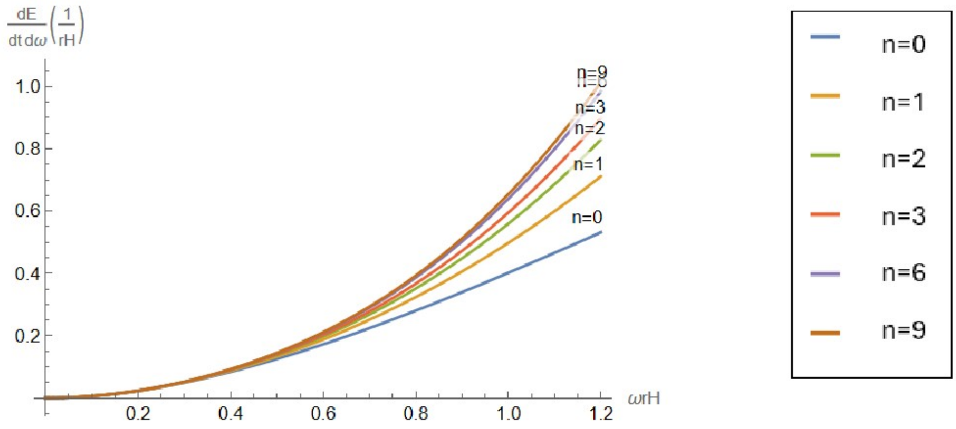

Figure 8: Energy emission rates of black holes in the case of Brane-localized Scalar emission with $l \geq 0$ for different n.

Finally, regarding the visualization of the graphical representations of energy, relation (166) was used, with $\sigma_{l,n}(\omega)$ given by relation (165). To calculate the term $\sum_l \sigma_{l,n}(\omega)$ the values of the greybody factor were added for the first 8 values of l (from $l = 0$ to $l = 7$) and for constant n. Like the bulk case, there is not much variation with the number of modes, so in the case here we present a general case, with 8 modes.

More specifically, Figure 8 shows the behavior of energy emission rates for particles with spin 0 in the low energy regime. As we can see, the corresponding power emission rates, as well as the flux emission rates, exhibit a universal behaviour according to which the energy, and the number of particles, emitted per unit time and energy interval is strongly enhanced, as n increases. This occurs due to the temperature, for the same reason it happens in the Bulk.

5 An application to primordial black holes

About 50 years ago, Hawking proposed the formation of primordial black holes (PBHs) [31], suggesting that black holes were electrically charged and, therefore, capable of capturing charged particles to form neutral ″atoms″, which was ultimately proven to be incorrect. And while later Zeldovich and Novikov (1967) [32] used a Newtonian argument to conclude that PBHs were unlikely to have formed, in 1974 a relativistic analysis refuted this Newtonian argument [33].

Primordial black holes (PBHs) are expected to have a mass corresponding to the cosmological horizon at their formation, which is significantly less than the mass of about 1 solar mass ($M_\odot$) of the smallest astrophysical black holes. This lead Hawking to explore the quantum effects of smaller black holes, resulting in his 1974 discovery that these black holes emit particles like a black body with a temperature inversely proportional to their mass ($T \propto M^{-1}$) and completely evaporate over a timescale proportional to the cube of their mass ($\tau \propto M^3$) [34]. Although Hawking's prediction has not yet been experimentally verified, it remains one of the most significant theoretical advancements of the late 20th century, as it integrates aspects of general relativity, quantum theory, and thermodynamics [35].

After Hawking's discovery, there was a flurry of articles concerning primordial black holes (PBHs). However, none of these articles could confirm their existence, and as a result the subject remained of minor interest for many years. However, in recent years the situation has changed radically and PBH publications have increased greatly. There are several reasons for this, but the most significant are likely: (a) the increasing interest in the possibility that primordial black holes (PBHs) larger than 10^{15} grams could account for dark matter in galactic halos, (b) the detection of gravitational waves by LIGO/Virgo/KAGRA (LVK) from merging binary black holes, some of which may be primordial in origin and (c) the idea that very large PBHs could serve as the seeds for the supermassive black holes (SMBHs) found in galactic centers [35].

In a black hole (here PBH), the Schwarzschild radius determines the size of the black hole's event horizon and is directly related to its mass (the greater the mass, the greater the radius). At the same time, the Hawking temperature is inversely proportional to the mass of the black hole, i.e. the lower the mass, the higher the temperature. This means that smaller black holes radiate more strongly. As the black hole emits Hawking radiation, it loses mass and shrinks. The rate of mass loss increases as its mass decreases. Additionally, the finite lifetime of the black hole is due to the slow but gradual loss of mass through Hawking radiation. When it loses all its mass, it disappears completely. This time depends on the initial mass of the black hole: the greater the mass, the longer its lifetimes.

Regarding Hawking radiation in the low-energy limit, the emissions are weak because the black hole's temperature is low. This means that for large black holes, which are in the low-energy limit, Hawking radiation is produced in very small amounts. The black hole loses mass more slowly because the energy it emits through radiation is extremely small. As a result, the rate of mass loss is very low, and the black hole requires much more time to evaporate [35].

Concerning the numerical solution to the problem of scalar radiation, it leads to a total radiation spectrum that takes the form of a Gaussian curve (for the radiation emission rate on the brane, see Figure 4(a) in [8], and for the radiation emission rate on the bulk, see Figure 6(b) in [8]), with the energy value at which the curve reaches its maximum determined by the temperature of the black hole. However, how do the properties of primordial black holes, whose mass range is currently considered to be very large (from microscopic to supermassive), change as a function of the number of extra dimensions and their mass?

In this chapter we give some numerical results for primordial black holes, of various masses and in various dimensions. More specifically, for $M_{PBH} = 50TeV$, $M_{PBH} = 10\mu g$, $M_{PBH} = 1M_{\odot}$, $M_{PBH} = 10^4 M_{\odot}$, and $M_{PBH} = 10^8 M_{\odot}$, the Schwarzschild radius r_H, the temperature T_H, and the half-life τ of the primordial black hole are calculated for $n = 0$, $n = 1$, $n = 2$, $n = 3$, $n = 4$, $n = 5$, $n = 6$ and $n = 7$. From equation (79), we observe that, for $n \neq 0$ the relation between r_H and $M \equiv M_{PBH}$ is not linear anymore, and that it is the fundamental Planck scale M_* that appears in the expression of the horizon radius and not the four dimensional one $M_P = 1.22 \times 10^{28} eV$. The latter feature is the main reason for the fact that extra dimensions facilitate the creation of low-mass black holes, as we will shortly see. Before elaborating on this last point, we need to make another comment first: in order to be able to ignore quantum corrections in our calculations and study the produced black holes by using semi-classical methods, the mass of the black hole must be, at least, a few times larger than the scale of quantum gravity M_*. Therefore, if we assume that $M_* = 10TeV$, a safe limit for the mass of the produced black hole would be $M_{PBH} = 50TeV$.

The modified properties of a higher-dimensional, Schwarzschild-like black hole, compared to those of a four-dimensional one with the same mass, were first studied in [36]. Now, we will discuss in detail the temperature of a PBH. The temperature of a black hole in $4 + n$ dimensions is given by the expression: [8]

$$T_H = \frac{(n+1)}{4\pi r_H},$$

where r_H is given by (79) with $M = M_{PBH}$. Finally, the timelife of black holes in $4 + n$ dimensions is given by:

$$\tau \sim \frac{1}{M_*} \left(\frac{M_{PBH}}{M_*} \right)^{(n+3)/(n+1)},$$

where $M = M_P$ when $n = 0$ and $M_* = 10TeV$ when $n \neq 0$.

Table 5. Black hole r_H, T_H and τ values, for different values of n, for $M_{PBH} = 50TeV$			
$n = 0$	$r_H \simeq 1.33 \times 10^{-52} km$	$T_H \simeq 1.40 \times 10^{45} K$	$\tau \simeq 3.71 \times 10^{-87} sec$
$n = 1$	$r_H \simeq 3.52 \times 10^{-23} km$	$T_H \simeq 1.06 \times 10^{16} K$	$\tau \simeq 1.65 \times 10^{-27} sec$
$n = 2$	$r_H \simeq 2.30 \times 10^{-23} km$	$T_H \simeq 2.42 \times 10^{16} K$	$\tau \simeq 9.62 \times 10^{-28} sec$
$n = 3$	$r_H \simeq 1.98 \times 10^{-23} km$	$T_H \simeq 3.77 \times 10^{16} K$	$\tau \simeq 7.36 \times 10^{-28} sec$
$n = 4$	$r_H \simeq 1.86 \times 10^{-23} km$	$T_H \simeq 4.99 \times 10^{16} K$	$\tau \simeq 6.26 \times 10^{-28} sec$
$n = 5$	$r_H \simeq 1.83 \times 10^{-23} km$	$T_H \simeq 6.10 \times 10^{16} K$	$\tau \simeq 5.63 \times 10^{-28} sec$
$n = 6$	$r_H \simeq 1.83 \times 10^{-23} km$	$T_H \simeq 7.11 \times 10^{16} K$	$\tau \simeq 5.21 \times 10^{-28} sec$
$n = 7$	$r_H \simeq 1.86 \times 10^{-23} km$	$T_H \simeq 8.03 \times 10^{16} K$	$\tau \simeq 4.92 \times 10^{-28} sec$

Table 6. Black hole r_H, T_H and τ values, for different values of n, for $M_{PBH} = 10\mu g$			
$n = 0$	$r_H \simeq 1.48 \times 10^{-38} km$	$T_H \simeq 1.26 \times 10^{31} K$	$\tau \simeq 5.19 \times 10^{-45} sec$
$n = 1$	$r_H \simeq 3.72 \times 10^{-16} km$	$T_H \simeq 9.99 \times 10^{8} K$	$\tau \simeq 20.56 sec$
$n = 2$	$r_H \simeq 1,11 \times 10^{-18} km$	$T_H \simeq 5.04 \times 10^{11} K$	$\tau \simeq 0.0002 sec$
$n = 3$	$r_H \simeq 6.44 \times 10^{-20} km$	$T_H \simeq 1.16 \times 10^{13} K$	$\tau \simeq 8.69 \times 10^{-7} sec$
$n = 4$	$r_H \simeq 1.20 \times 10^{-20} km$	$T_H \simeq 4.25 \times 10^{16} K$	$\tau \simeq 2.91 \times 10^{-8} sec$
$n = 5$	$r_H \simeq 4.03 \times 10^{-21} km$	$T_H \simeq 2.78 \times 10^{14} K$	$\tau \simeq 3.03 \times 10^{-9} sec$
$n = 6$	$r_H \simeq 1.87 \times 10^{-21} km$	$T_H \simeq 6.99 \times 10^{14} K$	$\tau \simeq 6.01 \times 10^{-10} sec$
$n = 7$	$r_H \simeq 1.06 \times 10^{-21} km$	$T_H \simeq 1.41 \times 10^{15} K$	$\tau \simeq 1.79 \times 10^{-10} sec$

Table 7. Black hole r_H, T_H and τ values, for different values of n, for $M_{PBH} = 1M_\odot$			
$n = 0$	$r_H \simeq 2.94 km$	$T_H \simeq 6.34 \times 10^{-8} K$	$\tau \simeq 4.06 \times 10^{70} sec$
$n = 1$	$r_H \simeq 5245 km$	$T_H \simeq 7.09 \times 10^{-11} K$	$\tau \simeq 8.11 \times 10^{77} sec$
$n = 2$	$r_H \simeq 6.47 \times 10^{-6} km$	$T_H \simeq 0.086 K$	$\tau \simeq 1.69 \times 10^{60} sec$
$n = 3$	$r_H \simeq 2.42 \times 10^{-10} km$	$T_H \simeq 3086.1 K$	$\tau \simeq 2.43 \times 10^{51} sec$
$n = 4$	$r_H \simeq 5.50 \times 10^{-13} km$	$T_H \simeq 1.69 \times 10^{6} K$	$\tau \simeq 1.21 \times 10^{46} sec$
$n = 5$	$r_H \simeq 9.72 \times 10^{-15} km$	$T_H \simeq 1.16 \times 10^{8} K$	$\tau \simeq 3.51 \times 10^{42} sec$
$n = 6$	$r_H \simeq 5.52 \times 10^{-16} km$	$T_H \simeq 2.37 \times 10^{9} K$	$\tau \simeq 1.05 \times 10^{40} sec$
$n = 7$	$r_H \simeq 6.49 \times 10^{-17} km$	$T_H \simeq 2.30 \times 10^{10} K$	$\tau \simeq 1.33 \times 10^{38} sec$

Table 8. Black hole r_H, T_H and τ values, for different values of n, for $M_{PBH} = 10^4 M_\odot$			
$n = 0$	$r_H \simeq 29428 km$	$T_H \simeq 5.15 \times 10^{-12} K$	$\tau \simeq 4.06 \times 10^{82} sec$
$n = 1$	$r_H \simeq 524480 km$	$T_H \simeq 7.09 \times 10^{-13} K$	$\tau \simeq 8.11 \times 10^{85} sec$
$n = 2$	$r_H \simeq 0.00014 km$	$T_H \simeq 0.004 K$	$\tau \simeq 7.83 \times 10^{66} sec$
$n = 3$	$r_H \simeq 2.42 \times 10^{-9} km$	$T_H \simeq 308.61 K$	$\tau \simeq 2.43 \times 10^{57} sec$
$n = 4$	$r_H \simeq 3.47 \times 10^{-12} km$	$T_H \simeq 262317 K$	$\tau \simeq 4.80 \times 10^{51} sec$
$n = 5$	$r_H \simeq 4.51 \times 10^{-14} km$	$T_H \simeq 2.46 \times 10^{7} K$	$\tau \simeq 7.56 \times 10^{47} sec$
$n = 6$	$r_H \simeq 2.06 \times 10^{-15} km$	$T_H \simeq 6.61 \times 10^{8} K$	$\tau \simeq 1.45 \times 10^{45} sec$
$n = 7$	$r_H \simeq 2.05 \times 10^{-16} km$	$T_H \simeq 7.27 \times 10^{9} K$	$\tau \simeq 1.33 \times 10^{43} sec$

Table 9. Black hole r_H, T_H and τ values, for different values of n, for $M_{PBH} = 10^8 M_\odot$			
$n = 0$	$r_H \simeq 2.94 \times 10^8 km$	$T_H \simeq 6.34 \times 10^{-16} K$	$\tau \simeq 4.06 \times 10^{94} sec$
$n = 1$	$r_H \simeq 5.24 \times 10^7 km$	$T_H \simeq 7.10 \times 10^{-15} K$	$\tau \simeq 8.11 \times 10^{93} sec$
$n = 2$	$r_H \simeq 0.003 km$	$T_H \simeq 0.00019 K$	$\tau \simeq 3.63 \times 10^{73} sec$
$n = 3$	$r_H \simeq 2.42 \times 10^{-8} km$	$T_H \simeq 30.086 K$	$\tau \simeq 2.43 \times 10^{63} sec$
$n = 4$	$r_H \simeq 2.19 \times 10^{-11} km$	$T_H \simeq 42967.8 K$	$\tau \simeq 1.91 \times 10^{57} sec$
$n = 5$	$r_H \simeq 2.09 \times 10^{-13} km$	$T_H \simeq 5.67 \times 10^6 K$	$\tau \simeq 1.63 \times 10^{53} sec$
$n = 6$	$r_H \simeq 7.67 \times 10^{-15} km$	$T_H \simeq 1.69 \times 10^8 K$	$\tau \simeq 2.02 \times 10^{50} sec$
$n = 7$	$r_H \simeq 6.49 \times 10^{-16} km$	$T_H \simeq 2.30 \times 10^9 K$	$\tau \simeq 1.33 \times 10^{48} sec$

As can be seen from the results of Table 5, for the mass $M_{PBH} = 50TeV$, the black hole radius r_H varies between $1.33 \times 10^{-52} km$ and $1.83 \times 10^{-23} km$ as n increases from 0 to 7. The temperature T_H decreases from $1.40 \times 10^{45} K$ to $7.11 \times 10^{16} K$, while the lifetime (τ) increases from $3.71 \times 10^{-87} sec$ to $5.21 \times 10^{-25} sec$. As n increases, the radius stabilizes around $1.83 \times 10^{-23} km$, while the temperature continues to decrease, and the lifetime increases significantly. In this case, for $M_{PBH} = 50TeV$, their properties resemble the ones of the microscopic black holes that could in principle be created at ground-based accelerators in the presence of extra dimensions. The higher dimensionality of spacetime makes their creation easier as it increases their horizon radius but also renders them cooler and thus longer-lived compared to their four-dimensional analogues.

Furthermore, for$M_{PBH} = 10\mu g$, Table 6, the event horizon radius varies from $1.48 \times 10^{-38} km$ to $1.06 \times 10^{-21} km$ a much larger range compared to the $M_{PBH} = 50TeV$ case. The temperature drops from $1.26 \times 10^{31} K$ to $1.41 \times 10^{15} K$ as n increases. The lifetime changes significantly, starting at $5.19 \times 10^{-45} sec$ and rising to $1.79 \times 10^{-10} sec$ for $n = 7$. The pattern shows rapid changes in the values, especially for the small n, compared to the $M_{PBH} = 50TeV$ case. In this case, for $M_{PBH} = 10\mu g$, the presence of the extra dimensions favours the creation of black holes with their properties resembling a lot the ones of the previous case. We note however that in this case it is the smaller values of the number of extra dimensions that support black holes with the most realistic and likely to observe properties.

Also, for $M_{PBH} = 1M_\odot$, Table 7, the event horizon radius starts from $2.94 km$ for $n = 0$ and decreases sharply to $6.49 \times 10^{-17} km$ for $n = 7$. The temperature shows a similar trend, ranging from $6.34 \times 10^{-8} K$ to $2.30 \times 10^{10} K$. The lifetime decreases from $4.06 \times 10^{70} sec$ to $1.33 \times 10^{38} sec$. The variations for this mass are more extreme than the smaller PBH masses, with much higher lifetimes and lower initial temperatures. Here, it is only the case $n = 1$ that may lead more easily to the creation of cooler and thus longer-lived black holes compared to the 4-dimensional case. The presence of more than 2 extra dimensions decreases in fact the possibility of black holes with a mass equal to one solar mass to be created and even in the case they do, they evaporate rather quickly.

The table 8 for $M_{PBH} = 10^4 M_\odot$ shows an event horizon radius that starts at $29428 km$ for $n = 0$ and reduces to $2.05 \times 10^{-16} km$ for $n = 7$. The temperature ranges from $5.15 \times 10^{-12} K$ to $7.27 \times 10^9 K$. The lifetime, like in the other tables, decreases significantly with increasing n, from $4.06 \times 10^{82} sec$ to $1.33 \times 10^{43} sec$. This trend mirrors the other tables, with larger masses exhibiting longer lifetimes and smaller radii as n increases. The situation here resembles very much the one of the previous case.

Finally, for the mass $M_{PBH} = 10^8 M_\odot$, Table 9, the radius varies from $2.94 \times 10^8 km$ to $6.49 \times 10^{-16} km$. The temperature starts from $6.34 \times 10^{-16} K$ and rises to $2.30 \times 10^9 K$ as n increases. The lifetime shows significant reductions, from $4.06 \times 10^{94} sec$ to $1.33 \times 10^{48} sec$. This massive black hole follows a similar pattern as the other tables, with much larger event horizons and longer lifetimes. As we can see, here, no values of n exist that enhances the creation of black holes. On the contrary, the higher-dimensional spacetime supports much smaller, hotter and thus shorter-lived supermassive black holes.

So from the above analysis, we can conclude that black holes with larger masses have much larger event horizon radius (r_H), lower temperatures (T_H), and significantly longer lifetimes (τ). This indicates that as the mass increases, the black hole becomes cooler and more stable with a larger event horizon. Conversely, black holes with smaller masses have very small event horizon radii, higher temperatures, and shorter lifetimes. This suggests that smaller black holes are hotter and more short-lived due to their higher Hawking radiation emission. Comparing the values across different mass scales, it is clear that for each value of n, the trends are consistent: larger mass black holes have larger event horizons, lower temperatures, and longer lifetimes. Additionally, it is important to highlight that the results indicate that the presence of extra spatial dimensions helps in the formation of black holes only in the case of small masses. For large black holes, there is an improvement only for $n = 1$. However, this case has been excluded because the size of the extra dimension would be equal to the Earth-Sun distance, and thus it would have already been detected through changes in the intensity of gravitational forces.

More specifically, in the case of $n = 1$, we can derive some important conclusions. From the following relation for R [37]:

$$R = 2 \times 10^{31/n-16} mm \times \left(\frac{1TeV}{M_{(4+n)}} \right)^{1+2/n},$$

we can deduce that if $M_{(4+n)} = 1TeV$, the resulting size is $R = 10^{12} m$, while if $M_{(4+n)} = 10TeV$, we have $R = 10^9 m$, a value that would have been observed in Cavendish experiments, if it existed. Therefore, if we ″pushed″ the value of $M_{(4+n)}$ to much higher values, we could reduce the value of R close to the phenomenological limit. However, this would likely also reduce the value of the horizon, making the formation of black holes-even those with small mass-very difficult.

6 Conclusions

The proposal of the existence of extra dimensions in the Universe has made significant progress in theoretical physics, potentially revolutionizing our understanding of four-dimensional cosmology, particle physics phenomenology, and black hole physics. By extending beyond the conventional four-dimensional framework, extra-dimensional theories provide novel insights and predictive power, suggesting profound modifications in the behavior of fundamental forces and particles, the structure and evolution of the cosmos, and the nature of black holes.

The recent resurgence in the hypothesis of extra space-like dimensions, which may be almost macroscopic in size or even non-compact, introduces a groundbreaking aspect to theoretical physics: the scale at which gravity becomes strong could be significantly lower than the traditional four-dimensional Planck mass M_P. This exciting development suggests that high-energy collisions between elementary particles, such as those anticipated at next-generation ground-based accelerators or occurring in Earth's atmosphere, might explore the energy regime of quantum gravity. Among the most remarkable implications is the potential formation of mini black holes from high-energy particle collisions with center-of-mass energies only a few times greater than the new gravity scale M_*. This prospect offers a unique opportunity to investigate quantum gravitational effects directly [8].

The literature offers various findings on the possibility of creating mini black holes during high-energy collisions. Traditional four-dimensional analyses have been expanded to include scenarios where colliding particles move through higher-dimensional spacetimes. Some new studies indicate that in head-on collisions, the mass of the resulting black hole decreases as the number of extra dimensions increases. Additionally, recent findings suggest that the emission of gravitational waves during these collisions diminishes with an increasing number of dimensions. This discrepancy suggests that a significant portion of the energy lost during the collision might be emitted in a form other than gravitational radiation. Conversely, in collisions with a non-zero impact parameter, which are more common, the likelihood of black hole production actually increases with more extra dimensions. When these findings are applied to realistic collisions between composite particles, the estimated black hole production cross-sections become significantly large by new physics standards, whether at the LHC or in the Earth's atmosphere [8]. These mini black holes, when quantum effects are considered, emit Hawking radiation into higher-dimensional spacetime in the form of both bulk and brane modes. Extending the four-dimensional emission rate calculations to higher dimensions is straightforward, but understanding the precise greybody factors for different fields in higher dimensions was challenging until recent advancements clarified these factors.

The aim of this work was to understand understand the behavior of Schwarzschild black holes in n-dimensional spacetime by computing Hawking radiation in the form of bulk and brane-localized scalar emission. Initially, in the first chapter, the useful mathematical tools of General Relativity were presented, specifically focusing on the concept and properties of the metric tensor, the connection, and the covariant derivatives, as well as the Riemann, Ricci, and Einstein tensors and the Ricci scalar. Additionally, in this first chapter, the Lagrangian formalism was introduced, and the Einstein equations were derived. Next, in the second chapter, the Schwarzschild solution in 4-dimensional space was derived, followed by a discussion on theories of extra dimensions. Then, the Schwarzschild solution in n-dimensions was derived, along with the equation of a scalar field in a curved background. It is important to mention again that, the spacetime will change if the assumption about spherical symmetry changes. Then in the third chapter we dealt with Hawking radiation from higher-dimensional black holes. We introduced the concept of Hawking radiation and then derived the radial equation, the absorption coefficient, and the greybody factor in n-dimensions, for the cases of bulk scalar field and brane-localized scalar emission for $l \leq 0$. These relationships were derived analytically in the low-energy limit. Additionally, in this chapter, we presented the relationship of the emission energy of black holes in the case of a bosonic field.

Then, in the fourth chapter, we presented the results for the cases of the bulk scalar emission and the brane-localized scalar emission, for the absorption coefficients the gray-body factors and the energy emission rates. For the absorption coefficients in the case of Bulk Scalar emission for $l \geq 0$, we found that when $l = 0$ we are dealing with the simplest form of emission, resulting in higher absorption coefficients. This indicates that the emission is more effective in this state. As l increases, the complexity of the emission increases, leading to lower absorption coefficients. At the same time, in the case where we have constant l and different n, the larger the n, the smaller the value of the absorption coefficient. Furthermore, regarding the greybody factor for the case of Bulk Scalar emission for $l \geq 0$ which is given in units of the horizon area A_H (since the quantity A_H is a purely geometric quantity and does not depend on ω), we found that the dominant contribution of the greybody factor from the lowest partial wave (with $l = 0$) indicates that basic emission processes are more significant, while higher-order contributions (with $l > 0$) provide less energy. Finally, we found that Increasing n enhances the energy emission capabilities. As n rises, black holes become more ″powerful″ in their emission processes, as indicated by rising temperatures. The increase in the energy emission rate with rising n implies that black holes in higher dimensions have greater potential for creating and releasing energy. This affects the physics of black holes and their behavior in various cosmological scenarios.

For the absorption coefficients in the case of Brane-localized scalar emission for $l \geq 0$, we found that for $l = 0$, the absorption coefficient remains constant regardless of the values of n. However, as l increases and n decreases, the absorption coefficient decreases, indicating that higher-order emissions are less efficient. Also, for constant l and varying n, the absorption coefficient is very small for high values of l. However, changes in n do not significantly affect the absorption coefficient. Additionally, the greybody factor has a constant value for $l = 0$ regardless of n and decreases as l increases. This indicates that the basic emission processes are dominant for low values of l, while higher-order contributions yield less energy. Finally, we observed that the energy emission rates and flux emission rates exhibit universal behavior, where the energy and number of particles emitted per unit time and energy interval are significantly enhanced as n increases. This occurs due to the temperature, similar to the bulk case. The connection between increasing n and enhanced emission rates suggests that temperature plays a crucial role in energy emission. As n increases, the black hole temperature also rises, leading to more pronounced emission rates.

Finally, in Chapter 5, we presented some calculations for the early Schwarzschild black holes. As we found, the black holes with lower mass ($M = 50TeV$), have properties resemble the ones of the microscopic black holes, where the higher dimensionality of spacetime makes their creation easier as it increases their horizon radius but also renders them cooler and thus longer-lived compared to their four-dimensional analogues. On the other hand for supermassive black holes ($M = 10^8 M_\odot$), the higher-dimensional spacetime supports much smaller, hotter and thus shorter-lived supermassive black holes.

In conclusion, greybody factors provide crucial information about the background around the emitting black hole and depend on the energy of the emitted particle and the dimensionality of spacetime. This implies that the greybody factor will alter the low-energy emission rate compared to the high-energy one. Additionally, the number of particles emitted is influenced by the number of extra dimensions, potentially allowing for the determination of spacetime dimensionality through the detection of Hawking radiation. The emission of brane-localized modes is undoubtly the most phenomenologically interesting effect since it involves Standard Model particles that can be easily detected during experiments. On the other hand, the emission of bulk modes will be only perceived as a missing energy signal by the observer on the brane. Nevertheless, the amount of energy lost in the bulk is crucially important as it determines the remaining available energy for emission on the brane. Although the possibility of the production and evaporation of mini black holes at the LHC is an exciting prospect, this will be possible only in the case where the fundamental scale of gravity M_* is indeed very close to $1TeV - 10TeV$. Nevertheless, there is absolutely no guarantee for that, and the only argument in favour of this particular value is the possible resolution of the hierarchy problem.

Finally, it is important at this point to mention that we do not take into account the backreaction of the field on the metric (the metric is considered to be unaffected by the emission of individual particles). In this work, we assume that the energy ω of the particles is small, and with this assumption, we ensure that the energy of the particle is much smaller than the mass of the black hole emitting it, and therefore the change in the metric is negligible. However, as the energy of the emitted particle increases, this approximation becomes less reliable. In this case, not only a numerical integration of the particle's equation of motion is required, but also a full simulation to describe the phenomenon with the backreaction of the field on the metric taken into account (for microscopic black holes, of course; in astrophysical or galactic cases, this need does not exist due to their large mass).

Appendix A

In the main text (in Section 2.1) we studied the case where $n = 0$ for the general form of our metric, in relation (57). Now we will perform the case where $\mathbf{n = 1}$. In this case we can write the metric in the form:

$$ds^2 = -A(r)\,dt^2 + B(r)\,dr^2 + r^2\left[d\theta_1^2 + sin^2\theta_1(d\theta_2^2 + sin^2\theta_2\,d\phi^2)\right]. \tag{167}$$

Then, from the equation (9) we can calculate again the non-zero Christoffel symbols:

$$\Gamma^1{}_{11} = \frac{B'(r)}{2B(r)},\quad \Gamma^0{}_{01} = \frac{A'(r)}{2A(r)},\quad \Gamma^1{}_{00} = \frac{A'(r)}{2B(r)},\quad \Gamma^1{}_{22} = -\frac{r}{B(r)},\quad \Gamma^1{}_{33} = -\frac{r}{B(r)}sin^2\theta_1,$$
$$\Gamma^1{}_{44} = -\frac{r}{B(r)}sin^2\theta_2 sin^2\theta_1,\quad \Gamma^2{}_{33} = -sin\theta_1\,cos\theta_1,\quad \Gamma^2{}_{44} = -sin\theta_1\,cos\theta_1\,sin^2\theta_2,$$
$$\Gamma^3{}_{32} = \frac{cos\theta_1}{sin\theta_1},\ \Gamma^3{}_{44} = -sin\theta_2\,cos\theta_2,\quad \Gamma^4{}_{42} = \frac{cos\theta_1}{sin\theta_1},\quad \Gamma^4{}_{43} = \frac{cos\theta_2}{sin\theta_2},\quad \Gamma^2{}_{21} = \Gamma^3{}_{31} = \Gamma^4{}_{41} = \frac{1}{r}$$

and the non-zero components of the Ricci tensor:

$$R_{00} = -\frac{A''(r)}{2B(r)} + \frac{A'(r)}{4B(r)}\left[\frac{A'(r)}{A(r)} + \frac{B'(r)}{B(r)}\right] - \frac{3}{2}\frac{A'(r)}{rB(r)} \tag{168}$$
$$R_{11} = \frac{A''(r)}{2A(r)} - \frac{A'(r)}{4A(r)}\left[\frac{A'(r)}{A(r)} + \frac{B'(r)}{B(r)}\right] - \frac{3}{2}\frac{B'(r)}{rB(r)} \tag{169}$$
$$R_{22} = \frac{2}{B(r)} - 2 + \frac{r}{2B(r)}\left[\frac{A'(r)}{A(r)} - \frac{B'(r)}{B(r)}\right] \tag{170}$$
$$R_{33} = sin^2\theta_1\,R_{22},\qquad R_{44} = sin^2\theta_1\,sin^2\theta_2\,R_{22}. \tag{171}$$

Furthermore, from the Einstein equations, we get:

$$\frac{1}{2}R_{00} + \frac{A(r)}{2B(r)}R_{11} + \frac{3A(r)}{2r^2}R_{22} = 0 \tag{172}$$
$$\frac{1}{2}R_{00} + \frac{A(r)}{2B(r)}R_{11} - \frac{3A(r)}{2r^2}R_{22} = 0. \tag{173}$$

Then, by adding and subtracting these equations, we arrive at the relations, respectively:

$$A'(r) + A(r)\frac{B'(r)}{B(r)} = 0 \tag{174}$$
$$R_{22} = 0. \tag{175}$$

From equation (174), we obtain:

$$B(r) = \frac{\Lambda}{A(r)} \to B'(r) = -\frac{A'(r)\Lambda}{A^2(r)} \tag{176}$$

and from equation (175):

$$\frac{2}{B(r)}-2+\frac{r}{2B(r)}\left[\frac{A'(r)}{A(r)}-\frac{B'(r)}{B(r)}\right]=0\Rightarrow r^2A'(r)+2rA(r)=2\Lambda r\rightarrow\frac{d}{dr}[r^2A(r)]=2\Lambda r \tag{177}$$

with solution:

$$A(r)=1+\left(\frac{C}{r}\right)^2 \tag{178}$$

$$B(r)=\left[1+\left(\frac{C}{r}\right)^2\right]^{-1}. \tag{179}$$

To find the constant, C we again use Gauss's law:

$$\int g\,ds=-4\pi GM \tag{180}$$

where g is the intensity of the gravitational field and $ds=r^3sin^2\theta_1 sin\theta_2 d\theta_1 d\theta_2 d\phi$.

Therefore we have:

$$gr^3\int_0^{\pi}sin^2\theta_1 d\theta_1\int_0^{\pi}sin\theta_2 d\theta_2\int_0^{2\pi}d\phi=-4\pi GM\rightarrow g=-\frac{2GM}{\pi r^3}. \tag{181}$$

Now, to find the potential and subsequently the constant C, we use the well-known relation $g=-\nabla\Phi$ and then:

$$\Phi=\int\frac{2GM}{\pi r^3}dr=-\frac{GM}{\pi r^2}. \tag{182}$$

Taking as an approximation the limit of the weak field $A(r)\rightarrow 1+2\Phi$, we have:

$$2\Phi=\frac{C^2}{r^2}\rightarrow\frac{-2GM}{\pi r^2}=\frac{C^2}{r^2}\rightarrow C^2=-\frac{2GM}{\pi}. \tag{183}$$

Then, for the equations (178), (179) we get:

$$A(r)=1-\frac{2GM}{\pi r^2}\equiv\left(1-\frac{r_H^2}{r^2}\right) \tag{184}$$

$$B(r)=\left(1-\frac{2GM}{\pi r^2}\right)^{-1}\equiv\left(1-\frac{r_H^2}{r^2}\right)^{-1} \tag{185}$$

where $r_H^2=\dfrac{2GM}{\pi}$ is the Schwarzschild radius in 5-dimensions.

So, the final form of the Schwarzschild metric in $\mathbf{n=1}$ is:

$$ds^2=-\left(1-\frac{r_H^2}{r^2}\right)dt^2+\left(1-\frac{r_H^2}{r^2}\right)^{-1}dt^2+r^2[d\theta_1^2+sin^2\theta_1(d\theta_2^2+sin^2\theta_2 d\phi^2)] \tag{186}$$

where $r_H^2 = \dfrac{2GM}{\pi}$.

In the case now where $\mathbf{n = 2}$, we can write the metric in the form:

$$ds^2 = -A(r)dt^2 + B(r)dr^2 + r^2\left[d\theta_1^2 + sin^2\theta_1\left(d\theta_2^2 + sin^2\theta_2(d\theta_3^2 + sin^2\theta_3 d\phi^2)\right)\right] \quad (187)$$

and then we can get the non-zero Christoffel symbols:

$$\begin{gathered}
\Gamma^1{}_{11} = \frac{B'(r)}{2B(r)}, \quad \Gamma^0{}_{01} = \frac{A'(r)}{2A(r)}, \quad \Gamma^1{}_{00} = \frac{A'(r)}{2B(r)}, \quad \Gamma^1{}_{22} = -\frac{r}{B(r)}, \quad \Gamma^1{}_{33} = -\frac{r}{B(r)}sin^2\theta_1, \\
\Gamma^1{}_{44} = -\frac{r}{B(r)}sin^2\theta_3 sin^2\theta_2, \quad \Gamma^2{}_{33} = -sin\theta_1\, cos\theta_1, \quad \Gamma^2{}_{44} = -sin\theta_2\, cos\theta_2\, sin^2\theta_3, \quad \Gamma^3{}_{32} = \frac{cos\theta_2}{sin\theta_2}, \\
\Gamma^3{}_{44} = -sin\theta_3\, cos\theta_3, \quad \Gamma^4{}_{42} = \frac{cos\theta_2}{sin\theta_2}, \quad \Gamma^4{}_{43} = \frac{cos\theta_3}{sin\theta_3}, \quad \Gamma^2{}_{21} = \Gamma^3{}_{31} = \Gamma^4{}_{41} = \Gamma^5{}_{51} = \frac{1}{r}, \\
\Gamma^5{}_{52} = \frac{cos\theta_1}{sin\theta_1}, \quad \Gamma^5{}_{53} = \frac{cos\theta_2}{sin\theta_2}, \quad \Gamma^5{}_{54} = \frac{cos\theta_3}{sin\theta_3} \quad \Gamma^1{}_{55} = -\frac{r}{B(r)}sin^2\theta_3 sin^2\theta_2 sin^2\theta_1, \\
\Gamma^2{}_{55} = -sin\theta_1\, cos\theta_1\, sin^2\theta_3\, sin^2\theta_2, \quad \Gamma^3{}_{55} = -sin\theta_2\, cos\theta_2\, sin^2\theta_3, \quad \Gamma^4{}_{55} = -sin\theta_3\, cos\theta_3
\end{gathered} \quad (188)$$

and the non-zero components of the Ricci tensor:

$$R_{00} = -\frac{A''(r)}{2B(r)} + \frac{A'(r)}{4B(r)}\left[\frac{A'(r)}{A(r)} + \frac{B'(r)}{B(r)}\right] - \frac{2A'(r)}{rB(r)} \quad (189)$$

$$R_{11} = \frac{A''(r)}{2A(r)} - \frac{A'(r)}{4A(r)}\left[\frac{A'(r)}{A(r)} + \frac{B'(r)}{B(r)}\right] - \frac{2B'(r)}{rB(r)} \quad (190)$$

$$R_{22} = \frac{3}{B(r)} - 3 + \frac{r}{2B(r)}\left[\frac{A'(r)}{A(r)} - \frac{B'(r)}{B(r)}\right] \quad (191)$$

$$R_{33} = sin^2\theta_1 R_{22} \quad (192)$$

$$R_{44} = sin^2\theta_2 sin^2\theta_1 R_{22} \quad (193)$$

$$R_{55} = sin^2\theta_3 sin^2\theta_2 sin^2\theta_1 R_{22}. \quad (194)$$

Then, from the Einstein equations, we get:

$$\frac{1}{2}R_{00} + \frac{A(r)}{2B(r)}R_{11} + \frac{4A(r)}{2r^2}R_{22} = 0 \quad (195)$$

$$\frac{1}{2}R_{00} + \frac{A(r)}{2B(r)}R_{11} - \frac{4A(r)}{2r^2}R_{22} = 0. \quad (196)$$

By adding and subtracting these equations, we arrive at the relations:

$$A'(r) + A(r)\frac{B'(r)}{B(r)} = 0 \quad (197)$$

$$R_{22} = 0. \quad (198)$$

As before, from relation (197) we have:

$$B(r) = \frac{\Lambda}{A(r)} \rightarrow B'(r) = -\frac{A'(r)\Lambda}{A^2(r)} \quad (199)$$

and from (198):

$$\frac{3}{B(r)} - 3 + \frac{r}{2B(r)}\left[\frac{A'(r)}{A(r)} - \frac{B'(r)}{B(r)}\right] = 0 \Rightarrow r^3A'(r) + 3A(r)r^2 = 3\Lambda r^2$$
$$\Rightarrow \frac{d}{dr}[r^3A(r)] = 3\Lambda r^2 \Rightarrow r^3A(r) = \Lambda(r^3 + C) \quad (200)$$

Then:

$$A(r) = 1 + \left(\frac{C}{r}\right)^3 \quad (201)$$
$$B(r) = \left[1 + \left(\frac{C}{r}\right)^3\right]^{-1}. \quad (202)$$

To find the constant, C we again use Gauss's law:

$$\int g\, ds = -4\pi GM \quad (203)$$

where g is the intensity of the gravitational field and $ds = r^4 sin^1\theta_3 sin^2\theta_2 \sin\theta_3 d\theta_1 d\theta_2 d\theta_3 d\phi$.

Then, we have:

$$gr^4 \int_0^\pi sin^3\theta_2 d\theta_1 \int_0^\pi sin^2\theta_2 d\theta_2 \int_0^\pi sin\theta_3 d\theta_3 \int_0^{2\pi} d\phi = -4\pi GM \rightarrow g = -\frac{3GM}{2\pi r^4}. \quad (204)$$

Therefore, to find the potential and subsequently the constant C, we use the well-known relation $\Phi = -\nabla g$ and then:

$$\Phi = \int \frac{3GM}{2\pi r^4} dr = -\frac{GM}{2\pi r^3}. \quad (205)$$

Taking as an approximation the limit of the weak field $A(r) \rightarrow 1 + 2\Phi$, we have:

$$2\Phi = \frac{C^3}{r^3} \rightarrow \frac{-2GM}{2\pi r^3} = \frac{C^3}{r^3} \rightarrow C^3 = -\frac{GM}{\pi}. \quad (206)$$

Then, for equations (201) and (202), we have:

$$A(r) = 1 - \frac{GM}{\pi r^3} \equiv \left(1 - \frac{r_H^3}{r^3}\right) \quad (207)$$
$$B(r) = \left(1 - \frac{GM}{\pi r^3}\right)^{-1} \equiv \left(1 - \frac{r_H^3}{r^3}\right)^{-1} \quad (208)$$

where $r_H^3 = \dfrac{GM}{\pi}$ is the Schwarzschild radius in 6-dimensions.

Then, the final form of the Schwarzschild metric in $\mathbf{n = 2}$ is:

$$ds^2 = -\left(1 - \frac{r_H^3}{r^3}\right) dt^2 + \left(1 - \frac{r_H^3}{r^3}\right)^{-1} dt^2 + r^2\left[d\theta_1^2 + sin^2\theta_1\left(d\theta_2^2 + sin^2\theta_2(d\theta_3^2 + sin^2\theta_3 d\phi^2)\right)\right] \quad (209)$$

where $r_H^3 = \dfrac{GM}{\pi}$.

Appendix B

In the main text (in Section 2.5) we studied the scalar field, for the case where we are in 4-dimensions, with the metric given by matrix (85). In this appendix we will study the behavior of the scalar field, for the cases where we are in 5 and 6 dimensions.

We start with the case of the 5-dimensional metric, where we have in matrix form:

$$g^{\mu\nu}_{(d=5)} = \begin{pmatrix} -1/h(r) & 0 & 0 & 0 & \\ 0 & h(r) & 0 & 0 & \\ 0 & 0 & 1/r^2 & 0 & \\ 0 & 0 & 0 & 1/(r^2 sin^2\theta_1) & \\ 0 & 0 & 0 & 0 & 1/(r^2 sin^2\theta_2 sin^2\theta_1) \end{pmatrix}. \tag{210}$$

We easily calculate that $g = -r^6 sin^4\theta_1 sin^2\theta_2 \to \sqrt{-g} = r^3 sin\theta_2 sin^2\theta_1$ and the scalar field has the form $\Phi = e^{-i\omega t} R_{\omega l}(r)\tilde{Y}_l(\Omega)$. Then from equation (83), we have:

$$\frac{1}{h(r)}\omega^2 \tilde{Y} R_{\omega l}\, e^{-i\omega t} + e^{-i\omega t}\frac{1}{r^3}\partial_r \left[r^3 h(r)\tilde{Y}\partial_r R_{\omega l}\right] + e^{-i\omega t}\frac{R_{\omega l}}{sin^2\theta_1}\partial_{\theta_1}\left(\frac{sin^2\theta_1}{r^2}\partial_{\theta_1}\tilde{Y}\right) + e^{-i\omega t}\frac{R_{\omega l}}{r^2 sin\theta_2}\partial_{\theta_2}\left(sin\theta_2 \partial_{\theta_2}\tilde{Y}\right) + e^{-i\omega t}\frac{R_{\omega l}}{r^2 sin^2\theta_2 sin^2\theta_1}\partial^2_\phi \tilde{Y} = 0. \tag{211}$$

Multiplying this equation by $(r^3 e^{i\omega t})/(R_{\omega l}\tilde{Y})$, we obtain the relation:

$$\frac{\omega^2}{h(r)}r^3 + \frac{2}{R_{\omega l}}\frac{d}{dr}\left(r^3 h(r)\frac{d}{dR}R_{\omega l}\right) + \frac{r}{sin^2\theta_1}\frac{1}{\tilde{Y}}\partial_{\theta_1}\left(sin^2\theta_1 \partial_{\theta_1}\tilde{Y}\right) + \frac{r}{sin\theta_2}\frac{1}{\tilde{Y}}\partial_{\theta_2}\left(sin\theta_2\partial_{\theta_2}\tilde{Y}\right) + \frac{r}{sin^2\theta_2 sin^2\theta_1}\frac{1}{\tilde{Y}}\partial^2_\phi\tilde{Y} = 0, \tag{212}$$

where:

$$\frac{1}{sin^2\theta_1}\frac{1}{\tilde{Y}}\partial_{\theta_1}\left(sin^2\theta_1\partial_{\theta_1}\tilde{Y}\right) + \frac{1}{sin\theta_2}\frac{1}{\tilde{Y}}\partial_{\theta_2}\left(sin\theta_2\partial_{\theta_2}\tilde{Y}\right) + \frac{1}{sin^2\theta_2 sin^2\theta_1}\frac{1}{\tilde{Y}}\partial^2_\phi\tilde{Y} = -l(l+2). \tag{213}$$

Therefore, the radial equation takes the form:

$$\frac{h(r)}{r^3}\frac{d}{dr}\left(r^3 h(r)\frac{d}{dr}R_{\omega l}\right) + \left[\omega^2 - \frac{h(r)}{r^2}l(l+2)\right]R_{\omega l} = 0. \tag{214}$$

In the case of the 6-dimensional metric, we have the matrix form:

$$g^{\mu\nu}_{(d=6)} = \begin{pmatrix} -1/h(r) & 0 & 0 & 0 & & \\ 0 & h(r) & 0 & 0 & & \\ 0 & 0 & 1/r^2 & 0 & & \\ 0 & 0 & 0 & 1/(r^2 sin^2\theta_1) & & \\ 0 & 0 & 0 & 0 & 1/(r^2 sin^2\theta_2 sin^2\theta_1) & \\ 0 & 0 & 0 & 0 & 0 & 1/(r^2 sin^2\theta_3 sin^2\theta_2 sin^2\theta_1) \end{pmatrix}. \tag{215}$$

Again, we easily calculate that $g = -r^8 sin^6\theta_1 sin^4\theta_2 sin^2\theta_3 \to \sqrt{-g} = r^4 sin\theta_1^3 sin^2\theta_2 sin\theta_3$ and the scalar field has the form $\Phi = e^{-i\omega t} R_{\omega l}(r)\tilde{Y}_l(\Omega)$. Then from equation (83), we have:

$$\frac{1}{h(r)}\omega^2 R_{\omega l}\tilde{Y} + \frac{\tilde{Y}}{r^4}\partial_r(r^4 h(r)\,\partial_r R_{\omega l}) + \frac{1}{sin^3\theta_1}\partial_{\theta_1}\left(sin^3\theta_1 \frac{R_{\omega l}}{r^2}\partial_{\theta_1}\tilde{Y}\right) + \frac{R_{\omega l}}{sin^2\theta_2}\partial_{\theta_2}\left(\frac{sin^2\theta_2}{r^2 sin^2\theta_1}\partial_{\theta_2}\tilde{Y}\right)$$
$$+ \frac{R_{\omega l}}{sin\theta_3}\partial_{\theta_3}\left(\frac{1}{r^2 sin^2\theta_1 sin^2\theta_2}\partial_{\theta_3}\tilde{Y}\right) + \partial_\phi\left(\frac{R_{\omega l}}{r^2 sin^2\theta_1 sin^2\theta_2 sin^2\theta_3}\partial_\phi\tilde{Y}\right) = 0. \quad (216)$$

and multiplying this equation by $(r^4/R_{\omega l}\tilde{Y})$, we obtain the relation:

$$\frac{\omega^2 r^4}{h(r)} + \frac{1}{R}\frac{d}{dr}\left(r^4 h(r)\,\frac{d}{dr}R_{\omega l}\right) + \frac{r^2}{\tilde{Y}}\frac{1}{sin^3\theta_1}\partial_{\theta_1}(sin^3\theta_1\partial_{\theta_1}\tilde{Y}) + \frac{r^2}{sin^2\theta_1 sin^2\theta_2}\partial_{\theta_2}(sin^2\theta_2\partial_{\theta_2}\tilde{Y})$$
$$+ \frac{r^2}{sin\theta_3}\partial_{\theta_3}\left(\frac{sin\theta_3}{sin^2\theta_1 sin^2\theta_2}\partial_{\theta_3}\tilde{Y}\right) + \frac{1}{r^4 sin^2\theta_1 sin^2\theta_2 sin^2\theta_3}\frac{d^2}{d\phi^2}\tilde{Y} = 0 \quad (217)$$

where:

$$\frac{r^2}{\tilde{Y}}\frac{1}{sin^3\theta_1}\partial_{\theta_1}(sin^3\theta_1\partial_{\theta_1}\tilde{Y}) + \frac{r^2}{sin^2\theta_1 sin^2\theta_2}\partial_{\theta_2}(sin^2\theta_2\partial_{\theta_2}\tilde{Y}) + \frac{r^2}{sin\theta_3}\partial_{\theta_3}\left(\frac{sin\theta_3}{sin^2\theta_1 sin^2\theta_2}\partial_{\theta_3}\tilde{Y}\right)$$
$$+ \frac{1}{r^4 sin^2\theta_1 sin^2\theta_2 sin^2\theta_3}\frac{d^2}{d\phi^2}\tilde{Y} = -l(l+3). \quad (218)$$

Therefore, the radial equation takes the form:

$$\frac{h(r)}{r^4}\frac{d}{dr}\left(r^4 h(r)\,\frac{d}{dr}R_{\omega l}\right) + \left[\omega^2 - \frac{h(r)}{r^2}l(l+3)\right]R_{\omega l} = 0. \quad (219)$$

References

[1] Caroll, M., S., *Spacetime and Geometry. An Introduction to General Relativity.* Addison Wesley: Chicago, Ilinois, 2003.

[2] Abramowitz, M., Stegun, I. A., *Handbook of Mathematical Functions with Formulas, Graphs, and Mathematical Tables.* Department of Commerce: United States, 1964.

[3] Hartle J. *Gravity: An Introduction to Einstein's General Relativity.* Adsidon Wesley, University of California: Santa Barbara, 2003.

[4] Wald, Robert, M., *General Relativity.* The University of Chicago Press: Chicago and London, 1984.

[5] Einstein, A., *Relativity the special and general theory.* New York: Henry holt and company, 1920.

[6] Bekenstein, Jacob, D., *Black Holes and Entropy.* Physical Review D, 1973, 7(8), 2333-2346.

[7] Hawking, S. W. *Particle creation by black holes.* Communications In Mathematical Physics, 1975, 43(3), 199–220.

[8] Kanti, P., *Black holes in theories with large extra dimensions: A Review*, Int. J. Mod. Phys. A **19**, 2004, 4899-4951.

[9] Kanti, P., March-Russell, J., *Calculable Corrections to Brane Black Hole Decay I: The Scalar Case.* Phys.Rev., 2002, 66(2), 1-16.

[10] Hobson, M. P., Efstathiou, G. P., Lasenby, A. N., *General Relativity: An Introduction for Physicists.* University Press: Cambridge, New York, 2006.

[11] Kanti, P., Winstanley, E., *Hawking radiation from higher-dimensional black holes.* Fundam.Theor.Phys., 2015, 178, 229-265.

[12] Harris, C. M., Kanti, P., *Hawking radiation from a (4+n)-dimensional black hole: exact results for the Schwarzschild phase.* JHEP10, 2003, 10(14), 1-38.

[13] Arkani-Hamed, N., Dimopoulos, S., Dvali, G., Kaloper, N., *Infinitely large new dimensions.* Phys. Rev. Lett., 2000, 84, 586-589.

[14] Reall, H. S., *Higher-dimensional black holes*, Int. J. Mod. Phys. D, 2012, 21(2), 1-15.

[15] Johnson, G., *Primordial Black Hole Constraints with Large Extra Dimensions.* JCAP, 2020, 9(46), 1-16.

[16] Chamblin, A., Hawking, S. W., Reall, H. S., *Brane world black holes.* Phys.Rev.D, 2000, 61(2), 1-8.

[17] Winstanley, E., *Hawking radiation from rotating brane black holes.* Conference on Black Holes and Naked Singularities, 2007, 1-18.

[18] Li, L. X., *A note on the Kaluza–Klein theory*. Classical Quantum Grav., 2023, 40(19), 1-8.

[19] Harmark, T., Obers, N. A., *General definition of gravitational tension*. Journal of High Energy Physics, 2004, 5(43), 1-17.

[20] Emparan, R., Reall, H. S., *Black holes in higher dimensions*. Living Reviews in Relativity, 2008, 11(1), 1-77.

[21] Polchinski, J., *Dirichlet-Branes and Ramond-Ramond Charges*. Physical Review Letters, 1995, 75(26), 4724-4727.

[22] Strominger, A., Vafa, C., *Microscopic Origin of the Bekenstein-Hawking Entropy*. Physics Letters B, 1996, 379(1-4), 99-104.

[23] Antoniadis, I., *A Possible new dimension at a few TeV*. Phys. Lett., 1990, B246(3-4), 377-384.

[24] Arkani-Hamed, N., Dimopoulos, S., Dvali, G., *The Hierarchy Problem and New Dimensions at a Millimeter*. Phys.Lett., 1998, 429, 263-272.

[25] Randall, L., Sundrum, R., *A large mass hierarchy from a small extra dimension*. Physical Review Letters, 1999, 83(17), 3370-3373.

[26] Maartens, R., *Brane-world gravity*. Living Reviews in Relativity, 2004, 7(7), 1-58.

[27] Tanaka, T., *Classical black hole evaporation in Randall-Sundrum infinite braneworld*. Progress of Theoretical Physics Supplement, 2003, 148, 307-316.

[28] Lee, J. G., Adelberger, E. G., Cook, T. S., Fleischer, S. M., Heckel, B. R., *New Test of the Gravitational $1/r^2$ Law at Separations down to $52\mu m$*. Phys.Rev.Lett., 2020, 124(10), 1-5.

[29] Kanti, P., Grain, J., Barrau, A., *Bulk and Brane Decay of a (4+n)-Dimensional Schwarzschild-De-Sitter Black Hole: Scalar Radiation*. Phys. Rev. D, 2005, 71(10), 1-18.

[30] Abramowitz, M., Stegun, I. A., *Handbook of Mathematical Functions with Formulas, Graphs, and Mathematical Tables*. Department of Commerce, 1964.

[31] Hawking, Stephen, *Gravitationally collapsed objects of very low mass*. Mon. Not. Roy. Astron. Soc., 1971, 152(1).

[32] Zeldovich, Y., Novikov, I., *The Hypothesis of Cores Retarded during Expansion and the Hot Cosmological Model*. Sov. Astron., 1967, 10(602).

[33] Carr, B., Hawking, S., *Black holes in the early Universe*. Mon. Not. R. astron. Soc., 1974, 168, 399–415.

[34] Hawking, Stephen, *Black hole explosions*. Nature, 1974. 248, 30–31.

[35] Carr, B. J., Clesse, S., Garcia-Bellido, J., Hawkins, M. R. S., Kuhnel, F. *Observational Evidence for Primordial Black Holes: A Positivist Perspective*. Phys.Rept., 2024, 1054, 1-68.

[36] Philip, C., A., Dimopoulos, S., March-Russell, J., *Black holes and submillimeter dimensions*. Phys.Lett.B 441, 1998, 96-104.

[37] Arkani-Hameda, N., Dimopoulosb, S., Dvalic, G., *Phenomenology, Astrophysics and Cosmology of Theories with Sub-Millimeter Dimensions and TeV Scale Quantum Gravity*. Phys.Rev.D, 1998, 59, 1-51.